Solid-State NMR Studies of DNA Structure and Dynamics

TODD M. ALAM and GARY P. DROBNY*,†

Department of Chemistry, University of Washington, BG-10, Seattle, Washington, and Department of Chemistry, University of Arizona, Tucson, Arizona

Contents

1.0 Introduction

The description of deoxyribonucleic acid (DNA) has evolved from the uniform, static double helix originally presented by Watson and Crick nearly 40 years ago.[1] The determination of X-ray crystal structures of several synthetic DNA oligomers[2-4] reveals that while these molecules have overall geometries which are similar to the structures obtained by fiber diffraction,[5] there is considerable sequence-dependent variability of the local structure.[6,7] Two-dimensional NMR studies indicate that such sequence-dependent variability may exist in DNA oligomers in solution as well.[8] An intriguing prospect is that this phenomenon provides the molec-

ular basis for the specificity of protein–DNA interactions. Therefore, it is important to determine how well-defined these structures are and the degree to which deviations occur from average structures. In other words, what are the internal dynamics of DNA?

Theoretical and experimental investigation of dynamics in polynucleotides has progressed at a rapid rate, involving many researchers and a variety of techniques and approaches, yet various descriptions of the internal motions in DNA are inconsistent or incomplete. Additional study is clearly required before we obtain

Todd M. Alam, an Arizona native, received his B.S. in chemistry/biology from Northern Arizona University in 1986 and his Ph.D. from the University of Washington in 1990. He is presently a National Eye Institute postdoctoral fellow at the University of Arizona. His research interests include the use of nuclear magnetic resonance to probe the reorientational dynamics in complex systems, in particular biological molecules.

Gary P. Drobny received his Ph.D. in chemistry from the University of California, Berkeley, in 1981. He is currently a Professor in the Department of Chemistry at the University of Washington, Seattle. His research interests include high-resolution and solid-state NMR studies of the structure and dynamics of biopolymers, liquid crystals, and synthetic polymers.
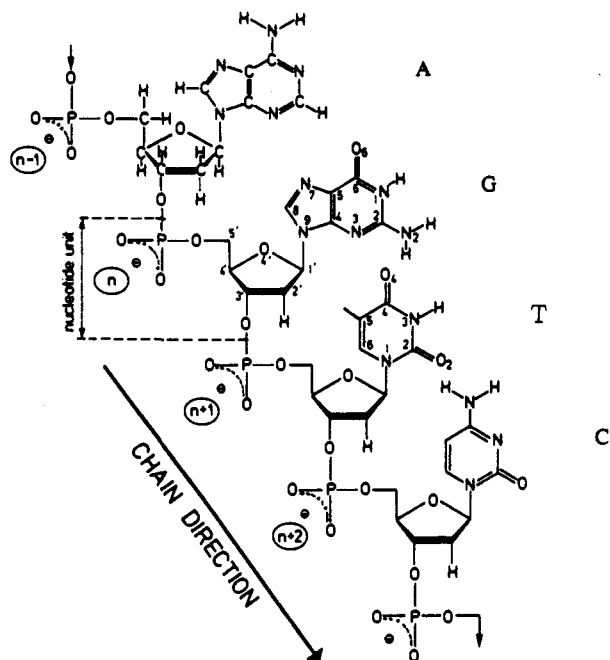
† University of Washington.

Figure 1. Representation of a polynucleotide chain containing the nucleosides deoxyadenosine (A), deoxyguanosine (G), deoxythymidine (T), and deoxycytidine (C). The chain direction is from the 5′- to the 3′-end as shown by arrow (adapted from Saenger (ref 9)).

Figure 2. Atomic numbering scheme and definition of the torsional angles within the polynucleotide chain (adapted from Saenger (ref 9)).

a thorough understanding of the flexibility and conformational fluctuations that occur in polynucleotides and the role that these dynamics may play in the biological function of these molecules.

This review describes the work of a number of groups using solid-state NMR, and particularly deuterium (^{2}H) NMR, to probe the internal dynamics of synthetic oligonucleotides and high molecular weight DNA. Hopefully this review will acquaint the reader with the potential of solid-state NMR to contribute to the ever-growing picture of the internal dynamics of polynucleotides.

1.1 DNA Structure: A Brief Review

As the repository of genetic information carried by chromosomes, nucleic acids play a prominent role in the cellular function of living organisms. To begin any discussion of DNA it is essential that the general structure be understood. The repeating unit in DNA is the nucleoside, composed of a β-D-2′-deoxyribose substituted at the C1′-position by one of four heterocyclic bases: thymine, cytosine, adenine, or guanine. These nucleosides are linked by 3′,5′-phosphodiester bonds to form a polynucleotide strand. A representation of a polynucleotide chain is shown in Figure 1, and the numbering scheme and various torsional angles within the nucleotide unit are shown in Figure 2. Two polynucleotide chains associate via hydrogen bonding between bases to form the classic double helix, shown in Figure 3. This double helix has been shown to exist in a number of conformations including A, B, and Z forms.[9] DNA in the A or B form has a right-handed helical structure, and these conformations may be distinguished on the basis of sugar puckering mode, base pair tilt, axial rise per residue, etc. The sugar rings in A-form DNA are observed to favor the C3′-endo puckering mode while in the B form sugar ring puckering
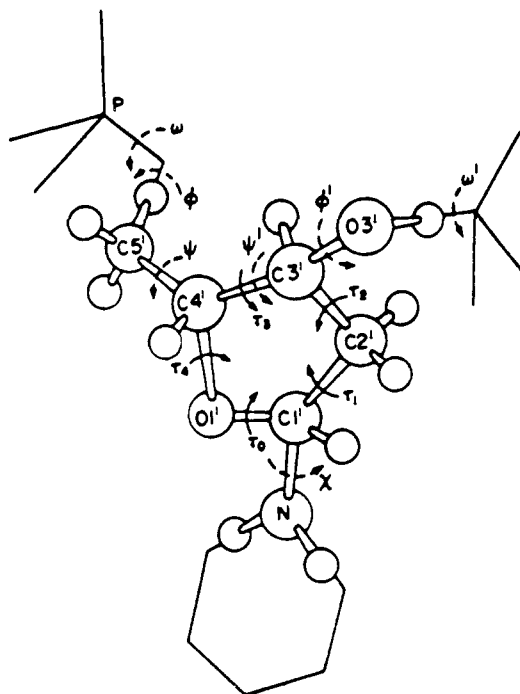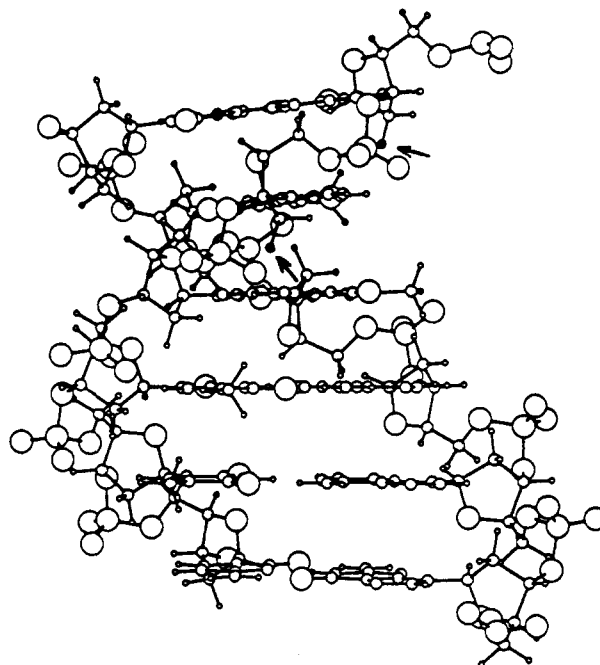
Figure 3. Molecular model of the DNA sequence [d(GAATTC)]$_2$ in the ideal B form. Small arrow denotes 2″ sugar proton.

is generally distributed about the C2′-endo mode. In the A form, axial rise per nucleotide is about 2.59–3.59 Å, but varies from 3.03 to 3.37 Å in B-form DNA. In A-form DNA the rotation per nucleotide about the helix axis is only about 30° but increases to 36°–45° in B-form DNA. Z DNA, a conformation observed only in nucleic acids such as poly(dG-dC), poly(dG-dm^{5}C), or the halogenated sequence poly(dI-dBr^{5}U), has a left-handed helical structure.

The role of hydration or water content is important in determining the structure and dynamics of nucleic acids. The repulsive phosphate–phosphate electrostatic

interaction is mediated by the dielectric constant of water and hydrated counterions, and water content is an important factor involved in the various conformational transitions that occur in DNA.[9] X-ray investigations of the structure of the hydration shells of DNA oligomers in single crystals[10,11] have been reported, as well as diffraction studies of the adsorption properties of DNA fibers.[12-14] The conclusions of the fiber diffraction studies are summarized below.

(1) Between 0% and 65% relative humidity (RH) (up to $W = 6$ mol of H_2O/mol of nucleotide) the phosphate oxygens are hydrated.

(2) The hydration of the base amino, imino, and keto groups occurs above 65% RH with $W = 13-15$.

(3) The primary hydration shell is completely occupied at ca. 80% RH and corresponds to $W \approx 20$.

(4) Further hydration is accompanied by swelling of the sample, and formation of the second hydration shell.

The A- to B-form transition is known to occur between 75% and 92% RH.[9] The exact point of this transition has been shown to vary with salt concentration,[137] where high concentrations of salt causes increased water uptake by the DNA, resulting in the formation of the B-form structure. The use of high salt concentrations in solid-state NMR studies increases the likelihood that the local, internal dynamics observed at low hydration levels are representative of those motions occurring in solution.

1.2 Internal Dynamics in DNA: Background

During the last 10 years, a number of studies of internal dynamics in DNA have appeared in the literature. It is not practical to review all the literature, but a brief survey of selected works will be presented in an attempt to represent the state of knowledge and the points of controversy.

In the late 1970s/early 1980s the first NMR studies of DNA motion appeared in the literature. Most of these efforts were relaxation studies of solutions of DNA fragments hundreds of base pairs in length. Many of these studies, notably work by Hogan and Jardetzky,[15] Bolton and James,[16] Bendall and James,[17] and Bendall, Laub, and James,[18] reported large amplitude internal local motions at rates in the neighborhood of 10^9 s^{-1}. It might be instructive to briefly review how these studies reached such conclusions.

Hogan and Jardetzky performed a number of relaxation measurements (T_1, T_2, NOE) on ^1H, ^{13}C, and ^{31}P nuclei in DNA fragments 140 and 260 base pairs in length. An analysis of the relaxation data based on a two site exchange model for internal motion in ellipsoids was performed[19] in which internuclear vectors were assumed to exist in two discrete configurations.

T_1 and T_2 values for ^{31}P as well as $^{31}P\{^1H\}$ NOEs were measured for 140 and 260 base pair long DNA fragments. In fitting their model to the data, the authors made numerous assumptions, including neglecting the contribution of collective torsional motions to nuclear relaxation, assuming that the relaxation of ^{31}P is purely dipolar and involves only the 3'-, 5'-, and 5''-protons (relaxation by the chemical shift anisotropy or CSA is neglected), and assuming that the ^{31}P-H3', ^{31}P-H5', and ^{31}P-H5'' distances do not change as a result of the motion. Using these assumptions, Hogan and Jardetzky fit their model expressions for T_1, T_2 and the NOE to

their data and found that a best fit resulted assuming ^{31}P-H vector fluctuations of $\pm 27°$ with a time constant of 2.2×10^{-9} s. Similar treatments of the ^{13}C and ^1H data resulted in base plane fluctuations of $\pm 20°$ with a time constant of 10^{-9} s and fluctuations of the deoxyribose sugar ring of $\pm 20°$ to $\pm 33°$ with a similar time constant.

Bolton and James[16] analyzed ^{31}P and ^{13}C NMR data on very long DNA fragments using a model developed by Woessner[20] in which a single internal rotation is superimposed on isotropic reorientation, and internuclear vectors diffuse freely. Assumptions regarding the absence of collective torsional effects in the relaxation, absence of CSA relaxation, and invariance of ^{31}P-H distances were made. The general conclusion of these studies is that large amplitude local motions occur on the nanosecond time scale in long DNA fragments. Continuing along these lines, James and co-workers performed proton[17,18] and ^{31}P[19] NMR relaxation measurements of supercoiled and circular DNA. Remarkably long proton and ^{31}P T_1 relaxation times were measured (>1 s for protons). These workers concluded again that extreme local mobility existed in these DNAs.

Following the publication of the Hogan-Jardetzky and Bolton-James studies, Lipari and Szabo[21] proposed a variety of models of internal motion in DNA including two-site jumps, fluctuations of the azimuthal angle of internuclear vectors (twisting), and wobbling of internuclear vectors. Lipari and Szabo were able to fit a variety of models to the Hogan-Jardetzky data, and all of these models implies the existence of large amplitude internal motion on the nanosecond time scale.

During the same period as the Bolton-James, Hogan-Jardetzky, and Lipari-Szabo work, a number of theories of internal motion in DNA were developed to interpret EPR and nanosecond fluorescence depolarization data. In particular Barkley-Zimm[22] developed an elastic model of semiflexible chain macromolecules in order to treat internal rotary Brownian motion in the DNA helix. From the model, a time distribution function of the angular orientation of a fluorescent probe embedded in a chain macromolecule was derived and used to compute the emission anisotropy. Comparison with published data for ethidium-DNA complexes indicated that the decay of the anisotropy arises primarily from twisting of the DNA helix and to a lesser extent from bending.

Robinson et al.[23] developed at about the same time a theory of the EPR response from a spin-labeled intercalator bound to DNA by solving the stochastic Liouville equation. The internal dynamics were treated in a discrete model in which disks (base pairs) are harmonically coupled together, the entire polymer undergoing Brownian rotational motion in solution. The theory accounted well for the temperature dependence of the rotational correlation time τ_R as well as the dependence of τ_R on the number of base pairs (N) in the DNA. A further study by Robinson and co-workers[24] measured EPR spectra of a family of spin-labeled probes noncovalently bound to DNA as functions of helix orientation, packing density, and temperature. The study indicated the presence of substantial torsional motion but no detectable bending on the EPR time scale. A very interesting feature of this work is

an analysis of the temperature dependence of the correlation time of a propidium probe in terms of several models of internal motion. In terms of a model of elastic rotational coupling between adjacent nucleotides, it was suggested that nucleotide pairs undergo random oscillations with a root mean square (rms) amplitude of 4°-5° at room temperature.

In 1979, Allison and Schurr[25a] published a dynamical model that incorporates the effect of collective torsional modes on an elastic fiber. In 1982, Allison et al.[25b] extended this model to include the effect of collective torsional modes as well as local reorienting motions of pertinent internuclear vectors in harmonic restoring potentials within a nucleotide unit, and end-over-end rotations of the helix axis. This model was used to calculate the dipolar and CSA contributions to T_1 and T_2 of ^{31}P in DNA. These authors demonstrated that collective torsional motions can contribute to T_1 relaxation and claimed that components of motion on the time scale observed by Bolton–James are manifested in collective torsional deformations. Torsional deformations exhibit an unusual correlation function: $\exp(-A/\sqrt{t})$, which results in an unusual field dependence of the dipolar and CSA relaxation rates. This model further predicts that assuming pure dipolar relaxation, ^{31}P–H vectors are expected to have rms local angular displacements of only 7° with a relaxation time of 1 ns, with collective torsional deformations dominating T_1. Should the CSA contribution to T_1 be as large as 40%, local rms displacements of the ^{31}P–H vector would increase to 12° with a relaxation time of 0.2 ns.

Langowski et al.[26] studied supercoiled DNA by ^{31}P NMR and measured a T_2 value of 2 ms, which lies well within the estimates of an extended Allison et al.[25] model using normal rigidities. These authors questioned the results of the Bendall–Laub–James study[18] and claimed that the conclusions of that study imposed upon the DNA one or more extreme properties such as enormously reduced bending or twisting rigidities.

It is clear from the above review that the nature of internal motions in DNA remains an unsettled issue. Part of the reason for lack of unanimity in reported views of the details of internal motions in DNA lies in the complicated nature of the NMR relaxation study. Interpretation of spin–lattice relaxation times in systems of dipolar-coupled nuclei can be a very complicated task, invariably requiring numerous assumptions concerning local molecular geometry and relaxation mechanism. This is especially true with ^{31}P data where a thorough analysis requires inclusion not only of dipolar terms in T_1 but also CSA and possibly dipolar/CSA cross terms. Such a treatment requires detailed knowledge of local geometry, principle values of the ^{31}P CSA tensor, and the orientation of the CSA tensor in a molecule-fixed frame. Certain internal motions (i.e. rotations about the O–C5 bond axis) would tend to change the ^{31}P[H] distance, thus complicating the analysis even further. Such bond rotations are generally neglected. In a recent analysis of NMR data acquired by the Kearns group,[27] Schurr and Fujimoto[28] conclude that using their model of DNA motion and certain structural assumptions, large amplitude internal motions need not be superimposed on collective torsional motions to account for the data. However, these authors conclude that "the low precision of present knowledge about solution structure does not allow a definitive statement about the rms amplitudes of local angular motions of the bases to be made independent of any structural or geometric assumptions". Thus to achieve progress in defining the internal dynamics of DNA, it would seem reasonable to seek a spectroscopic technique in which motional processes could be studied without the necessity of making detailed and possibly unsubstantiated assumptions on local structure.

2.0 Solid-State NMR

Solid-state NMR, and particularly ^2H NMR, has long been recognized as being particularly suited to the study of polymer dynamics. The advantages of ^2H NMR to the study of the internal dynamics of DNA are (1) Deuterium is a nonperturbing probe. The replacement of protons with deuterium has a negligible effect on the structure and dynamics of DNA. (2) Deuterium is a spin $I = 1$ nucleus and therefore possesses an electric quadrupole moment. The interaction of the nuclear electric quadrupole moment with surrounding electric field gradients (EFG) dominates the solid-state NMR spectrum of deuterium relaxation as well. Because the quadrupolar interaction is a single nucleus property, few structural assumptions are required to analyze the line shape or relaxation. (3) Different types of motion can be distinguished through analysis of the ^2H line shape or through the analysis of ^2H Zeeman relaxation. (4) The dynamic range of ^2H NMR is large. Relaxation investigations allow motions from 10^6–10^{10} Hz to be probed, while analysis of the solid echo line shape allows motions in the 10^4–10^6 Hz range to be studied. Even longer time scale motions can be probed from the study of spin-alignment echos.[139] This feature of ^2H NMR is particularly useful because a number of internal motions in DNA such as helical bending and Rousse–Zimm coil deformations occur at very long time scales. (5) A disadvantage is that isotopic labeling is required due to the low natural abundance of deuterium. This can prove to be an overall advantage since unique information can be obtained by site-specific labeling.

The study of the internal dynamics of DNA by solid-state ^2H NMR involves the interpretation of the influence of internal motions on the ^2H NMR spectral line shape and relaxation. Section 2.1 provides a brief overview of the essential elements of ^2H NMR. Section 2.2 presents a review of the quadrupolar line shape and describes the effect on the ^2H line shape of several discrete and continuous motions. Section 2.3 focuses on the influence that various types of internal dynamics exert on the observed Zeeman (T_1) relaxation rate.

2.1 General Deuterium NMR Theory

A comprehensive discussion of the principles of solid-state NMR is beyond the scope of this review. The theoretical material presented in this section will be the bare essentials, hopefully allowing an understanding of the subsequent solid-state ^2H NMR investigations of high molecular weight DNA and synthetic oligonucleotides. Those readers interested in a more thorough discussion of solid-state NMR are referred to several excellent and detailed texts[29-31] and reviews.[32,33] Those readers desiring less theoretical detail, however, may skip sections 2.2 and 2.3 and proceed directly to

the experimental sections 3.0–3.2, where, when the need arises, references are made to specific equations in sections 2.2 and 2.3.

In general the Hamiltonian for an NMR spin system can be written as a sum of terms

$$\mathcal{H} = \mathcal{H}_{ext} + \mathcal{H}_{int} \tag{1}$$

The interaction with external magnetic fields ($\mathcal{H}_{ext}$) includes the Zeeman interaction with the static magnetic field ($\mathcal{H}_z = -\gamma I_o B_o$) and the interaction with the radio frequency magnetic field of the pulse ($\mathcal{H}_{rf} = -\gamma I B_{rf}$). The Hamiltonian describing the interaction with internal or local fields ($\mathcal{H}_{int}$) can involve couplings to other spins (homonuclear and heteronuclear dipolar interactions) or coupling to the local environment (chemical shift and quadrupolar).

For nuclei with spin angular momentum ≥ 1, $\mathcal{H}_{int}$ is dominated by the quadrupolar Hamiltonian $\mathcal{H}_Q$, which can be conveniently expressed in terms of irreducible spherical tensors:[34]

$$\mathcal{H}_Q = C^Q \sum_{l=0}^{2} \sum_{m=-1}^{+1} (-1)^m T_{lm} R_{l-m} \tag{2}$$

where $C^Q = eQ/2\hbar$.

For the quadrupolar interaction on the spherical tensor representation of the spin operators is defined as

$$T_{2,0} = \frac{1}{\sqrt{6}}[3I_z^2 - I^2] \qquad T_{2,\pm 1} = \mp\frac{1}{2}[I_z I_\pm + I_\pm I_z]$$

$$T_{2,\pm 2} = \frac{1}{2}I_\pm^2 \tag{3}$$

where the magnetic field B_0 defines the z axis of the laboratory frame. The EFG tensor is described in the principal axis system (PAS) using a spherical representation:

$$\rho_{20} = \left(\frac{3}{2}\right)^{+1/2} eq \qquad \rho_{2,\pm 1} = 0 \qquad \rho_{2,\pm 2} = \eta eq/2 \tag{4}$$

The parameters eq and η are related to the Cartesian components of the EFG tensor, V_{xx}, V_{yy}, and V_{zz}, by $V_{zz} \equiv eq$ and $\eta \equiv (V_{xx} - V_{yy})/V_{zz}$.

The transformation of these tensor elements to the laboratory frame is accomplished using the rotation matrix with elements $D^{(2)}_{nn'}(\alpha\beta\gamma)$. The convention $D^{(2)}_{nn'}(\alpha\beta\gamma) = \exp{-i(\alpha n + \gamma n')}d^{(2)}_{nn'}(\beta)$ with rotation through the angles $(\alpha\beta\gamma)$ is used.[35] The irreducible coupling elements expressed in the laboratory frame are represented by $R^Q_{2,n}$ and are given in terms of the tensors in the PAS using the relation

$$R^Q_{2,n} = \sum_{n'=-2}^{2} \rho_{2,n'} D^{(2)}_{n'n}(\Phi\Theta\Gamma) \tag{5}$$

where $(\Phi\Theta\Gamma)$ is the solid angle describing the transformation from the PAS to the lab frame (LAB).

Since the static magnetic field is large in comparison to the magnitude of the internal interaction $\mathcal{H}_{int}$, only those components that commute with the Zeeman interaction ($[\mathcal{H}_z, \mathcal{H}'_{int}] = 0$) contribute in first order to the observed spectrum. This part of the internal Hamiltonian $\mathcal{H}'_{int}$ is referred to as the secular component and is the only portion considered further. The secular
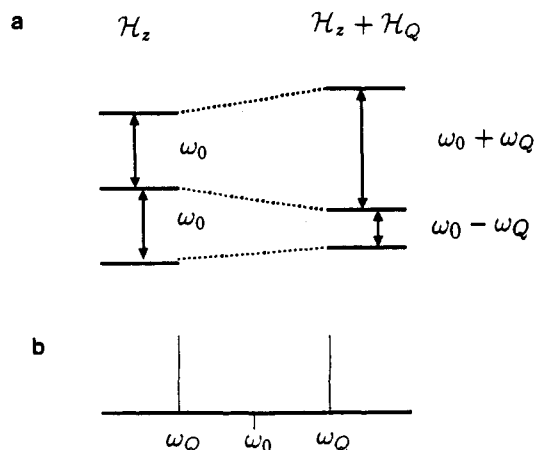

Figure 4. (a) The effects of the first-order quadrupolar perturbation on the energy levels of a spin $I = 1$ nucleus in a high magnetic field. The degenerate transition under the Zeeman interaction $\mathcal{H}_z$ are split by quadrupolar interaction $\mathcal{H}_Q$. (b) The resulting spectrum for a single value of the quadrupolar interaction at $\omega_0 \pm \omega_Q$.

orientation-dependent quadrupolar perturbation Hamiltonian is given by

$$\mathcal{H}_Q = C^Q T^Q_{20} R^Q_{20} \tag{6}$$

Expressing the coupling tensor in the principal axis system using eq 5 gives

$$\mathcal{H}_Q = C^Q T^Q_{20} \sum_{n'=-2}^{2} \rho_{2n'} D^{(2)}_{n'0}(\Phi\Theta\Gamma) \tag{7}$$

It should be noted that the rotation matrix $D^{(2)}_{n'0}(\Phi\Theta\Gamma)$ is independent of Γ. This simply means that in the case of the secular quadrupolar Hamiltonian the resonant frequency does not vary with its orientation about the Z_{lab} axis. The resulting Hamiltonian is

$$\mathcal{H}_Q = C^Q T^Q_{20} \rho_{20}[3 \cos^2\Theta - 1 + \eta \sin^2\Theta \cos 2\Phi] \tag{8}$$

The energy levels for a spin $I = 1$ nucleus and the resulting quadrupolar perturbation are depicted in Figure 4. A spin $I = 1$ nucleus is a three-level system. Under the influence of a Zeeman interaction, $\mathcal{H}_z$, two degenerate transitions at a frequency ω_0 occur. In the presence of the quadrupolar $\mathcal{H}_Q$, this degeneracy is removed, resulting in two transitions at $\pm\omega_Q$ about the Zeeman frequency ω_0 (see Figure 4b), where

$$\omega_Q = 3\pi/4\left(\frac{e^2qQ}{h}\right)[3 \cos^2\Theta - 1 + \eta \sin^2\Theta \cos 2\Phi] \tag{9}$$

The quantity (e^2qQ/h) is called the quadrupolar coupling constant (QCC), and η is called the asymmetry parameter.

Thus far it has been tacitly assumed that only one orientation of the EFG tensor with respect to the magnetic field B_0 exists. If the NMR sample consists of domains or molecules where the orientation of the molecular axis or director are randomly oriented with respect to the magnetic field, a classic powder pattern or Pake doublet is obtained which is the superposition of these transitions. The spectral intensity $I(\omega)$ integrated over a frequency range $\delta\omega = \omega_a - \omega_b$ (referred to a curve of constant frequency) is equal to the superposition of transitions for all orientations Θ, Φ that
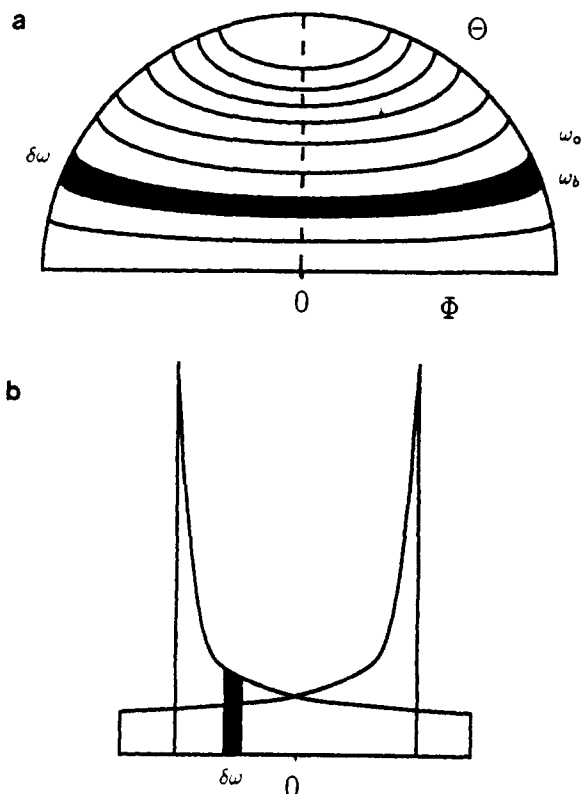
a

b

Figure 5. (a) Illustration of the constant frequency curve for an axially symmetric EFG tensor in stereographic projection. (b) The Pake doublet spectra resulting from both transitions is composed of two mirror image powder spectra. The shaded region corresponds to that in part a.

correspond to frequencies in the interval. Examples of curves of constant frequency and the resulting powder pattern are presented in Figure 5. The calculation of the intensity for the interval $\delta\omega$ reduces to determination of the area between two curves of constant frequency ω_a and ω_b

$$\int_{\omega_b}^{\omega_a} I(\omega) \, d\omega = N \int_{\Theta_a}^{\Theta_b} \int_{\Phi_b}^{\Phi_a} \sin \Theta \, d\Theta \, d\Phi \qquad (10)$$

The resulting line shapes for random and partially ordered solids have been treated in detail elsewhere.[33,34]

2.2 Dynamic and Motional Processes

Internal dynamics and molecular motion can modulate the angular-dependent frequencies ω_Q. If the motion is slow on the time scale of ω_Q^{-1} the observable effects on the quadrupolar echo line shape are minimal. Spectra in this limit are usually referred to as static line shapes, allowing the determination of the static quadrupolar coupling constant QCC_{static} and static asymmetry parameter η_{static}. If the motion is on the time scale of ω_Q^{-1}, distinct spectral distortions of the line shape can occur.[36]

If the molecular motion is fast on the time scale of ω_Q^{-1}, the resonant frequencies are defined using effective values of the averaged quadrupolar coupling constant QCC_{eff} and asymmetry parameter η_{eff}.

The evolution of the spin system under the influence of dynamics can be monitored in the general case through the use of the density matrix. The overall formalism for the simulation of evolution for a spin I = 1 nuclei subject to radio frequency (rf) pulses of du-

ration t_p, pulse delays of τ_i, and exchange is given by[37]

$$\dot{\rho} = i[\rho, \mathcal{H}] + k(P\rho P - \rho) \qquad (11)$$

where $\mathcal{H}$ describes both the quadrupolar interactions and the rf pulse, k is the exchange rate, and P is the exchange operator. The exchange operator acts only on the site labels of the spin operators, such that $PI_{x1}^{\alpha}P = I_{x1}^{\beta}$.

The spin-density operator can be expressed as a linear combination of operators forming a complete basis set

$$\rho(t) = \sum m_i(t)O_i \qquad (12)$$

In the Liouville representation, eq 11 can be written as a set of coupled differential equations

$$\dot{m}_i = \sum_j L_{ij}m_j \qquad (13)$$

whose general solution is

$$\mathbf{M}(t) = \exp{(\mathbf{L}t)}\mathbf{M}(0) \qquad (14)$$

where the column vector $\mathbf{M}$ is composed of the expansion coefficients given by the relationship in eq 12. The signal $S(t)$ is obtained by evaluating the trace of the product of the density matrix $\rho(t)$ with the operator $\sum_{N\alpha=1}I_{x1}^{\alpha}$ or $\sum_{\alpha=1}^{N}I_{y1}^{\alpha}$, where the index α labels the site.

$$S(t) = Tr[\sum_{\alpha=1}^{N} I_{x1}^{\alpha}\rho(t)] \qquad (15)$$

Evaluation of this trace results in a subset selection of the vector $\mathbf{M}$ such that a nonzero element implies that the operator m_i is associated with I_{x1} or I_{y1} for the site α in question.

The general procedure described above is required to treat dynamics in the regime where the rate of the motion is on the order of ω_Q^{-1}. In the limit where the motion is fast on the time scale of ω_Q^{-1}, determination of the resulting quadrupolar line shape is simplified. In this regime the resulting line shape is dependent on the equilibrium conformational populations $P(\Omega)$, and is independent of the exchange rate. The analysis of line shapes is accomplished through calculation of the averaged quadrupolar coupling constant QCC_{eff} and averaged asymmetry parameter η_{eff} such that the resulting line shape is defined by

$$\omega_Q = 3\pi/4\left(\frac{e^2qQ}{h}\right)_{eff} [3 \cos^2 \Theta - 1 + \eta_{eff} \sin^2 \Theta \cos 2\Phi] \qquad (16)$$

The reduction in the quadrupolar coupling constant is typically discussed in terms of an order parameter S_{ij}. Since the order parameter is not necessarily symmetric and its correct use will involve η_{eff}, we refrain from utilizing it here and instead define a simpler "reduction factor" Λ to describe the motional averaging of the quadrupolar coupling constant.

$$\Lambda = \left(\frac{e^2qQ}{h}\right)_{eff} / \left(\frac{e^2qQ}{h}\right)_{static} \qquad (17)$$

2.2.1 Discrete Dynamics

If the motion is fast in comparison to ω_Q^{-1}, the eigenvalues of the motionally averaged or quasistatic EFG

tensor $\bar{V}_{ll}^{PAS}$ replace the static principal components of V_{ll}^{PAS}. The motionally averaged EFG tensor is an orientational-dependent average weighted by the equilibrium distribution $P(\Omega)$. For discrete processes:

$$\bar{V}_{kl} = \sum_j P(\Omega_j) V_{kl}(\Omega_j) \qquad (18)$$

Considering only an axial symmetry component (η_{static} = 0) and the conventions of Torchia and Szabo[38] the resonant frequency for an N site libration in the fast exchange limit is given by

$$\omega_Q = K^Q \rho_{20} \sum_{j=1}^{N} p_{eq}(j) \sum_{a=-2}^{+2} d_{0a}^{(2)}(\Theta) d_{0a}^{(2)}(\theta_j) \cos [a(\phi_j - \Phi)] \qquad (19)$$

where $K^Q = \pm(3/2)^{1/2} eQ/2\hbar$, $\rho_{20} = (3/2)^{1/2} eq$, and $p_{eq}(j)$ is the equilibrium probability of jth site. The angles Θ and Φ describe the orientation of the magnetic field in the crystal frame, while θ_j and ϕ_j describe the orientation of the crystal frame in the PAS of the jth site.

In the analysis of experimental ^2H NMR line shapes obtained from selectively deuterated DNA, a number of discrete motional models will prove useful. The procedure for obtaining expressions for unequal site probabilities is to diagonalize the averaged EFG tensor $\bar{V}$, allowing the eigenvalues or principal components to be determined by inspection. For the case in which the static EFG tensor is axially symmetric in the PAS

$$V^{PAS} = -\frac{eq}{2} \begin{pmatrix} 1 & 0 & 0 \\ 0 & 1 & 0 \\ 0 & 0 & -2 \end{pmatrix} \qquad (20)$$

the EFG tensor in a given site (Ω_j) is obtained from V^{PAS} using the orthogonal transformation $r(\Omega)$[39]

$$V(\theta_j) = r^\dagger(\Omega_j) V^{PAS} r(\Omega_j) \qquad (21)$$

It follows from the axial symmetry of V^{PAS} only two Euler angles $\Omega_j = (\theta_j, \phi_j)$ are required to orient $V(\Omega_j)$, resulting in

$$V(\Omega_j) = -\frac{eq}{2} \times$$

$$\begin{pmatrix} 1-3\cos^2\phi_j\sin^2\theta_j & 3/2\sin 2\phi_j\sin^2\theta_j & 3/2\cos\phi_j\sin 2\theta_j \\ 3/2\sin 2\phi_j\sin^2\theta_j & 1-3\sin^2\phi_j\sin^2\theta_j & -3/2\sin\phi_j\sin 2\theta_j \\ 3/2\cos\phi_j\sin 2\theta_j & -3/2\sin\phi_j\sin 2\theta_j & 1-3\cos^2\theta_j \end{pmatrix} \qquad (22)$$

The averaged EFG tensor resulting from a 2-fold libration or 2-fold jump with a half-angle θ_0 is obtained using eqs 18 and 22 to give

$$\bar{V} = -\frac{eq}{2} \begin{pmatrix} 1-3\sin^2\theta_0 & 0 & \xi_{12}^-(3/2)\sin 2\theta_0 \\ 0 & 1 & 0 \\ \xi_{12}^-(3/2)\sin 2\theta_0 & 0 & 1-3\cos^2\theta_0 \end{pmatrix} \qquad (23)$$

where the difference in equilibrium site populations is given by $\xi_{12}^- = [p_{eq}(1) - p_{eq}(2)]$. Diagonalization of this averaged tensor allows the principal components to be easily determined. Contours depicting the variation of the reduction factor Λ and η_{eff} as a function of the half-angle θ_0 and site probability $p_{eq}(1)$ are presented in Figures 6 and 7. The variation in line shape is found to differ slowly with $p_{eq}(1)$, suggesting that a wide range
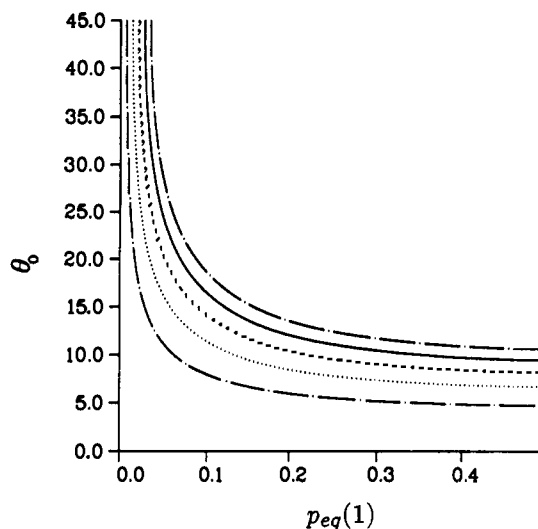

Figure 6. Variation in the reduction factor Λ for a discrete two-site jump as a function of equilibrium population $p_{eq}(1)$ and the half-angle of displacement, θ_0. Contours are shown for specific values of Λ; 0.99 (— ·), 0.98 (· ·), 0.97 (– –), 0.96 (—), 0.95 (— ·).

Figure 7. Variation in the effective asymmetry parameter η_{eff} for a discrete two-site jump as a function of equilibrium population $p_{eq}(1)$ and the half-angle of displacement θ_0. Contours are shown for specific values of η_{eff}; 0.01 (– –), 0.02 (· ·), 0.03 (— ·), 0.04 (—), 0.05 (· -).

of site populations could easily account for small observed values of η_{eff}.

Expressions for a four-site libration are obtained in the same manner as described above. Assuming the libration is characterized by half-angles θ_0 and ϕ_0, the averaged tensor is obtained again using eqs 18 and 22:

$$\bar{V} = -\frac{eq}{2} \times$$

$$\begin{pmatrix} \xi_{34}^+ + \xi_{12}^+(1-3\sin^2\theta_0) 0 & & \xi_{12}^-(3/2)\sin 2\theta_0 \\ 0 & \xi_{12}^+ + \xi_{34}^+(1-3\sin^2\phi_0) & -\xi_{34}^-(3/2)\sin 2\phi_0 \\ \xi_{12}^-(3/2)\sin 2\theta_0 & -\xi_{34}^-(3/2)\sin 2\phi_0 & \xi_{12}^+(1-3\cos^2\theta_0) + \\ & & \xi_{34}^+(1-3\cos^2\phi_0) \end{pmatrix}$$

$$(24)$$

where $\xi_{ij}^\pm = [p_{eq}(i) \pm p_{eq}(j)]$. Contours showing the behavior of η_{eff} and Λ as a function of the half-angles θ_0 and ϕ_0 for different site populations are presented in Figure 8.

Figure 8. Variation in the reduction factor Λ and the effective asymmetry parameter η_{eff} for a discrete four-site libration as a function of the two half-angles of displacement θ_0 and ϕ_0 with the equilibrium populations $p_{eq}(1) = p_{eq}(2) = p_{eq}(3) = p_{eq}(4) = 0.25$. Contours are shown for specific values of Λ (lower left concentric circles), 0.99 (— ·), 0.98 (· ·), 0.97 (– –), 0.96 (—), 0.95 (— ·), and specific values of η_{eff}, 0.01 (– –), 0.02 (· ·), 0.03 (— ·), 0.04 (—), 0.05 (– –).

The final discrete model which will prove useful in our discussion of DNA line shapes is the trans–gauche isomerization between three sites defined by the angles $\phi_1 = 0°$, $\phi_2 = 120°$, $\phi_3 = 240°$ and θ. The averaged EFG tensor for this three site jump motion is

$$\overline{V} = -\frac{eq}{2} \times$$

$$\begin{pmatrix} p_{eq}(1)(1 - 3 \sin^2 \theta) + & -\xi_{23}^-(3\sqrt{3}/4) \sin^2 \theta & p_{eq}(1)(3/2) \sin 2\theta \\ \xi_{23}^+(1 - 3/4 \sin^2 \theta) & p_{eq}(1) + & -\xi_{23}^+(3/4) \sin 2\theta \\ -\xi_{23}^-(3\sqrt{3}/4) \sin^2 \theta & \xi_{23}^+(1 - (9/4) \sin^2 \theta) & -\xi_{23}^-(3\sqrt{3}/4) \sin 2\theta \\ p_{eq}(1)(3/2) \sin 2\theta & -\xi_{23}^-(3\sqrt{3}/4) \sin 2\theta & 1 - 3 \cos^2 \theta \\ -\xi_{23}^+(3/4) \sin 2\theta & & \end{pmatrix}$$

$$(25)$$

Contour plots displaying the behavior of Λ and η_{eff} as a function of the site populations are shown in Figures 9 and 10.

2.2.2 Continuous Dynamics

The quadrupolar line shape resulting from fast continuous dynamics is obtained in a manner analogous to that for a discrete process. The residual or averaged EFG tensor $\overline{V}(\Omega)$ is a weighted average based on the equilibrium distribution of molecular orientations $P(\Omega)$. For continuous processes, this is given by

$$\overline{V}(\Omega) = \int d\Omega \, P(\Omega) V(\Omega) \qquad (26)$$

where the equilibrium distribution is determined by the potential $U(\Omega)$ through the Boltzmann distribution

$$P(\Omega) = Z^{-1} e^{-U(\Omega)\beta} \qquad (27)$$

$$Z = \int_0^\infty e^{-U(\Omega)} \, d\Omega \qquad (28)$$

where Z is the partition function, the parameter β is identified with $1/k_B T$ (T is the absolute temperature

Figure 9. Variation in the reduction factor Λ for a discrete three-site jump as a function of the equilibrium population $p_{eq}(i)$ and the relative ratio of the remaining fractions $[p_{eq}(j) - p_{eq}(k)]/[p_{eq}(j) + p_{eq}(k)]$. Contours are shown for the specific values of Λ: 0.95 (— ·), 0.90 (· ·), 0.85 (– –), 0.80 (—), 0.75 (— ·), 0.70 (· ·), 0.65 (– –), 0.60 (—), 0.55 (— ·), 0.50 (· ·), 0.45 (– –), 0.40 (—).

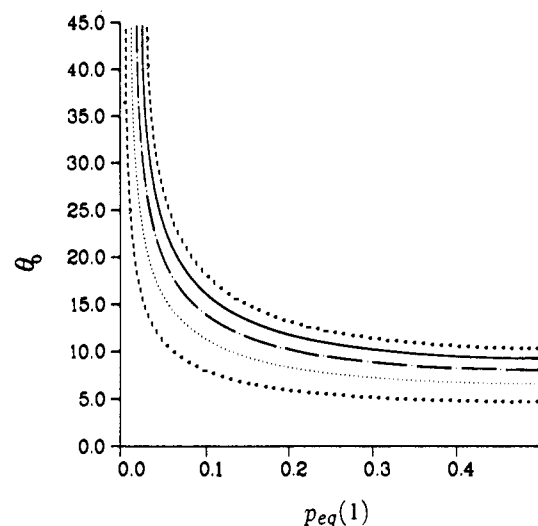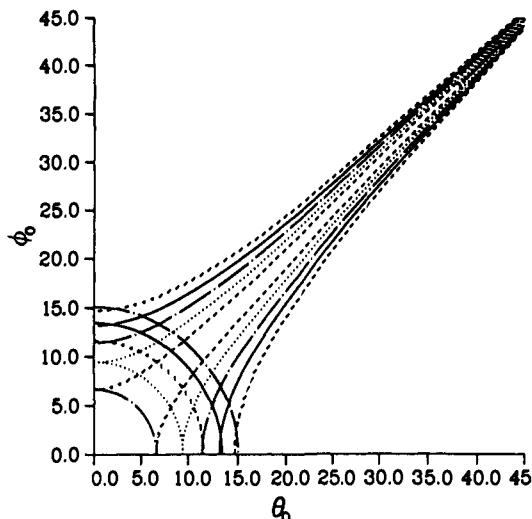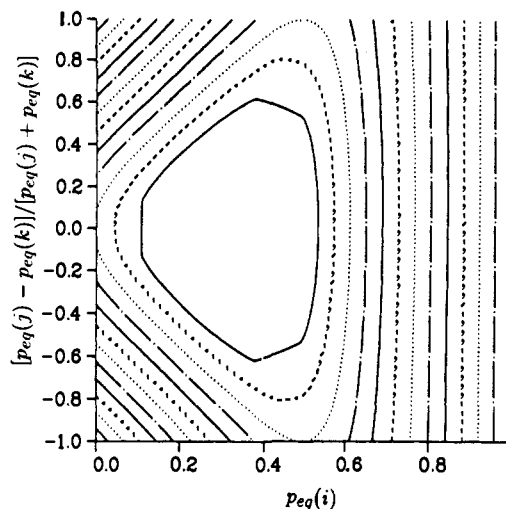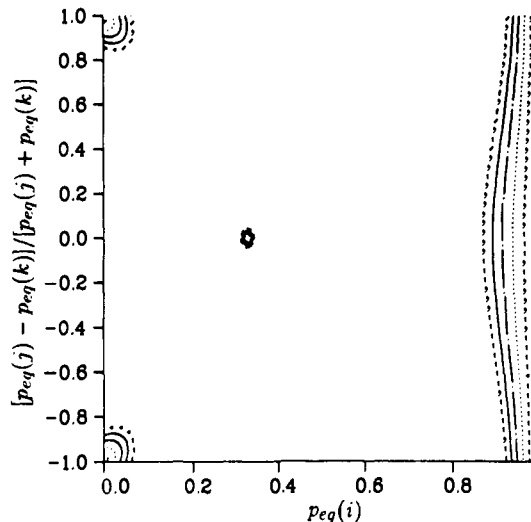**Figure 10.** Variation in the effective asymmetry parameter η_{eff} for a discrete three-site jump as a function of the equilibrium population $p_{eq}(i)$ and the relative ratio of the remaining fractions $[p_{eq}(j) - p_{eq}(k)]/[p_{eq}(j) + p_{eq}(k)]$. Contours are shown for specific values of η_{eff}; 0.02 (– –), 0.04 (· ·), 0.60 (— ·), 0.08 (—), 0.10 (– –).

and k_B is the Boltzmann constant).

The fast limit line shape for a CD bond undergoing motion within a harmonic potential is obtained using eqs 22 and 26. The harmonic potential is defined as $U(\theta_0) = f\theta_0^2$ or $U(\phi_0) = f\phi_0^2 \sin^2 \theta$, depending on whether θ or ϕ is allowed to be time dependent. Two distinctly different motional processes involving a harmonic potential are presented.

The first process considered can be described as a continuous libration and is depicted in Figure 11. The potential is $U(\theta_0) = f\theta_0^2$, with the angle of displacement defined as θ_0 and the force constant f. The potential is symmetric about $\theta = 0°$. This results in equilibrium populations $P(\Omega) = P(-\Omega)$, reducing the integration range to $\int_0^\pi$ in the analysis. Analytical expressions for individual tensor elements were obtained by evaluating the integral over the range $\int_0^\infty$. Extension of the upper limit to infinity is justified because the exponential of

$$U = f\theta_0^2$$

Figure 11. Representation of the continuous librational harmonic potential defined by $U(\theta_0) = f\theta_0^2$ where f is the force constant and θ_0 is the angle of displacement from equilibrium.

Figure 12. Variation of (a) the reduction factor Λ and (b) the effective asymmetry parameter η_{eff} for a continuous librational motion in the one-dimensional harmonic potential $U(\theta_0) = f\theta_0^2$ as a function of the force constant f.
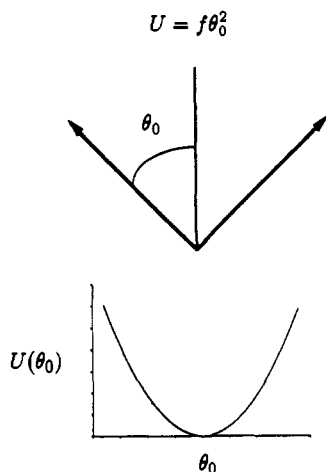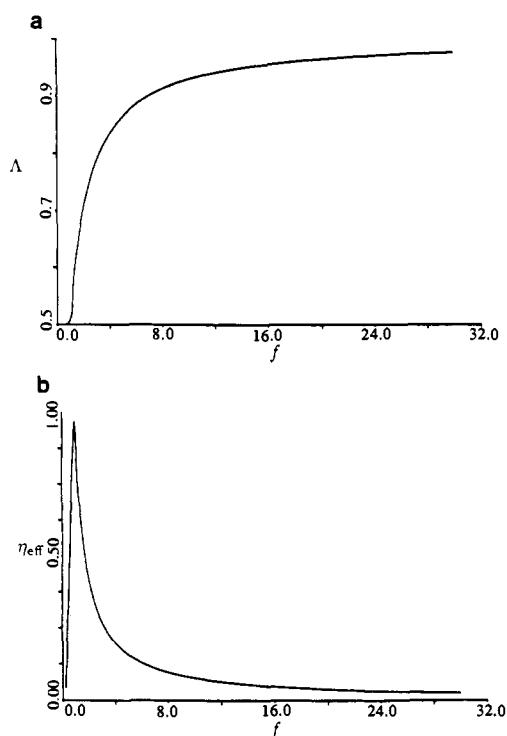
the Boltzmann distribution dominates the first terms in the integral. The resulting averaged EFG tensor is

$$\overline{\mathbf{V}}(U = f\theta_0^2) = -\frac{eq}{2} \int_0^\infty \frac{e^{-f\beta\theta_0^2}}{Z} \times$$

$$\begin{pmatrix} 1 - 3\cos^2\phi\sin^2\theta_0 & 3/2 \sin 2\phi\sin^2\theta_0 & 0 \\ 3/2 \sin 2\phi\sin^2\theta_0 & 1 - 3\sin^2\phi\sin^2\theta_0 & 0 \\ 0 & 0 & 1 - 3\cos^2\theta_0 \end{pmatrix} d\theta_0$$

$$(29)$$

It should be noted that the angle ϕ commutes with Φ (which is the angle describing the crystal to lab transformation). This commutation produces averaged line-shape parameters QCC_{eff} and η_{eff} that are invariant

$$U = f\phi_0^2 \sin^2\theta$$
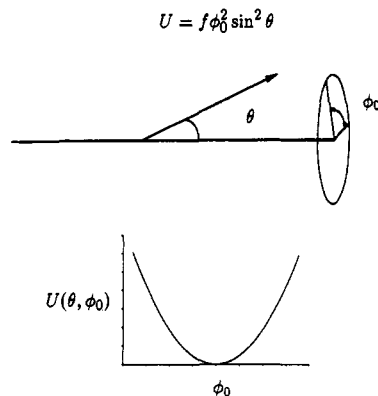
Figure 13. Representation of the one-dimensional harmonic potential defined as $U(\phi_0) = f\phi_0^2 \sin^2\theta$, where f is the force constant and ϕ_0 is the half-angle of displacement. The angle between the V_{zz} element of the EFG tensor and the motional axis is defined as θ.
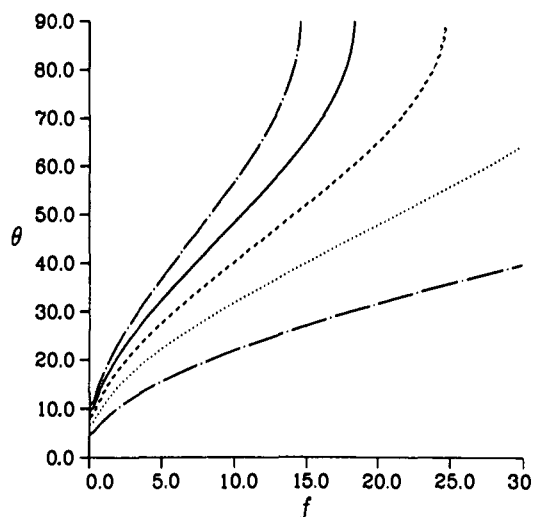
Figure 14. Variation of the reduction factor Λ for the one-dimensional harmonic potential $U(\phi_0) = f\phi_0^2 \sin^2\theta$ (see Figure 13) as a function of the angle θ and the force constant f. Contours are shown for specific values of Λ: 0.99 (— ·), 0.98 (· ·), 0.97 (— —), 0.96 (—), 0.95 (— ·).

to changes in ϕ. This invariance to ϕ allows the value of $\phi = 0$ to be used without loss of generality, and results in a diagonal averaged EFG tensor. The behavior of Λ and η_{eff} with variation in the force constant is shown in Figure 12. At low force constants, motion in the plane is nearly uniform, resulting in the reduction factor $\Lambda = \frac{1}{2}$ as is expected. In this limit the motion is also symmetric, leading to an averaged asymmetry parameter $\eta_{\text{eff}} = 0$. With increasing force, constant Λ approaches the value of 1. This simply reflects the fact that with a steep harmonic potential the dynamics are reduced, restricting the deuterium to a limited range of the potential with little motional averaging. The behavior of the average asymmetry parameter with increasing values of the force constant shows distinct maximum of $\eta_{\text{eff}} \approx 1$ at $f \approx 0.95k_BT$, followed by a steady decrease with higher values of f.

A similar continuous motional model is depicted in Figure 13. The dynamics are governed by the potential $U(\phi) = f\phi_0^2 \sin^2\theta$. The motion occurs on the edge of a cone defined by the time-independent angle θ. In the limit that $\theta = 90°$, this is equivalent to the continuous libration within a plane discussed above. For other θ angles the dynamic process is expected to have differing

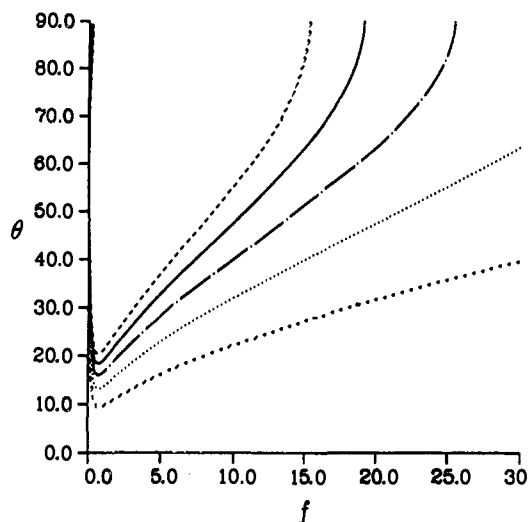**Figure 15.** Variation of the effective asymmetry parameter η_{eff} for the one-dimensional harmonic potential $U(\phi_0) = f\phi_0^2 \sin^2 \theta$ (See Figure 13) as a function of the angle θ and the force constant f. Contours are shown for specific values of η_{eff}: 0.01 (- -), 0.02 (· ·), 0.03 (— ·), 0.04 (—), 0.05 (- -).

effects on the line shape. The averaged tensor is evaluated as described previously, resulting in

$$\overline{V}(U = f\phi_0^2) = -\frac{eq}{2} \int_0^\infty \frac{e^{-f\beta\phi_0^2}}{Z} \times$$

$$\begin{pmatrix} 1 - 3\cos^2\phi_0\sin^2\theta & 0 & 3/2\cos\phi_0\sin 2\theta \\ 0 & 1 - 3\sin^2\phi_0\sin^2\theta & 0 \\ 3/2\cos\phi_0\sin 2\theta & 0 & 1 - 3\cos^2\theta \end{pmatrix} d\phi_0$$

(30)

The influence of the angle θ and the force constant f on the line-shape parameters are shown in Figures 14 and 15. It is interesting to note that if $\theta = 0$ the motion has no effect on the line shape since the C–D bond points along the axis of motion.

2.3 Zeeman Relaxation

In this section the effect of molecular motion on the observed Zeeman relaxation rate will be considered. In particular, expressions for the Zeeman relaxation rate corresponding to a number of motional models relevant to the study of the internal dynamics of DNA will be derived. As was mentioned earlier, ^2H NMR relaxation is particularly convenient to analyze because the relaxation dynamics of deuterium are dominated by the quadrupolar mechanism. To appreciate this consider that the quadrupolar coupling of a deuterium nucleus bound to an aliphatic carbon is typically on the order of 150–200 kHz. In comparison, the dipolar interaction between a deuteron and a proton is only on the order of 10 kHz, and the dipolar interaction between two deuterons is even smaller. Therefore, to an excellent approximation, in systems of deuterium nuclei, Zeeman relaxation is dominated by fluctuations of the quadrupolar interaction, which in turn are produced by molecular motions. To express these fluctuations the total Hamiltonian can be rewritten, in the absence of a radio frequency field, as[29,32,33]

$$\mathcal{H} = \mathcal{H}_z + \langle \mathcal{H}_Q \rangle + (\mathcal{H}_Q(t) - \langle \mathcal{H}_Q(t) \rangle)$$

(31)

where $\mathcal{H}_z$ refers to the Zeeman interaction, $\mathcal{H}_Q(t)$ is the time-dependent quadrupolar Hamiltonian, and $\langle \mathcal{H}_Q \rangle$ is the time-independent or static component of the quadrupolar interaction. Transformation of the Hamiltonian to the interaction frame of $\mathcal{H}_0 = \mathcal{H}_z + \langle \mathcal{H}_Q \rangle$ using the unitary operator $U = \exp[-i\mathcal{H}_0 t]$ allows the evolution of the density matrix to be written as

$$d\rho'/dt = -i[\mathcal{H}'_r(t), \rho']$$

(32)

where $\rho' = U\rho U^{-1}$ and the transformed relaxation Hamiltonian $[\mathcal{H}'_r(t)]$ is given by

$$\mathcal{H}'_r(t) = U(\mathcal{H}_Q(t) - \langle \mathcal{H}_Q(t) \rangle)U^{-1} = U\mathcal{H}_r(t)U^{-1}$$

(33)

Evolution of the density matrix under the relaxation Hamiltonian $\mathcal{H}_r$ is governed by a master equation, which is best framed in terms of the relaxation Hamiltonian expressed in an irreducible tensor basis:

$$\mathcal{H}_r(t) = C^Q \sum_{m=-2}^{+2} (-1)^m T_{2m} R_{2-m}$$

(34)

where $C^Q = eQ/2\hbar$.

The master equation is written in the interaction frame of the Zeeman Hamiltonian as

$$d\rho^*/dt = i[\rho^*, \langle \mathcal{H}_Q \rangle] - C^2 \sum_{m=m'=-2}^{+2} (-1)^{m+m'} \exp(i(m + m')\omega_0 t)[T_{2m}[T_{2m'}, \rho^*(t) - \rho_0^*]] \times$$

$$\int_0^\infty \langle R_{2-m}(t) R_{2-m'}(t - \tau) \rangle \exp(-im'\omega_0\tau) d\tau$$

(35)

where ρ^* is the density matrix in this new rotating frame

$$\rho^* = V\rho V^{-1}, \quad V = \exp(i\mathcal{H}_z t)$$

(36)

Also note that the operators T_{lm} are modified by a factor of $\exp(\pm i\omega_Q t)$ due to the static component $\langle \mathcal{H}_Q \rangle$, but since $\omega_Q \ll \omega_0$, these factors are ignored.

In the determination of relaxation rates only slow changes in the elements of the density matrix are of interest, not the rapid oscillations on the order of the Larmor frequency ω_0. Inspection of eq 35 reveals that only those secular terms with $m = -m'$ need to be retained, resulting in the evolution expression

$$d\rho^*/dt = i[\rho^*, \langle \mathcal{H}_Q \rangle] - (C^Q)^2 \sum_{m=-2}^{+2} [T_{2m}[T_{2-m}, \rho^*(t) - \rho_0^*]] \times \int_0^\infty \langle R_{2-m}(t) R_{2m}(t - \tau) \rangle e^{-i_m'\omega_0\tau} d\tau$$

(37)

Defining the correlation function

$$C'_m(t) = \langle R_{2-m}(t) R_{2m}(t - \tau) \rangle$$

(38)

followed by a redefinition of time scales and rescaling, leads to the autocorrelation function

$$C_m(t) = \langle R_{2-m}(0) R_{2m}(t) \rangle / (\rho_{20})^2$$

(39)

The spectral density function is related to the autocorrelation function by the cosine Fourier transform

$$J_m^Q(m\omega_0) = (-1)^m 2 \int_0^\infty C_m(t) \cos(\omega t) dt$$

(40)

The relaxation of individual elements of the spin-density matrix can be expressed in terms of the spectral densities presented in eq 40. The relaxation of the Zeeman polarization, also referred to as spin–lattice relaxation, is obtained by examining the evolution of the coefficient m_{z1} of the operator I_z

$$\dot{m}_{z1} = -(m_{z1} - m_{z1}^{eq})/T_1 \qquad (41)$$

where the initial equilibrium density matrix contains only the matrix element m_{z1}^{eq}. This leads to the well-known expression

$$R_1 = \frac{1}{T_1} = \frac{1}{3}\left(\frac{3e^2qQ}{4\hbar}\right)^2 [J_1(\omega_0) + 4J_2(2\omega_0)] \qquad (42)$$

Similarly the decay of quadrupolar order is given by:

$$R_{1Q} = \frac{1}{T_{1Q}} = \left(\frac{3e^2qQ}{4\hbar}\right)^2 [J_1(\omega_0)] \qquad (43)$$

In the absence of rf fields, the decay of the quadrupolar echo intensity may be described by the relaxation of the two transverse components of magnetization that decay to zero as $\exp(-t/T_{2e})$ where

$$\frac{1}{T_{2e}} = \frac{1}{2}\left(\frac{1}{T_{2a}} + \frac{1}{T_{2b}}\right) \qquad (44)$$

and

$$\frac{1}{T_{2a}} = \frac{1}{3}\left(\frac{3e^2qQ}{4\hbar}\right)^2\left[\frac{3}{2}J_0(0) + \frac{5}{2}J_1(\omega_0) + J_2(2\omega_0)\right] \qquad (45)$$

$$\frac{1}{T_{2b}} = \frac{1}{3}\left(\frac{3e^2qQ}{4\hbar}\right)^2\left[\frac{3}{2}J_0(0) + \frac{1}{2}J_1(\omega_0) + J_2(2\omega_0)\right] \qquad (46)$$

The decay of the quadrupolar echo as a function of the pulse delays τ_1 and τ_2 determines T_{2e}. This should not be confused with inhomogeneous decay T_2^*, which describes the dephasing of magnetization in the transverse plane. This dephasing is refocused by the quadrupolar echo pulse sequence.

2.3.1 Models for Localized Motions

Localized internal motions in DNA such as base librations, sugar ring conformational interconversions, and motions of the phosphodiester backbone may be modeled as discrete jumps and in some cases continuous librations about one or more axes. In this section correlation functions for several models of single axis and multiaxis discrete jump-type motions will be presented.

Recall that the elements R_{lm} can be constructed from the irreducible coupling elements described in the PAS through

$$R_{lm} = \sum_{n'=1}^{+1} \rho_{ln'}D_{n'm}^{(l)}(\Omega(t)) \qquad (47)$$

The time-dependent fluctuations in R_{lm} can result from changes in $\Omega = (\alpha,\beta,\gamma)$ or from changes in the principal values $\rho_{ln'}(t)$. We will consider only the case where the time dependence results from motional variation in the orientation angle $\Omega(t)$. The T_1 relaxation rate for deuterium is dominated by the quadrupole coupling mechanism; thus only second-rank coupling components are nonzero. Utilizing the symmetry relationship of the rotation matrix $D_{mm'}^{(2)*}(\Omega) = (-1)^{m-m'}D_{-m-m'}^{(2)}(\Omega)$ expression of the correlation function in the PAS system yields

$$C_m(t) = \sum_{nn'aa'=-2}^{+2} \frac{\rho_{2n}\rho_{2n'}}{(\rho_{20})^2} \langle D_{na}^{(2)*}(\Omega_{pc}(0))D_{n'a}^{(2)}(\Omega_{pc}(t)) \rangle \times$$
$$\langle D_{am}^{(2)*}(\Omega_{cl}(0))D_{a'm}^{(2)}(\Omega_{cl}(t)) \rangle \qquad (48)$$

where the Euler angles β_{cl},α_{cl} are the spherical polar angles (Θ,Φ) describing the orientation of the crystal axis in the laboratory frame. The approximation of $\eta = 0$ is valid for deuterium bound to carbon (especially for aliphatic deuterons) producing an axially symmetric coupling tensor that contributes only terms with $n = n' = 0$. Each term in the sum is assumed to be the simple product of two functions

$$C_m(t) = \sum_{aa'=-2}^{+2} C_{aa'}(t)G_{aa'mm}(t) \qquad (49)$$

where

$$C_{aa'}(t) = \langle D_{0a}^{(2)*}(\Omega_{pc}(0))D_{0a}^{(2)}(\Omega_{pc}(t)) \rangle \qquad (50)$$

is the internal correlation function describing the motion of the C-D bond in the base pair reference frame, and

$$G_{aa'mm}(t) = \langle D_{am}^{(2)*}(\Theta(0)\Phi(0))D_{a'm}^{(2)}(\Theta(t)\Phi(t)) \rangle \qquad (51)$$

is the correlation function describing the motion of the base pair subunit in the laboratory reference frame.

Expressions for spin–lattice relaxation in solids for various motional models were treated extensively by Torchia and Szabo.[38] They presented explicit expressions for the correlation function $C_{aa'}(t)$ and the resulting T_1 relaxation for N site jump motions. In the following section the two site and three site jump models will be investigated, including a characterization of the anisotropic behavior of T_1 relaxation across the powder pattern. This jump formalism will be extended to investigate T_1 relaxation for an asymmetric four-site jump.

Correlation functions for an N-site jump are obtained using the formalism presenetd by Szabo and Wittebort.[41,42] In general the correlation function for a jump process is given by

$$\langle f(\Omega(0))g(\Omega(t)) \rangle = \sum_{kl} f(\Omega^l)p_{eq}(l)g(\Omega^k)p(kt|l0) \qquad (52)$$

where $p_{eq}(l)$ is the probability of configuration l at equilibrium and $p(kt|l0)$ is the conditional probability that if site l is occupied at time $t = 0$ site k will be occupied at time t, subject to the initial conditions

$$p(kt|l0) = \delta_{kl}, \ t = 0 \qquad (53)$$

$$\lim_{t\to\infty} p(kt|l0) = p_{eq}(k) \qquad (54)$$

It has been assumed that the probability of site i at time t $(p_i(t))$ satisfies the master equation

$$\frac{\partial p_i(t)}{\partial t} = \sum_{j=1}^{N} R_{ji}p_j(t) \qquad (55)$$

where R_{ji} is the exchange rate between site j and i. The correlation function can now be determined from the eigenvalue problem

$$\mathbf{RX} = -\lambda\mathbf{X} \qquad (56)$$

The correlation function is now given by

$$\langle f(\Omega(0))g(\Omega(t)) \rangle = \sum_{nlj=0}^{N-1} e^{-\lambda_n t}X_l^{(0)}X_l^{(n)}X_j^{(0)}X_j^{(n)}f(\Omega_l)g(\Omega_j) \qquad (57)$$
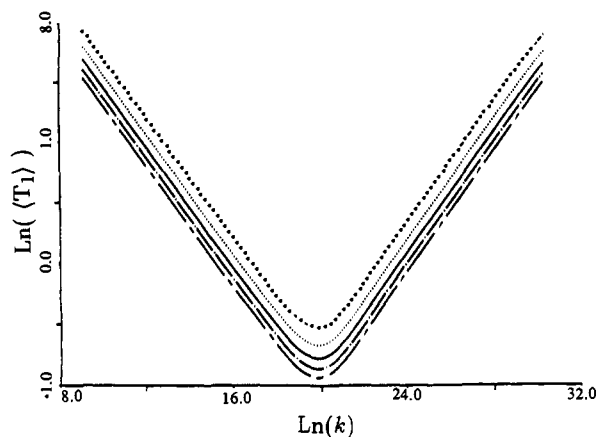
Figure 16. Variation of the powder average spin–lattice relaxation $\langle T_1 \rangle$, as a function of the jump rate k, for a two-site jump of equal site probabilities. All calculations are for the resonant frequency $(\omega_0/2\pi) = 76.75$ MHz and a quadrupolar coupling constant of QCC = 170 kHz. Relaxation curves for different angles of displacement θ_0 are shown: $6°$ (- -), $8°$ ($\cdot\cdot$), $10°$ (—), $12°$ (— $\cdot$), $14°$ (- - -).

where λ_n and X^n are the nth eigenvalue and eigenvector of the diagonalized $\mathbf{R}$ matrix, and Ω_j describes the orientation of site j.

In deuterium studies relaxation rates are often determined from quadrupole echo intensity. This so-called "powder average" is the spatial average of all orientations and neglects the anisotropic behavior of T_1 relaxation. The error introduced by this method is often small and the simplification in calculating T_1 expressions is significant. It is possible to take the explicit T_1 expression and determine the powder average by integration over all spatial orientations (either numerically or analytically). The same result can be obtained more easily if the averaging is taken into account in the original T_1 derivation. The effects on the correlation function $G_{aa'mm}(t)$ are easily determined

$$\langle \mathbf{D}^{(2)*}_{am}(\Theta(0)\Phi(0))\mathbf{D}^{(2)}_{a'm}(\Theta(t)\Phi(t)) \rangle = $$
$$\delta_{mm}\langle \mathbf{D}^{(2)*}_{a0}(\Theta(0)\Phi(0))\mathbf{D}^{(2)}_{a'0}(\Theta(t)\Phi(t)) \rangle \quad (58)$$

revealing that the spectral density is independent of m. In the case where the correlation function $G_{aa'mm}(t)$ has no time dependence (i.e. the crystal does not move with respect to the laboratory frame) the orthogonality relationship gives[35]

$$\int d(\Omega_{cl})\, \mathbf{D}^{L*}_{MN}(\Omega_{cl})\mathbf{D}^{l}_{mn}(\Omega_{cl}) = $$
$$((8\pi^2)/(2l + 1))\delta_{L,l}\delta_{M,m}\delta_{N,n} \quad (59)$$

such that only diagonal terms of $G_{aa'mm}$ survive, contributing a normalization factor of $1/5$. Inserting these results into eq 49 gives

$$C(t) = \frac{1}{5}\sum_{a=-2}^{+2} C_{aa}(t) \quad (60)$$

In this manner the powder average T_1 expressions can be quickly determined.

As a simple example, consider a 2-fold jump motion.[38] Using the relation between the Euler and spherical polar angles, $(\beta_{pc},\gamma_{pc}) = (\theta,\pi - \phi)$, where (θ,ϕ) are the spherical polar angles describing the orientation of the PAS V_{zz} tensor element in the crystal frame. The orientation of the PAS V_{yy} tensor element is specified by α_{pc}. For a two-site jump the orientations are described by $\theta_1 = \theta_0$ and $\phi_1 = 0°$ and $\theta_2 = \theta_0$ and $\phi_2 = 180°$,

with the equilibrium populations being $p_{eq}(1)$ and $p_{eq}(2)$. The interconversion is represented by the two rate constants

$$1 \underset{k_{21}}{\overset{k_{12}}{\rightleftharpoons}} 2 \quad (61)$$

The equilibrium populations must satisfy microreversibility producing

$$p_{eq}(1) = k_{21}/(k_{12} + k_{21})$$
$$p_{eq}(2) = k_{12}/(k_{12} + k_{21}) \quad (62)$$

The internal correlation function for a two-site jump is given by

$$C^{Jmp}_{aa}(t) = d^{(2)}_{0a}(\theta_0)d^{(2)}_{0a}(\theta_0)\Gamma^{Jmp}_{aa}(t) \quad (63)$$

where

$$\Gamma^{Jmp}_{aa}(t) = \langle \exp(ia\phi_0(0)) \exp(-ia'\phi_0(t)) \rangle \quad (64)$$

With eq 52, this correlation function is

$$\Gamma^{Jmp}_{aa}(t) = [p_{eq}(1) + (-1)^a p_{eq}(2)][p_{eq}(1) + $$
$$(-1)^{a'} p_{eq}(2)] + e^{-t/\tau_c}p_{eq}(1)p_{eq}(2)[1 - (-1)^a][1 - (-1)^{a'}] \quad (65)$$

with the correlation time τ_c being defined as $\tau_c = 1/k_{12} + k_{21}$. It is important to note that the only time-dependent terms of $\Gamma^{Jmp}_{aa}(t)$ that have nonzero diagonal elements are $a = a' = \pm1$, and $a = -a' = \pm1$. Full T_1 expressions have appeared in the literature (see eq 37 and Table 2 in ref 38) and will not be reproduced here. In the extreme narrowing limit ($\omega\tau_c \ll 1$), the relaxation expression becomes

$$\frac{1}{T_1} = $$
$$\left(\frac{3e^2qQ}{4\hbar}\right)^2 \tau_c p_{eq}(1)p_{eq}(2) \sin^2\theta_0(1 + 3\sin^2\Theta\sin^2\Phi) \quad (66)$$

The powder average expressions for a two-site jump are easily determined from eqs 63 and 64, where only the components with $a = a' = \pm1$ contribute to the spectral density. The internal correlation function reduces to

$$C^{Jmp}_{aa}(t) = \frac{3}{2}p_{eq}(1)p_{eq}(2)e^{-t/\tau_c}\sin^2 2\theta_0 \quad (67)$$

which yields the powder average relaxation expression

$$\left\langle \frac{1}{T_1} \right\rangle = \frac{2}{5}\left(\frac{3e^2qQ}{4\hbar}\right)^2 p_{eq}(1)p_{eq}(2)$$
$$\left[\frac{\tau_c}{1 + \tau_c^2\omega_0^2} + \frac{4\tau_c}{1 + 4\tau_c^2\omega_0^2}\right]\sin^2 2\theta_0 \quad (68)$$

Figure 16 shows $\langle T_1 \rangle$ relaxation for a two-site jump of equal site populations as a function of θ_0 and jump rate k. Utilizing these expressions the rate of motion can be determined from T_1 measurements.

The internal correlation function for an N equivalent site jump ($N \geq 3$) has also been obtained.[38] The orientations of the N sites are assumed to be $\theta_j = \theta = \beta_{pm}$ and $\phi_j = 2\pi j/N$, $j = 0, 1, ..., N - 1$. The rate constant

between site j and $j + 1$ is k. The internal correlation function is the same as in eq 63 with

$$\Gamma_{aa'}(t) = \exp\left[-4kt\ \sin^2\ (\pi a/N)\right] \qquad a \equiv a'(\text{mod } N)$$
$$= 0 \text{ otherwise}$$

$$(69)$$

A three site nearest neighbor jump model can describe the internal dynamics of a methyl group. For equal rates the correlation time τ_c is defined as $\tau_c = (3k)^{-1}$. The nonzero elements of the internal correlation function are

$$\Gamma_{aa'}^{Me}(t) = 1 \qquad a = a' = 0$$
$$= e^{-t/\tau_c} \qquad a = a' = \pm 1, \pm 2, \text{ and } |a - a'| = 3$$

$$(70)$$

The fact that the three-jump model $\Gamma_{aa'}^{Me}(t)$ is nondiagonal leads to nonexponential decay, a result of the T_1 expressions being dependent on both the angles Θ and Φ, while the line shape is a function of the angle Θ only. In general this nonexponential decay is difficult to observe experimentally and vanishes in the extreme narrowing limit. Full T_1 expressions have been presented earlier (see eq 39 and Table 2 of ref 38) and will not be reproduced here. In the extreme narrowing limit ($\omega \tau_c \ll 1$), the T_1 relaxation for a methyl group ($\theta = \beta_{pm} = 70.5°$) is still dependent on the angle of the orientation of the C_3 symmetry axis

$$\frac{1}{T_1} = \frac{4}{9}\left(\frac{3e^2qQ}{4\hbar}\right)^2 \tau_c(1 + \cos^2\Theta)$$

$$(71)$$

Powder average relaxation expressions are obtained recalling that only the diagonal terms ($a = a'$) contribute in the internal correlation function. The time-dependent terms of $C_{aa'}^{Me}(t)$ that survive are $a = a' = \pm 1$, ± 2. By utilizing eqs 58 and 61, the powder average relaxation expression $\langle T_1 \rangle$ becomes

$$\left\langle\frac{1}{T_1}\right\rangle = \frac{1}{8}\left(\frac{3e^2qQ}{4\hbar}\right)^2 [0.8\{\sin^4\theta + \sin^2 2\theta\}g(\tau_c,\omega_0) +$$
$$3.2\{\sin^4\theta + \sin^2 2\theta\}g(\tau_c,2\omega_0)] \quad (72)$$

where $g(\tau_c,\omega_0) = \tau_c/(1 + \omega_0^2\tau_c^2)$.

Powder average $\langle T_1 \rangle$ expression were obtained using the formalism of a N-site jump. The asymmetric four-site libration is described by the site orientations

$$\Omega_1 = (0,\theta_0,0) \qquad \Omega_2 = (0,\phi_0,90) \qquad \Omega_3 = (0,-\theta_0,0)$$
$$\Omega_4 = (0,-\phi_0,90)^{\cdot} \qquad (73)$$

If the equilibrium site populations are considered to be equal [$p_{eq}(i) = 0.25$], a global jump rate k defines the dynamics. Diagonalization of R_{ij} for an all-site jump results in the powder average relaxation shown in Figure 17 as a function of the jump rate k, the angles θ_0 and ϕ_θ, and the resonant frequency ω_0.

Expressions for T_1 relaxation involving more complicated models can be obtained following the same procedure. The effects of several distinct motions on the internal correlation function $C_{aa'}(t)$ can be obtained by following the multiaxis approach of Wittebort.[42] Recalling the definition of the internal correlation function given in eq 50, expressions for multiaxis models can be obtained by successive transformations of the Wigner rotation matrices.[43] Assuming that all internal motions are independent, the required internal corre-
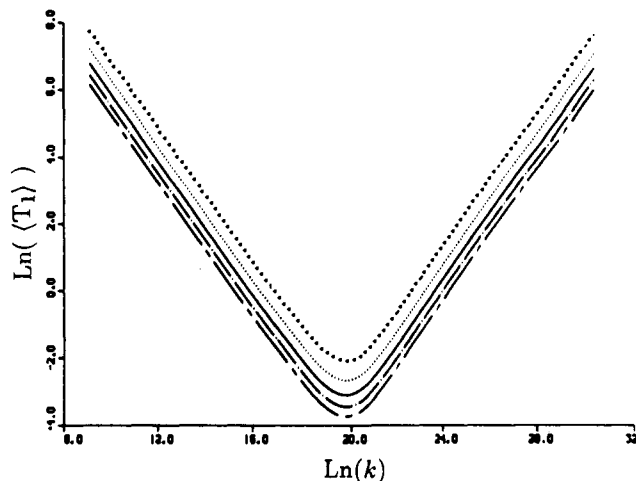

Figure 17. Variation of the powder average spin–lattice relaxation $\langle T_1 \rangle$, as a function of jump rate k, for a four-site libration with equal site probabilities. All calculations are for the resonant frequency of $(\omega_0/2\pi) = 76.75$ MHz and the quadrupolar coupling constant QCC = 170 kHz. Relaxation curves are presented for different amplitudes of displacement: $\theta_0 = 10°$, $\phi_0 = 5°$ ($\cdot\cdot$); $\theta_0 = 10°$, $\phi_0 = 10°$ ($-\cdot$); $\theta_0 = 10°$, $\phi_0 = 15°$ ($-\ -\ -$); $\theta_0 = 10°$, $\phi_0 = 20°$ ($-\ -$), and $\theta_0 = 10°$, $\phi_0 = 25°$ ($-$).

lation function $C_{aa'}(t)$ for n different motional frames is

$$\langle D_{0a}^{*(2)}(\Omega_{pc}(0))D_{0a}^{(2)}(\Omega_{pc}(t))\rangle =$$
$$\sum_{b_1 b'_1...b_n b'_n=-2}^{+2} \langle D_{0b'_1}^{*(2)}(\Omega_{p1}(0))D_{0b'_1}^{(2)}(\Omega_{p1}(t))\rangle \times$$
$$... \langle D_{b_n a}^{*(2)}(\Omega_{nc}(0))D_{b'_n a}^{(2)}(\Omega_{nc}(t))\rangle \quad (74)$$

where Ω_{p1} and Ω_{nc} are the Euler angles for the PAS to the first internal axis, and the nth axis to crystal transformation, respectively. This expression allows multiaxis motions of the methyl group in the labeled oligonucleotide to be addressed, but can be easily extended to describe motions at other sites if the appropriate correlation functions are used.

2.3.2 Models for Motion of the Helix

Accounting for helix motion within the oligonucleotide was accomplished with the internal correlation function $C^{Hlx}(\Omega(t))$ using eq 72, and restricting the evaluation of T_1 to powder pattern averaged expressions ($a = a'$). Here it is assumed that all motions are contained in the internal correlation function $C_{aa}(t)$. It can be shown that this is equivalent to taking the helix motion correlation function $C_{aa}^{Hlx}(\Omega(t))$ into consideration during the crystal to lab transformation. The internal correlation function is then factored into various individual terms and assuming these motions are uncorrelated the expression is

$$C_{aa}(t) = \sum_{b_1 b'_1...b_n b'_n=-2}^{+2} C_{b_1 b'_1}^1(\Omega_{p1}(t)) \times ... \times C_{b_n b'_n aa}^{Hlx}(\Omega_{nc}(t))$$

$$(75)$$

where Ω_{ij} represents the Euler angles for the i-to-j frame transformation, and Ω_{nc} represents the nth frame-to-crystal axis transformation. If the angles α_{nc}, β_{nc} are considered to be time independent, the helix motion is described by the time dependence of $\gamma_{nc}(t)$ and represents motion about the long axis of the oligonucleotide. The angles α_{nc}, β_{nc} lack time dependence, but are crucial in describing the orientation of the helix motions with

Figure 18. Variation of the powder average spin–lattice relaxation $\langle T_1 \rangle$, as a function of the helix diffusion constant D, for a multiaxis motion involving helix diffusion and a methyl three-site jump (see the text). All calculations are for a resonant frequency of $(\omega_0/2\pi)$ = 76.75 MHz, a quadrupolar coupling constant QCC = 159 kHz, and β_{mc} = 90°, unless otherwise specified. Relaxation curves are presented for different methyl jump rates: k = 9.8 × 10^{10} Hz (—); k = 9.8 × 10^{10} Hz, β_{mc} = 0° (· ·); k = 3.33 × 10^{10} Hz (– –), 3.3 × 10^9 Hz (— ·); k = 3.3 × 10^8 Hz (– – –).

respect to the previous frame.

As an illustration of a correlation function involving helix motion, consider the case of a methyl three-site jump in addition to an uncorrelated free diffusion motion about the long axis of the helix. The internal correlation function is given by

$$C_{aa}(t) = \sum_{bb'=-2}^{+2} (-1)^{b-b'} d_{0b}^{(2)}(\beta_{pm}) d_{0b}^{(2)}(\beta_{pm}) \Gamma_{bb'}^{Me}(t) d_{ba}^{(2)}(\beta_{mc}) \times$$
$$d_{ba}^{(2)}(\beta_{mc}) \Gamma_{aa}^{Hlx}(t) \quad (76)$$

where β_{pm} describes the angle between the PAS system and the C_3 symmetry axis of the methyl group, and β_{mc} describes the orientation of this symmetry axis to the helix axis. The correlation function $\Gamma_{bb'}^{Me}(t)$ is given by eq 70 while the helix motion with a diffusion coefficient D is given by the correlation function[43,44]

$$\Gamma_{aa'}^{Hlx}(t) = \delta_{aa'} \exp(-a^2 Dt) \quad (77)$$

In this example, setting the angle α_{mc} to zero places one site of the methyl motion parallel to the helix Z axis. Powder average relaxation $\langle T_1 \rangle$ as a function of the diffusion coefficient D and the methyl jump rate k are presented in Figure 18.

Another possible model is motion within a restricted potential in γ_{nc}

$$U(\gamma_{nc}(t)) = 0 \quad -\gamma_0 \leq \gamma_{nc} \leq \gamma_0$$
$$= \infty \quad \text{otherwise} \quad (78)$$

The correlation function has been discussed in detail elsewhere[42,45] and is given by

$$\Gamma_{aa'}^{Hlx}(t) = \sum_{n=0}^{\infty} \Gamma'_{aa'n}(\gamma_0) \exp(-Dn^2\pi^2 t/4\gamma_0^2) \quad (79)$$

where

$$\Gamma'_{aa'0}(\gamma_0) = \frac{\sin(a\gamma_0)\sin(a'\gamma_0)}{aa'\gamma_0^2} \quad (80)$$

$$\Gamma_{aa'n}(\gamma_0) =$$
$$[aa'\gamma_0^2[\cos(a\gamma_0)\cos(a'\gamma_0)(1-(-1)^n) +$$
$$\sin(a\gamma_0)\sin(a'\gamma_0)(1+(-1)^n)]]/$$
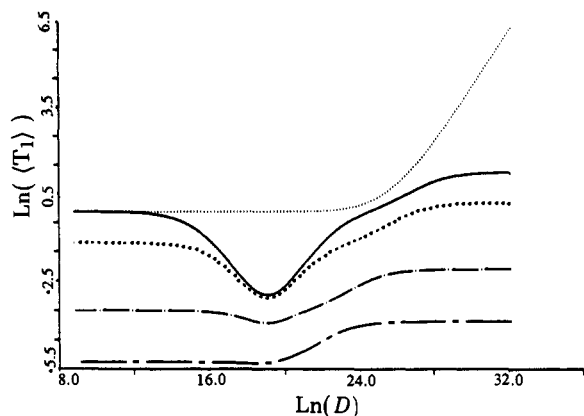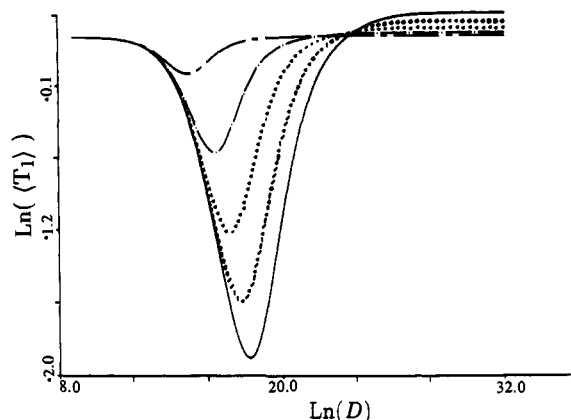$$[(a\gamma_0)^2 - (n\pi/2)^2][(a'\gamma_0)^2 - (n\pi/2)^2] \quad (81)$$

Figure 19. Variation of the powder average spin–lattice relaxation $\langle T_1 \rangle$, as a function of the helix diffusion constant D, for a multiaxis motion involving a restricted helix motion and a methyl three-site jump (see the text). All calculations are for a resonant frequency of $(\omega_0/2\pi)$ = 76.75 MHz, β_{pm} = 70.5°, β_{mc} = 90°, a three-site jump rate of k = 9.8 × 10^{10} Hz, and a quadrupolar coupling constant of QCC = 159 kHz. Relaxation curves are presented for different amplitudes of restricted helix motion γ_0: 6° (– – –), 12° (— ·), 18° (– –), 24° (· ·), 30° (—).

The series falls off as $1/n^2$ and the expression converges quickly, requiring only a limited number of terms in the infinite sum. To simulate restricted helix diffusion for a methyl-labeled dodecamer the correlation function given in eq 79 is substituted into eq 76. Figure 19 shows $\langle T_1 \rangle$ relaxation for a combined methyl group three-site jump and a restricted helix motion as a function of the diffusion rate D and the angle of maximum displacement γ_0.

The final model for helix motions is the collective torsional model developed by Schurr and co-workers.[46–49] This model treats the oligonucleotide as a linear array of N + 1 identical rods connected by Hookean springs opposing torsional and bending deformations. For short fragments of DNA, or in the case of oligonucleotides at low hydration levels, bending deformations can be neglected (i.e. setting any bending correlation function equal to 1). The exclusion of bending and tumbling may not be fully justified at high hydration levels. The internal correlation function for a three site jump methyl motion and collective torsional motion used for powder average $\langle T_1 \rangle$ relaxation calculations is given by

$$C_{aa}(\Omega_{pc}(t)) = \sum_{bb'=-2}^{+2} C_{bb'}^{Me}(t) C_{bb'aa}^{Tor}(t)$$

where the twisting correlation function is

$$C_{bb'aa}^{Tor}(t) = \exp(-i\alpha_{mc}(b-b')) d_{ba}^{(2)}(\beta_{mc}) d_{b'a}^{(2)}(\beta_{mc}) \Gamma_{aa}^{Tor}(t)$$
$$\Gamma_{aa}^{Tor}(t) = \langle \exp[ia(\gamma(t) - \gamma(0))] \rangle \quad (82)$$

As discussed earlier, the angles α_{mc}, β_{mc} describe the orientation of the helix axis with respect to the jump axis. Setting α_{mc} to zero corresponds to one of the jump sites in the methyl being parallel to the helix axis. In the previous two sections a methyl-jump motion was been used in conjunction with different helix motions, but other types of motions can be employed. A two-site jump or libration correlation function $C_{bb'}^{Lib}(t)$ or a combined methyl–libration correlation function could replace the methyl correlation function $C_{bb'}^{Me}(t)$. In the instance of a two-site jump, the angle α_{mc} = 0° or 90° orients the *direction* of the libration parallel or per-

pendicular to the helix Z axis, respectively. The angle $\beta_{mc} = 90°$ orients the C_3 symmetry axis perpendicular to the helix Z axis.

This torsional model was used previously to describe the internal dynamics in base-labeled oligonucleotides.[50] In that study a two site jump model and a torsional helix motion was used to describe the dynamics. Unfortunately, the transformation between the jump axis and the helix axis was overlooked. This omission corresponds to setting $\beta_{mc} = 0°$, placing the CD bond almost parallel to the helix axis (the Z axis of the two-site jump is parallel) and corresponding torsional motions. In this orientation, motion about the helix axis is not expected to have a major effect on relaxation. Similar observations have been noted for fluorescence depolarization and ^{13}C NMR.[51,52] This missing transformation stimulated Kintanar and co-workers to remove portions of the internal correlation function that can contribute to the spectral densities. The $\langle T_1 \rangle$ relaxation for the base and methyl group studies will be compared using the formalism presented below. The twisting correlation function for the mth subunit is given by

$$[\Gamma_{aa}^{Tor}]_m =$$

$$\exp\,(-a^2 D_\parallel t)\,\exp\,(-a^2[\sum_{l=2}^{n+1} d_l^2 Q_{ml}^2(1 - \exp\,(-t/\tau_l))]) \tag{83}$$

where

$$D_\parallel = k_B T/(N + 1)\gamma$$

$$\tau_l = \gamma/4\alpha\,\sin^2\left[(l - 1)\frac{\pi}{2}(N + 1)\right]$$

$$d_l^2 = k_B T/4\alpha\,\sin^2\left[(l - 1)\frac{\pi}{2}(N + 1)\right]$$

The parallel diffusion rate is represented by $D_\parallel$, τ_l corresponds to the relaxation time of the lth mode, and d_l^2 represents the mean displacement of the lth mode. The remaining symbols include the rotational friction factor γ, the torsional force constant α, the absolute temperature T, the Boltzmann constant k_B, and, finally, the transformation matrix Q_{ml}, which is given by

$$Q_{ml} = [2/(N + 1)]^{1/2}\cos\,[(m - 1/2)$$
$$(l - 1)\pi/(N +1)] \qquad l \geq 2 \tag{84}$$

The previous ^{2}H NMR relaxation studies that employed collective torsional modes utilized analytical expressions for the various time zones of the correlation function, but for sufficiently small subunit numbers, $N < 50$, direct use of the correlation function in eq 83 is possible. If the relaxing motion occurs at a time t sufficiently large $(t \gg \tau_2)$, the exponential terms in the sum of eq 83 will approach a limiting value and contribute to the scaling factor $B(\infty)$, while in the first term in Γ_{aa} contributes a single exponential decay. This time zone is call the uniform mode zone and the correlation function is given by

$$[\Gamma_{aa}^{Tor}(t)]_m = \exp\,(-a^2 D_\parallel t)[B_a(\infty)]_m \tag{85}$$

where

$$[B_a(\infty)]_m = \exp\,(-a^2[\sum_{l=2}^{N+1} d_l^2 Q_{ml}^2]) \tag{86}$$

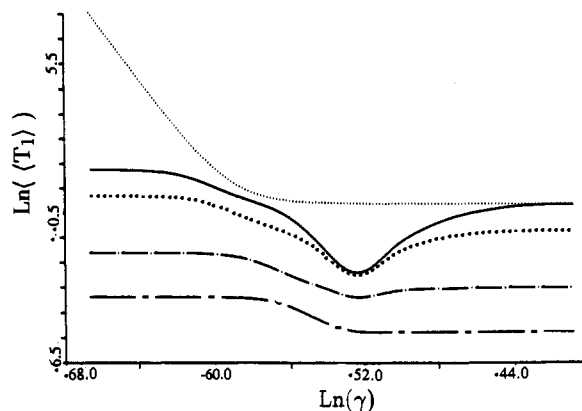For a small number of base units this expression can be obtained exactly and, for the dodecamer, presents

Figure 20. Variation of the powder average spin–lattice relaxation $\langle T_1 \rangle$, as a function of the friction factor γ, for a multiaxis motion involving a collective torsional motion and a methyl three-site jump (see the text). All calculations are for a dodecamer with a torsion constant $\alpha = 4.0 \times 10^{-12}$ dyn cm, a resonant frequency of $(\omega_0/2\pi) = 76.75$ MHz, $\beta_{pm} = 70.5°$, $\beta_{mc} = 90°$ (unless otherwise specified), and a quadrupolar coupling constant of QCC = 159 kHz. Relaxation curves are presented for different methyl three-site jump rate; $\beta_{mc} = 0°$, $k = 9.8 \times 10^{10}$ Hz ($\cdot\,\cdot$); $k = 9.8 \times 10^{10}$ Hz (—), $k = 3.3 \times 10^{10}$ Hz (- -), $k = 3.3 \times 10^9$ Hz (— $\cdot$), $k = 3.3 \times 10^8$ Hz (- - -).

no computational difficulty. For short oligonucleotides, higher torsional modes are not expected to contribute significantly and manifest themselves in a reduction of $B(\infty)$ and the residual amplitude of the uniform mode. The degree of this reduction depends on the value of the torsional spring constant considered, but in general was found to be $B(\infty) \geq 0.90$ for the range investigated. The small angular displacements of the higher modes allows the first exponential to be expanded

$$[\Gamma_{aa}^{Tor}(t)]_m = \exp\,(-a^2 D_\parallel t)\{1 - a^2\sum_{l=2}^{N+1} d_l^2 Q_{ml}(1 - \exp$$

$$(-t/\tau_l)) + 1/2(a^2\sum_{l=2}^{N+1} d_l^2 Q_{ml}(1 - \exp\,(-t/\tau_l)))^2 - ...\} \tag{87}$$

Figure 20 shows $\langle T_1 \rangle$ relaxation as a function of the methyl-jump rate and frictional constant.

3.0 Solid-State NMR Studies of DNA Dynamics and Structure

Having completed a review of the manner in which molecular dynamics affects the solid state NMR line shape and nuclear Zeeman relaxation rate, a review of the experimental implementation of these principles to the study of the internal dynamics and structure of DNA will be presented. Although sections 2.2 and 2.3 emphasized ^{2}H NMR, nuclei other than deuterium have been used as probes of dynamics and structure in high molecular weight DNA. Our review will address such work as well. The review of experimental work in this field will be divided into two sections. Section 3.1 will deal with the extensive literature consisting of solid state NMR studies of high molecular weight DNA. A number of groups have contributed to this field, and an effort has been made to cite as much of that literature as possible, while confining discussion to certain selected works. The interested reader is encouraged to consult the bibliography if further information is desired. Section 3.2 describes our own solid state NMR studies of the structure and dynamics of selectively labeled synthetic oligonucleotides.

3.1 NMR Studies of High Molecular Weight DNA

3.1.1 ^{31}P NMR Studies

Some of the earliest solid state NMR studies of DNA probed the conformation and dynamics of the phosphodiester backbone. Shindo and co-workers, for example, used the chemical shift anisotropy (CSA) of ^{31}P to study backbone conformation and dynamics of highly oriented Li–DNA fibers in the A, B, and C forms.[53] Those authors observed the ^{31}P line shape as a function of the orientation of the fiber axis relative to the magnetic field. At parallel orientations the spectra of A- and B-form DNA consisted of a single resonance in each case about 50 ppm wide at half the maximum intensity, while the spectrum of C-form DNA at parallel orientation spanned the entire range of ^{31}P chemical shifts (about 170 ppm). At perpendicular orientations DNA fibers in the A form displayed a somewhat broader resonance but fibers in the B form displayed a narrow resonance. At intermediate rotation angles (45°, for example), the spectrum of A form fibers was reminiscent of a powder pattern while B-form fibers displayed a broadened, featureless resonance. In general A-form fibers were equilibrated at 79% RH and B-form fibers were equilibrated at about 98% RH.

The authors analyzed these line shapes in the following way. The chemical shift tensor in the PAS, A_p, was related to the tensor in the frame of the goniometer by a series of frame transformations:

$$A_g = R_m^{-1}R_d^{-1}R_p^{-1}A_pR_pR_dR_m \qquad (88)$$

R_p transforms the tensor from the PAS to a molecule-fixed frame, while R_m transforms the tensor into the frame fixed to the goniometer. The transformation R_d describes misalignment of the fiber and consists of an rotation from an intermediate molecular frame M′ to the molecular frame M. Of the three Euler angles (α, β, γ) which locate the CSA tensor β and γ are determined by phosphodiester coordinates which the authors obtained from Landridge et al.[54] for B-form DNA or from Arnott and Hukins[55] for A-form DNA. Thus the chemical shift frequency δ_{zz} corresponding to a fiber rotation angle Φ was determined to be dependent on α and two angles ϕ and θ which described the fiber misalignment:

$$\delta_{zz}(\alpha,\phi,\theta) = 1/2[A_g(1,1) + A_g(2,2)] + 1/2[A_g(1,1) - A_g(2,2)] \cos(2\Phi) + 1/2[A_g(1,2) + A_g(2,1)] \sin(2\Phi) \qquad (89)$$

Calculated spectra for A- and B-form fibers predicted a broad doublet at 90° orientation, a singlet at 0°, and a triplet at 45°. Experimental data, however, did not display a doublet at perpendicular orientations but rather a singlet which was particularly evident for B-form fibers. The authors attributed this discrepancy to rapid molecular rotation aboutt he helix axis which would be especially effective in narrowing the resonance of highly hydrated B-form fibers. The authors went on to address certain questions concerning the B-form spectra: (i) why was the parallel spectrum so broad (~41 ppm), (ii) why was the perpendicular spectrum narrower than the parallel by 10 ppm? The first question was addressed by assuming that the orientation of the DNA varied either due to lack of truly parallel alignment between the fibers, lack of orienta-

tion of the DNA molecules relative to the fiber axis, or both. The authors attributed the difference between the parallel and perpendicular line widths as due to a distribution of phosphodiester group orientations with DNA and claimed that a difference of 9 ppm in observed line widths could be accounted for by a variation in the angle β of about ±7°.

Rupprecht and co-workers have reported a number of NMR studies of highly oriented DNA fibers.[56] In particular, those workers reported a ^{31}P NMR study of oriented fibers of calf thymus DNA in the A form which challenged the conclusions of the Shindo study.[53] Rupprecht and co-workers acquired proton-enhanced ^{31}P spectra at a variety of temperatures and goniometer rotation angles. Spectral simulations agreed with experimental spectra if the following assumptions were made: (i) no motional averaging of the ^{31}P chemical shifts, (ii) the orientation of the ^{31}P chemical shift anisotropy tensor as reported by Kohler and Klein[138] was assumed, (iii) samples of oriented DNA were considered to be composed of crystallites which are oriented relative to one another such that their dispersion about the experimentally determined zero angle is Gaussian with standard deviation between 2° and 10°, and (iv) the intrinsic line width for fibrous A-form DNA was assumed to be about 0.5–1.0 kHz (5–10 ppm). Given these assumptions, Rupprecht and co-workers concluded that the backbone of A-form DNA forms a rigid lattice and that the structure of the phosphodiester backbone is regular in structure.

Recent ^{31}P NMR studies by Harbison and co-workers[57] of oriented films of salmon sperm DNA report similar line shapes to those obtained previously by Shindo et al.[53] and Nall et al.[56] Those authors used magic angle spinning (MAS) techniques to determine the orientational distribution function $P(\chi,\phi,\psi)$ of the ^{31}P CSA tensor. The position of the maximum in $P(\chi,\phi,\psi)$ was centered at $\chi = 65°$, $\phi = 62°$, in good agreement with the studies of Nall et al. and Shindo et al. The authors concluded that although the phosphate backbone orientation is consistent with the fiber diffraction models of Arnott and Hukins,[55] heterogeneity of both the isotropic chemical shift and CSA tensor orientation occurs.

Another interesting example of the application of solid-state ^{31}P NMR spectroscopy to the study of DNA structure and dynamics has been reported by Rill and co-workers who have studied a variety of mesomorphic phases formed by DNA at high concentrations.[58] The paper by Strzelcka and Rill is an experimental study of the isotropic to cholesteric transition of DNA in which the authors use polarizing microscopy and solid-state ^{31}P NMR to characterize the phase diagram. Using polarizing microscopy, those workers found samples with concentrations of 130, 137, 145, and 150 mg/mL to be biphasic over the 20–70 °C range examined. The two lowest concentration samples were highly viscous and appeared transparent. Microscopic examination revealed trace amounts of cholesteric phase as small spherulites, and samples with concentrations of 157 and 164 mg/mL were liquid crystalline up to 44° and 56°, respectively.

Solid-state ^{31}P NMR was used to study the 157 and 165 mg/mL samples. At room temperature the ^{31}P resonance was symmetric and broader than expected

for an isotropic sample, but narrower than a powder pattern. Upon heating, a sharp resonance appeared on the downfield side of the broad resonance. This sharp resonance was due to the appearance of the isotropic phase. The asymmetric disposition of the isotropic phase resonance relative to the cholesteric phase resonance indicates that the latter phase is magnetically ordered, a fact which was confirmed by polarizing microscopy. Because the integrated areas of the resonances are proportional to the number of molecules in the isotropic and cholesteric phases, the phase diagram can be established from ^{31}P NMR spectra obtained from samples of varying concentration.

The phase diagram calculated for 146 base pair DNA at a Na^+ activity of 0.21 was found to be in qualitative agreement with the predictions of Flory theory[59] and the observed behavior of rodlike, nonelectrolyte polymers. There is a narrow region of coexistence of the isotropic and cholesteric phases, and the phase boundary is weakly temperature dependent. In general, the diagram compares well to the repulsive region of the phase diagram for rodlike molecules with axial ratio of 20 as predicted by the theory of Warner and Flory.[60]

Thus far our review of ^{31}P NMR has revealed general features of the backbone structure of DNA fragments oriented in fibers and the nature of the isotropic–cholesteric phase transition in samples of hydrated DNA, but little specific information on the nature of the internal dynamics of polynucleoides. Early solid-state NMR studies of the internal dynamics of DNA were reported by Opella and co-workers who used ^{2}H and ^{31}P NMR to study the dynamics of high molecular weight DNA. DiVerdi and Opella[61] studied high molecular weight calf thymus DNA in the B form as a function of temperature using deuterium NMR. Those workers deuterated DNA by exchanging the H8 protons of the purine bases. This study found that although ^{31}P NMR shows nonaxial averaging of the ^{31}P CSA tensor at rates $>10^4$ Hz, little or no averaging of the ^{2}H powder pattern occurred, causing the authors to conclude that large amplitude motions of the bases do not occur at nanosecond time scales. Those authors observed that the nonaxial ^{31}P line shape precluded the fast, axial motion proposed by Shindo and co-workers[53] for B-form DNA in fibers.

Another example of the application of ^{31}P NMR to the study of DNA dynamics has been reported by Mai et al.[62] Those authors studied the ^{31}P line shape, spin–lattice relaxation, and ^{31}P–H NOE of high molecular weight calf thymus DNA fragments as a function of hydration level and observed that the motional narrowing of the ^{31}P powder pattern generally increases with hydration level, beginning with low amplitude, high frequency ($>10^4$ Hz) motions at low hydration levels. At about 85% relative humidity the transition from A to B form occurs with a sudden decrease in line width which the authors attribute to fluctuations of the backbone of at least $\pm30°$ at a minimum frequency of 10^4 Hz. No detailed motional model was proposed.

3.1.2 ^{15}N and ^{13}C NMR Studies

Besides solid-state ^{31}P NMR spectroscopy, both ^{13}C and ^{15}N NMR have been demonstrated to be useful in the study of DNA structure and dynamics. For example, Opella and co-workers have uniformly ^{15}N labeled

DNA by growing *Escherichia coli* on a medium with ^{15}NH$_4$SO$_4$ as the sole source of nitrogen.[63] The DNA extracted from the bacteria was primarily in the form of 6800 base pair duplex viral replicative intermediate. Using proton-enhanced ^{15}N MAS spectroscopy at a Larmor frequency of 40 MHz, the authors reported 15 well-resolved lines resulting from the chemically distinct nitrogen nuclei of DNA. Two-dimensional ^{15}N–^{15}N NMR spin-exchange experiments performed for mixing times of 2, 4, and 6 s showed variations in cross peak intensity, and the spectrum was further simplified by using the heteronuclear dipolar coupling between ^{15}N and protons as a selection mechanism. Cross peaks between ^{15}N nuclei without bonded protons were selected in this way. With this approach the authors proposed studying the structure of DNA fragments much larger than the DNA oligomers currently under study by high-resolution NMR methods.

Harbison and co-workers[57] have determined DNA sugar ring puckering using solid state ^{13}C NMR spectroscopy. From a series of model nucleotides and nucleosides those authors correlated the ^{13}C chemical shift with deoxyribose ring conformation and found that 3'-endo conformers have 3'- and 5'-chemical shifts significantly upfield (5–10 ppm) from comparable 3'-exo and 2'-endo conformers. These trends appeared to be maintained in high molecular weight calf thymus DNA with ^{13}C chemical shifts confirming that A-form DNA is primarily 3'-endo and both B- and C-form DNA are largely 2'-endo.

3.1.3 ^{2}H NMR Studies

Following early ^{2}H NMR studies of DNA by Opella and co-workers[61] and James and co-workers,[64] the first attempt to quantitatively model the ^{2}H dynamics of DNA was reported in a series of papers by the Kearns and Vold groups.[65-69] This work has involved ^{2}H NMR studies of hydrated samples of randomly oriented calf thymus DNA[66] as well as ^{2}H NMR studies of oriented DNA fibers.[65,67-69] The latter studies have been performed in collaboration with the Rupprecht group.

^{2}H NMR studies of the effects of hydration were reported for calf thymus DNA deuterated at the A8 and G8 positions.[66] The results of this study are summarized in Table I. Samples of Li–DNA and Na–DNA were hydrated over appropriate saturated salt solutions to produce the relative humidities given in Table I. ^{2}H NMR spectra and relaxation times were recorded at 38.4 and 76.8 MHz. An example of the ^{2}H NMR spectrum of Li–DNA is given in Figure 21, which was obtained at a frequency of 38.4 MHz from a sample equilibrated at 66% RH. For this spectrum, simulation yields a QCC$_{eff}$ of 173 $\pm$ 1 kHz and an asymmetry parameter η_{eff} of 0.065 $\pm$ 0.010. Comparable values for dry, oriented Li–DNA are QCC$_{eff}$ = 179 $\pm$ 1 kHz and η_{eff} = 0.06 $\pm$ 0.01. As shown in Figure 22, at higher relative humidities the amplitude of the quadrupolar echo was diminished and the spectrum narrowed.

The most complete set of ^{2}H spin–lattice relaxation data vs W were obtained for Li–DNA samples.at 25 °C and are displayed in Figure 23, along with the ^{31}P T_1 data reported by Mai et al.[62] Li–DNA is reported to remain in the B form down to hydration levels of 23% RH at $W \approx 1.4$ the T_1 was found to be about 7 s. Between W = 5 and W = 6 T_1 dropped steeply. Further

TABLE I. Deuterium Quadrupole Splittings and Relaxation Rates of Randomly Aligned DNA with Na^{+} or Li^{+} as Counterion[c]

% RH	W (mol of H_2O/ mol of nucleotide)	38.4 MHz		76.8 MHz		T_1(76.8 MHz)/ T_1(38.4 MHz)
		δ, kHz	T_1, s	T_1, s	T_{2e}, μs	
			Li–DNA			
0	1.4	126 ± 2		7.3 ± 1.4		
6	2.8			4.2 ± 0.5		
35	4.5	123 ± 2		2.0 ± 0.2		2.3 ± 0.3
52	6.3			0.62 ± 0.08	256 ± 25	
66	7.7	122 ± 2	0.20 ± 0.01	0.38 ± 0.02	245 ± 42	1.9 ± 0.2
75	9.8	122 ± 2	0.15 ± 0.01	0.26 ± 0.01	271 ± 24	1.7 ± 0.2
75	9.8[a]			0.22 ± 0.02		
75	10.0[b]			0.26 ± 0.03		
84	12.1	119 ± 2	0.09 ± 0.02	0.20 ± 0.01	193 ± 17	2.2 ± 0.5
88	19.7			0.068 ± 0.01	124 ± 33	
92	22.6			0.062 ± 0.01	132 ± 16	
			Na–DNA			
66	7.2			0.30 ± 0.02		
75	8.4			0.27 ± 0.03		
84	9.8			0.21 ± 0.04		
92	20.8			0.045 ± 0.006		

[a] Measured at 30 °C. [b] Lyophilized DNA. [c] Measurements were performed at 25 °C and various levels of hydration. Reprinted with permission from ref 66, copyright 1986 American Chemical Society.

Li–DNA at 66% RH

Frequency (kHz)
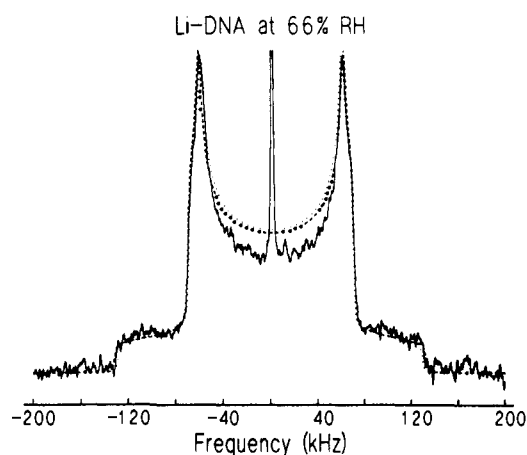
Figure 21. 38.4-MHz deuterium quadrupolar echo spectrum of Li–DNA at 66% RH and 25 °C. The spectrum was obtained with 64 000 scans using 2-μs 90° pulse times and a 2-kHz Gaussian broadening was applied to the free induction decay. Theoretical powder patterns were calculated assuming θ_0, ϕ_0 = 6°, 10° (—) and θ_0, ϕ_0 = 10°, 14°. The central narrow line is due to deuterium in the water of hydration (reprinted from ref 66; copyright 1986 American Chemical Society).
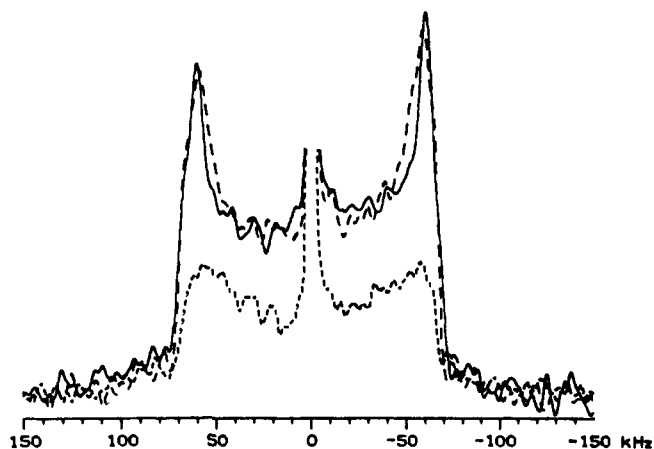
Figure 22. Deuterium quadrupolar echo spectra of Li–DNA equilibrated at 75% (—), 84% (- -), and 88% RH (- - -) recorded at 76.8 MHz and 25 °C using 4-μs 90° pulse times (reprinted from ref 66; copyright 1986 American Chemical Society).

T_1 (s)

w (mol H_2O / Nucleotide)
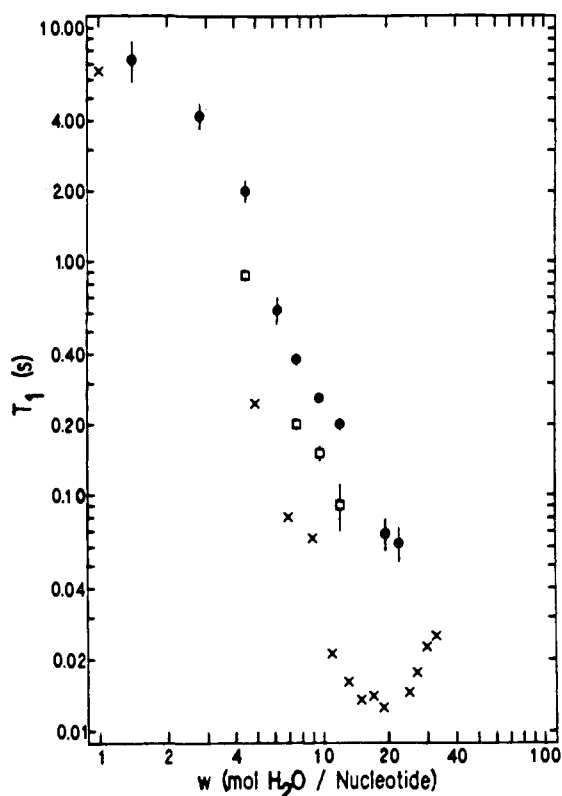
Figure 23. Deuterium spin–lattice relaxation times T_1 as a function of hydration level W. The solid circles (●) were measured at 76.8 MHz and the open squares (□) at 38.4 MHz for Li–DNA. The crosses (×) represent [31]P T_1's obtained from Table 1 of ref 62, divided by 20 for ease of comparison. Since the driest of the samples still contained some water, it has been assumed to contain one H_2O per nucleotide (reprinted from ref 66; copyright 1986 American Chemical Society).

increase in hydration resulted in a monotonic decrease to $T_1 \approx 62$ ms at $W = 22$.

To explain the decrease in QCC, the authors assumed that all librational motions were in the fast regime compared to the width of the powder pattern. Then the spectrum can be simulated using an appropriate fast regime model. The authors chose as a starting point for modeling the restricted motion of C–D bonds, the

diffusion-in-a-cone model. This model yields the expression for the effective QCC: $QCC_{eff} = QCC_{static} \cdot S_{zz}$, where the uniaxial order parameter is defined as $S_{zz} = 1/2(\cos \theta_0)(1 + \cos \theta_0)$ and θ_0 is the half angle of the cone. Application of this model to the observed decrease in QCC from 0% RH to 84% RH yields $S_{zz} = 0.968$ and $\theta_0 = 12°$ at 66% RH and $S_{zz} = 0.944$ and $\theta_0 = 16°$ at 84% RH.

A more realistic model proposes that the C–D bonds undergo restricted diffusion in two perpendicular planes, one of which is the purine base plane (for further discussion of the effect of continuous dynamics models on the ^{2}H line shape, see section 2.2.2). The frequency of a quadruplanar isochromat is then given by:[65]

$$\nu = \pm(3/4)QCC_{static}[(1/2) \times (3 \cos^2 \beta - 1)f(\eta,\theta_0) - (1/2)(\sin^2 \beta \cos 2\gamma)g(\eta,\theta_0,\phi_0)] \quad (90)$$

where

$$f(\eta,\theta_0) = \left[1 - \eta - (3 + \eta)\frac{\sin 2\theta_0}{2\theta_0} \right] \quad (91)$$

and

$$g(\eta,\theta_0,\phi_0) = \frac{1}{4}\left(\frac{\sin 2\phi_0}{2\phi_0} \right)\left[3(\eta - 1) - (3 + \eta) \frac{\sin 2\theta_0}{2\theta_0} \right] \quad (92)$$

In the above equations β is the angle between the DNA helix axis and the magnetic field, γ is the angle of rotation of the CD vector around the DNA helix axis, η is the static asymmetry parameter, and the CD bonds are assumed to fluctuate over the intervals $(-\phi_0, +\phi_0)$ and $(90° - \theta_0, 90° + \theta_0)$. Simulations using this model are given in Figure 21 for $\theta_0, \phi_0 = 6°, 10°$ (dashed line) and $\theta_0, \phi_0 = 10°, 14°$ (dotted line), and these simulations appear to bracket the experimental data. Therefore best estimates of the motion of the purine base planes at 66% RH are $\theta_0 = 8° \pm 2°$ and $\phi_0' = 12° \pm 2°$.

The T_1 data in Table I impose the condition T_1 (76.8)/T_1 (38.4) = 2.0 ± 0.4. Assuming that the motions under consideration occur in the fast regime relative to the time scale of the [2]H Larmor frequency, the spin-lattice relaxation rate is given by eq 42. The spectral densities $J_1(\omega_0)$ and $J_2(\omega_0)$ depend upon the orientation between the CD bond and the magnetic field, thus:[70]

$$J_M(M\omega_0,\beta) = \sum_{N=-2}^{+2} J_N(M\omega_0,0)[d_{NM}^{(2)}(\beta)]^2 \quad (93)$$

The authors then attempted to fit their relaxation data using a cone diffusion model. (For further discussion of the effect of continuous and discrete motions on the Zeeman relaxation rate, see section 2.3.1.) For cone angles less than 60°, $J_N(M\omega_0,0)$ is given by[69]

$$J_N(M\omega_0,0) = C_N\frac{6b_N/D_R}{1 + (M\omega_0)^2(b_N6/D_R)^2} \quad (94)$$

where D_R is the rotational diffusion constant from which a correlation time $\tau_N = b_N/D_R$ is defined and C_N are the amplitudes of the appropriate correlation functions. Using eqs 92–94, the authors found it im-

possible to find any values of cone correlation times that satisfy the constraint T_1 (76.8)/T_1 (38.4) = 2.0. The authors suggested that collective torsional models may offer an alternative to diffusion models (see section 2.3.2).

^{2}H NMR relaxation and line shape studies of A-form and B-form DNA in oriented fibers have also been reported.[65] Vold et al. reported a study of ^{2}H line shape as a function of hydration at a resonance frequency of 38.4 MHz for oriented high molecular weight calf thymus DNA. Using the continuous libration model described in eqs 90–92, the authors estimated librational amplitudes of $\phi_0 = 13° \pm 2°$ and $\theta_0 = 10° \pm 2°$ for B-form DNA at 66% RH.

Shindo, Torchia, and co-workers also reported a ^{2}H NMR study of oriented fibers of salmon sperm DNA.[71] The authors observed that the QCC derived from the ^{2}H spectrum of randomly oriented DNA samples was about 5.0 kHz smaller than in model compounds and simulated this reduction in QCC using a four-site discrete jump model (see section 2.2.1) deducing motional amplitudes of 8.1° and 8.9°. Like Vold and co-workers, a drastic drop in T_1 was observed at higher hydration levels, and the authors sought to simulate this trend using the T_1 expression for cone diffusion derived by Torchia and Szabo.[38] The cone angle θ_0 was assumed to be the average of the four-site fluctuation angles: 8.5°. Two solutions for the correlation times were obtained: 2.5×10^{-10} and 3.6×10^{-8} s, but only the longer value was consistent with the strong field dependence of T_1. The spin–lattice relaxation was measured at two frequencies: 38.5 and 76.8 MHz with a reported ratio of 2.9, somewhat larger than that reported by the Vold and Kearns groups. Shindo et al. also failed to simulate the field dependence of T_1 with a simple cone diffusion model.

On the basis of a line shape analysis applied to spectra obtained from oriented DNA fibers, it was determined that the purine base planes of the A form of DNA were tilted about 70° relative to the helix axis, and although the orientation of purine base planes in B-form DNA varied significantly, they were on the average perpendicular to the helix axis. In contrast to the 79% RH DNA powder patterns, at 92% RH the ^{2}H spectrum could not be simulated using fast motion limit models alone. Shindo et al. observed that only the perpendicular components of the powder pattern have significant intensity and interpret this fact as indicating that the DNA molecule undergoes rotation about the helix axis with a correlation time in the intermediate range (10^{-4}–10^{-7} s). The authors sought to simulate the effect on the line shape of a restricted rotation about the helix axis with an N-site jump model (see section 2.2.1). It was found that a maximum rotation amplitude of 150°, i.e. root-mean-square (rms) fluctuation for each jump Φ_{rms} of at least 30°, was required to simulate the observed 92% RH DNA spectrum, at a jump rate on the order of $(2 \pm 1) \times 10^6$ s^{-1}, which is approximately equal to $\omega_Q/2\pi$. Restricted diffusion about the helix axis does not account for the precipitous drop in T_1 which occurs at higher hydration levels, however. To simulate the decrease in T_1 which occurs for hydration levels over 79% RH the rms amplitude of the four-site jump is increased to 13.5° and the correlation time is decreased to $\tau_c = 1.5 \times 10^{-8}$ s.

TABLE II. Experimental Spectral Densities for Solid Li-DNA°

% relative humidity	librational amplitudes		ω_0 = 38.4 MHz			ω_0 = 76.8 MHz			frequency dependence		
	tilt θ_0, deg	twist ϕ_0, deg	$J_1(\omega_0)$, ps	$J_2(2\omega_0)$, ps	J_1/J_2	$J_1(\omega_0)$, ps	$J_2(2\omega_0)$, ps	J_1/J_2	J_1^{lo}/J_1^{hi}	J_2^{lo}/J_2^{hi}	J_1^{hi}/J_2^{lo}
35	7 ± 2	10 ± 2	1.2 ± 0.1	0.28 ± 0.06	4.3 ± 1.0						
66	10 ± 2	12 ± 2	6.1 ± 0.3	1.4 ± 0.1	4.4 ± 0.4	2.8 ± 0.1	0.50 ± 0.05	5.6 ± 0.6	2.2 ± 0.1	2.8 ± 0.3	2.0 ± 0.2
75	12 ± 2	13 ± 2	8.6 ± 0.4	2.6 ± 0.3	3.3 ± 0.4	4.2 ± 0.1	0.93 ± 0.08	4.5 ± 0.4	2.0 ± 0.1	2.8 ± 0.4	1.6 ± 0.2
84	15 ± 2		16.0 ± 1.2	8.4 ± 1.2	1.9 ± 0.3						

° Reprinted with permission from ref 67, copyright 1988 Academic Press.

Studies of static disorder and librational motions[67] and conformation[68] in films of oriented Li–DNA and Na–DNA have also been performed by Vold and Kearns in collaboration with the Rupprecht group. The authors used ^{2}H NMR line shape analysis to measure static base tilts as well as anisotropic motional amplitudes as a function of hydration and temperature in oriented DNA films. At a hydration level of $W = 10$ (about 80% RH) the tilt angle is close to zero with a distribution of tilt angles about this mean which cannot exceed 9°. A slightly greater distribution is observed at lower hydration levels with the average base tilt being about 23° at 75% RH. Amplitudes for tilting motions are dependent on hydration and range from 4° for the driest and 15° for the wettest samples, with slightly larger amplitudes observed for twisting motions. The tilting motion is suppressed at low temperature while the twisting appears independent of temperature.

Studies of T_1 and T_{1Q} at 38.4 and 76.8 MHz have enabled a measurement of the spectral densities $J_1(\omega_0)$ and $J_2(2\omega_0)$ as a function of field[69] (see section 2.3, in particular eqs 42 and 43). Results of that study are displayed in Table II. A comparison of J_1 and J_2 at two fields shows that J_1 is inversely proportional to the Larmor frequency. Although J_2 depends more strongly on field, perhaps as $\omega^{-3/2}$, neither the J_1 nor the J_2 frequency dependence is strong enough to be due to diffusive motion, which in the range of relaxation rates encountered here should be proportional to ω^{-2}. In fact it is clear from the data in Table II that J_1 is greater than J_2 in all cases. For the three driest samples, the ratio of J_1/J_2 falls in the range 3.3–5.6, dropping to 1.9 ± 0.3 at 38.4 MHz and 84% RH. Defining β at including the angle between the base normal and the helix axis and the angle between the helix axis and the magnetic field, the authors show that the following relation holds between the correlation functions of interest for small β:

$$C_1(t)/C_2(t) = \beta^2 \qquad (95)$$

Thus for $\beta \leq 22°$, the ratio of the correlation functions must be less than 0.14. Although the ratio of J_1 and J_2 does not obey such a simple relationship, at the sample orientation used in the study, the authors argue that the ratio of J_1 to J_2 must be substantially less than one for torsional motions occurring about the base pair plane normal. Because at the three lowest degrees of hydration the ratio is substantially greater than one, in-plane torsions are not considered to contribute substantially to the relaxation of these samples, although the decreasing trend of the ratio as hydration is increased indicates that contributions from torsional motions may be on the increase. Other motional models

including diffusion-in-a-cone were considered, but a satisfactory fit to the data was not achieved.

3.2 Internal Dynamics of Synthetic Oligonucleotides

In the last section the literature describing solid-state NMR studies of the internal dynamics and structure in high molecular weight DNA was reviewed. In summary, numerous investigations of DNA base dynamics and backbone dynamics have detected the occurrence of significant internal motions which increase in amplitude and rate as hydration is increased. However, the exact nature of these motions remains a point of controversy. In this section, ^{2}H NMR studies of the internal dynamics of specifically labeled oligonucleotides will be described. Before proceeding with the review, however, it is reasonable to discuss the motivation for studying the internal dynamics of DNA oligomers.

NMR studies of DNA reviewd thus far have involved samples of uniformly labeled, high molecular weight DNA. Such work, while capable of elucidating general dynamic properties of purine bases or the phosphodiester backbone, cannot define the localized dynamics at specific points in the DNA sequence. In fact, the sequence dependence of internal DNA dynamics has not been addressed by any of the studies reviewed thus far. To address the question of the sequence dependence of local DNA structure and dynamics, or to investigate the perturbation of local dynamics or structure produced by the site-specific binding of a drug or a regulatory protein, the same sample control that has been exercised in X-ray crystallography and high-resolution two-dimensional NMR must be exercised in solid-state NMR studies: DNA oligomers of known sequence and length must be synthesized.

The study of specifically labeled DNA oligomers has additional advantages. Synthetic protocols exist for introducing deuterium nuclei at a number of sites in the furanose rings and at the 5'-methylene group, in addition to a number of sites in the purine and pyrimidine bases, thus allowing the study of specific points outside the base region. The internal dynamics of short DNA oligomers may be somewhat simpler than the dynamics of high molecular weight DNA. We have already reviewed the complex nature of the collective torsional motions which some have claimed may dominate the Zeeman relaxation of deuterium-labeled DNA at high hydration levels. However, as explained in section 2.3.2, the amplitudes and rates of collective torsional modes are length dependent. As the length of the DNA decreases, torsional dynamics approach the rigid rod limit,[72] which is reasonably straightforward to treat.

Clearly, the dynamic and structural properties of synthetic DNA oligomers merit study by solid-state NMR.

However, which DNA sequence should be selected for study? A natural choice would be a sequence which has been studied by other structural methods such as high resolution NMR or X-ray crystallography. A brief survey of the literature offers an obvious candidate: the DNA dodecanucleotide [d(CGCGAATTCGCG]₂. This self-complementary dodecamer contains the *Eco*RI restriction endonuclease recognition site, d(GAATTC), and has been extensively studied in both the liquid and crystalline states. The sequence was the first oligonucleotide crystallized in the B form, and has been the subject of several X-ray diffraction investigations.[73–77] Information on the dynamics and local mobility within the crystal have been obtained from isotropic thermal factors[78] and segmented rigid body analysis.[79] Studies of the geometry of the hydration sphere have also been performed.[80,81]

The sequence [d(CGCGAATTCGCG)]₂ has also been investigated using high-resolution two-dimensional NMR.[82] A solution structure has been obtained from NOE data using distance geometry methods,[83] and a preliminary investigation of sugar conformation has also been reported.[84] These X-ray and NMR studies have sought to elucidate the structural basis of the specific interaction between the sequence d(GAATTC) and the restriction enzyme, so before describing solid state NMR studies of the internal dynamics and structure of the DNA dodecamer, a brief background on the restriction endonuclease will be provided.

Deoxyribonucleic acid type II restriction endonucleases and modification methylases are host-specific enzymes that act as barriers for interstrain transfer of DNA between cell lines. Foreign DNA is subjected to rapid endonucleolytic hydrolysis, to produce 3′-hydroxyl and 5′-phosphoryl termini, if it does not contain the characteristic DNA modification of that particular strain. The modification enzyme catalyzes the methyl transfer from *S*-adenosyl-L-methionine (AdoMet) to a DNA sequence specific for that host. This methylation of a DNA site is also recognized by the restriction enzyme and renders the cellular DNA resistant to endonuclease activity.[85]

The *Eco*RI endonuclease exists in solution as an equilibrium mixture of dimer and tetramer proteins. For activity in vivo, type II endonucleases require only Mg²⁺ ion and unmodified DNA. The restriction activity results from the enzyme introduction of two staggered single-strand breaks. The methyl modification of the restriction site at the exocyclic amino group yields N-6 methyladenine. The continued activity of the methylase enzyme is required to insure viability of the cell. The modification enzyme is functional as a monomer. This observation has led to the suggestion that the mechanism of endonuclease and methylase recognition differ.[85] Besides the site specific recognition by the *Eco*RI endonuclease, the enzyme also binds nonspecifically without hydrolysis. This has prompted investigation into the hypothesis of the nonspecific complex diffusing along the DNA to enhance the rate of formation for the site-specific complex.[86,87]

Chemical modification and base substitution studies have led to a qualitative assessment of contacts important in endonuclease and methylase activity. Contacts with the methyl group of the thymidine are important in the recognition of the methylase enzyme, but have a reduced effect on the endonuclease activity. Contacts with the adenine and guanine bases also influence the site-specific interactions. Recent studies into the energetics of specificity for the *Eco*RI endonuclease recognition have proposed the formation of an activated complex.[68] These investigations also reveal

$$E + DNA \rightleftharpoons E\text{–}DNA \rightleftharpoons [E\text{–}DNA]^* \qquad (96)$$
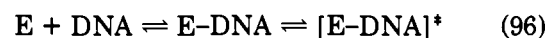
that site discrimination cannot be fully accounted for by the energetics of base contacts, but may also involve the free energy of phosphate contacts (ΔG_{phos}), the free energy of conformational reorganization (ΔG_{reorg}), and energy changes due to hydration.

The relative structural simplicity of the type II enzymes has made these systems attractive subjects for studies of protein–DNA interactions, and the [d(CGCGAATTCGCG)]₂ sequence has been a standard reference for structural, chemical, and dynamical investigations. As was mentioned above, the sequence [d(CGCGAATTCGCG)]₂ was the first oligonucleotide crystallized containing a complete turn of B-form DNA[77] and has been the subject of extensive X-ray structural studies. The crystal structures of the *Eco*RI endonuclease with the dodecanucleotide CGCGAATTCGCG and tridecanucleotide TCGCGAATTCGCG have also been reported,[88,89] and though detailed information of these systems has provided insight into protein–DNA interactions, a complete description is still lacking. The importance of major structural or conformational changes for the activity of DNA endonuclease and methylation recognition has been seen as minimal. The involvement of cruciform or bulge structures have been ruled out in the systems studied, but the contribution of local fluctuations in the sequence-specific recognition has not been fully addressed and needs to be considered to further understand the mechanism underlying the biophysical interaction between this DNA sequence and the restriction enzyme.

3.2.1 Base Dynamics In [d(CGCGAATTCGCG)]₂

In this section the internal dynamics of the DNA dodecamer [d(CGCGAATTCGCG)]₂ are investigated using [*methyl*-²H]-2′-deoxythymidine incorporated into the bases of dT7 and dT8. Quadrupolar echo line shapes, spin–lattice relaxation times (T_1), and quadrupolar decay times (T_{2e}) have been obtained as a function of hydration, allowing the development of a motional model to describe the internal dynamics of the dT7 and dT8 bases in the oligonucleotide [d(CGCGAAT*T*CGCG)]₂. The dominant motion is the fast reorientation of the methyl group about the C_3 symmetry axis, but as will be shown, other motions manifest themselves within the observed spectral line shape. Since the methyl group is rigidly attached to the pyrimidine base, it is influenced by base dynamics as well as overall molecular dynamics. Due to the partial averaging by rotational motion of the methyl group, the line shape is sensitive to motions on a slower time scale than those of previous base-labeled studies of high molecular weight DNAs. The results are compared to previous NMR studies of selectively and nonselectively base-labeled [d(CGCGAATTCGCG)]₂.

TABLE III. Line-Shape Parameters and Relaxation Rates of [*methyl*-^{2}H]-2'-Deoxythymidine-Labeled [d(CGCGAAT*T*CGCG)]$_2$[a]

% RH	W	% RI[b]	QCC$_{eff}$, kHz	η_{eff}	$\langle T_1 \rangle$, ms	$\langle T_{2e} \rangle$, μs	$\langle T_{2e} \rangle$, μs[c]
dry	0.0	1.00	51.5 ± 0.5	0.05	357 ± 23	396 ± 45	
66	5.0	0.99	51.5 ± 0.5	0.05	260 ± 13	316 ± 31	
75	10.4	0.86	51.0 ± 0.5	0.05	204 ± 10	252 ± 25	250
80	11.6	0.80	50.5 ± 0.5	0.05	213 ± 11	244 ± 23	250
88	16.3	0.40	45.5 ± 0.5	0.06	173 ± 12	142 ± 20	135
90	21.2	0.43	–[d]	–[d]	161 ± 08	115 ± 10	163
92	26.6	0.62	20.5 ± 0.5	∼0	146 ± 07	200 ± 18	218
92	29.6	0.79	20.0 ± 0.5	∼0	127 ± 06	230 ± 20	213
95	39.8	0.60	15.0 ± 0.5	∼0	103 ± 06	249 ± 24	256
98	69.9	–	∼0[e]	∼0[e]	–	–	

[a] Experiments performed at 298 K. [b] Relative intensity with respect to dry dodecamer. [c] Value obtained from simulation. [d] Intermediate rate line shape. [e] Observed only isotropic component.

Investigation of the Hydrated Dodecamer: Experimental Results

This section describes the investigation of [*methyl*-^{2}H]-2'-deoxythymidine-labeled [d(CGCGAAT*T*CGCG)]$_2$ as a function of hydration. The value of QCC$_{static}$ assumed in this study was obtained from ^{2}H NMR studies of [*methyl*-^{2}H]-2'-deoxythymidine monomer.[90] Water adsorption, W (mol of H$_2$O/mol of nucleotide), as a function of relative humidity for the sodium dodecamer is given in Table III. The results are similar to those presented previously for high molecular weight DNA.[12,91] Humidity studies on the lyophilized dodecamer did reveal a slightly higher W than that observed in previous investigations of oriented films or fibers and most likely results from the increased amount of salt present.[92]

Solid-state ^{2}H spectra, spin–lattice relaxation times $\langle T_1 \rangle$, and quadrupolar echo decay times $\langle T_{2e} \rangle$ were obtained at 76.75 MHz for [*methyl*-^{2}H]-2'-deoxythymidine-labeled [d(CGCGAAT*T*CGCG)]$_2$ as a function of relative humidity (RH) ranging from dry (W = 0.0) to 98% RH (W = 69.9). Effective quadrupolar coupling constants QCC$_{eff}$, effective asymmetry parameters η_{eff}, relative intensities (RI), $\langle T_1 \rangle$, and $\langle T_{2e} \rangle$ are given in Table III. Representative line shapes as a function of hydration level are given in Figure 24.[93]

Up to a relative humidity of 80% RH (W = 11.6), no significant changes of the observed line shape are observed aside from a 1.0-kHz reduction in QCC$_{eff}$. The effective asymmetry parameter remains constant throughout this range. (Figure 24A,B). The line shape undergoes a slight loss of center intensity with increasing humidity through 88% RH. Beginning with 88% RH (W = 16.3), a 5.0-kHz reduction in QCC$_{eff}$ with respect to 80% RH (W = 11.6) was observed, followed by drastic reduction to 20.5 kHz at 92% RH (W = 26.6) and 15 kHz at 95% RH (W = 39.8) (Figure 24C,E,F). The line shape at 90% RH (W = 21.2) is a signature of intermediate rate motion occurring within the sample and therefore could not be characterized by an effective QCC or η. (Figure 24D). Above W ≈ 25, the turbid appearance of the sample cleared when placed in the magnetic field, behavior characteristic of aligned samples. Beginning at W ≈ 20, an isotropic component became conspicuous and increased in relative magnitude until at W = 69.9 only a central isotropic line was observed. At low hydration levels this isotropic component was attributed to residual HOD, while at higher humidity levels it results from isotropic regions within the sample.
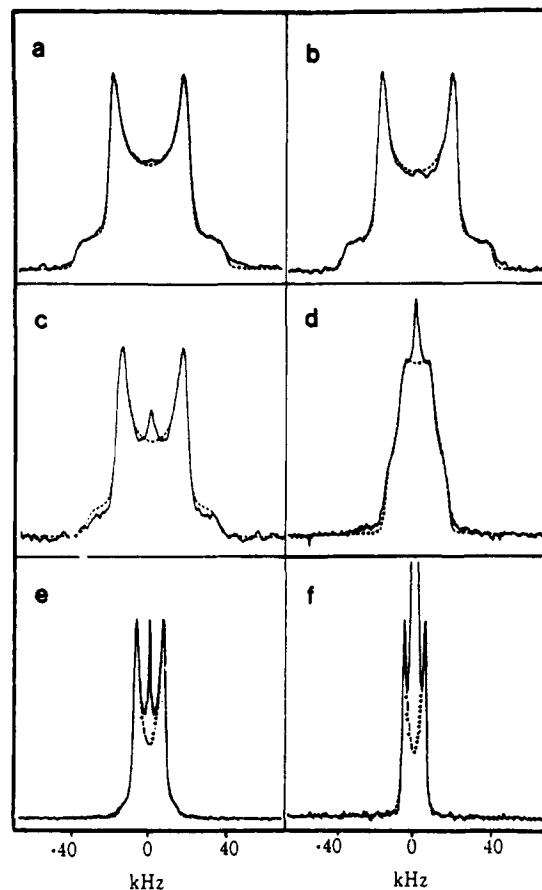
Figure 24. Experimental (—) and simulated (- -) 76.75-MHz deuterium quadrupole echo spectra of [*methyl*-^{2}H]-2'-deoxy-thymidine-labeled [d(CGCGAAT*T*CGCG)]$_2$ at various hydration levels W (mol of H$_2$O/mol of nucleotide). The simulated spectra were calculated as described in text, ignoring the central isotropic component. Spectra for pulse delay of 50 μs at (A) dry lyophilized powder, W ≈ 0, 12 000 scans; (B) 75% RH, W = 10.4, 24 000 scans; (C) 88% RH, W = 16.3, 32 000 scans; (D) 90% RH, W = 21.2, 28 500 scans; (E) 92% RH, W = 26.6, 32 000 scans; (F) 95% RH, W = 39.8, 8000 scans.

Increasing the level of hydration from the lyophilized powder produced a loss in relative intensity (RI) through 90% RH (W = 21.2), followed by a surprising increase in signal intensity beginning at 92% RH (W = 26.6). Similar attenuation of quadrupolar echo intensity as a function of hydration has been reported in samples of high molecular weight DNA (see section 3.1.3), resulting in the complete loss of the quadrupolar echo at hydration levels greater than 92% RH. Preliminary data at 92% RH (W = 24.9) on the base-labeled dodecamer revealed a signal with a reduction in

QCC$_{eff}$ of $\sim$100 kHz, and a RI of $\sim$0.09.[94] Quadrupolar echo spectra of salmon sperm DNA films and oriented fibers have been reported as high as 98% RH, but lacked discussion concerning the extent of relative intensity loss.[71]

Corresponding behavior of $\langle T_{2e} \rangle$ with increasing humidity was observed with a 4-fold decrease through 90% RH ($W = 21.1$) followed by an increase in $\langle T_{2e} \rangle$ above 92% RH ($W = 26.6$); see Table III. Significant loss in signal intensity with variation in pulse delay was observed (for example, see Figure 3A in ref 93), while anisotropic T_{2e} effects were not as pronounced as in previous studies.[50,71] This result is not readily apparent unless the spectra are scaled to the same relative intensity. The largest degree of anisotropic behavior with variation in pulse delay was observed for 90% RH ($W = 21.2$).

Spin–lattice relaxation times, $\langle T_1 \rangle$, decreased by a factor of 3.5 from dry to 95% RH ($W = 39.8$). The most dramatic decrease occurred between the "dry" and 66% RH samples, followed by a plateau at higher hydration levels. Relaxation times for the dry sample were significantly different than those observed for the monomer [$methyl$-^{2}H]-2'-deoxythymidine.[90] It should be noted that the relaxation recovery curves were found to be highly nonexponential in the dry sample. The anisotropic relaxation behavior of the deoxythymidine methyl group undergoing a 3-fold jump would be expected to give multiexponential relaxation if a powder average recovery is monitored.[38] These deviations from a single exponential relaxation are difficult to distinguish and were not discernible in the monomer studies.[90] Presently the signal to noise ratio of the deuterated dodecamer and available instrumentation does not allow a thorough analysis of the anisotropic behavior of T_1 within the dodecamer, and for this reason powder average $\langle T_1 \rangle$'s were determined and anisotropic effects ignored. The dry sample relaxation data was subsequently fit using an equally weighted double exponential upon the belief that the extreme nonexponential behavior was the result of two labeled methyl group sites in the dodecamer experiencing different motional environments. This resulted in $\langle T_1 \rangle$ values of 921 and 107 ms for the equally weighted biexponential fit, and a $\langle T_1 \rangle$ of 357 ms for a single exponential fit, compared to the $\langle T_1 \rangle$ of 1.12 s observed for the dry monomer. Relaxation recovery for all remaining humidities investigated were fit using a single exponential. The biexponential behavior of the dry sample may reflect differences in local environment between the monomer [$methyl$-^{2}H]-2'-deoxythymidine and the dodecamer, but these differences were not pursued further.

Analysis of Dodecamer Dynamics: Local Internal Dynamics

Analysis of NMR powder line shapes has provided insight into the internal dynamics of DNA. Numerous models have been presented to explain various aspects of previous ^{2}H and ^{31}P solid-state NMR studies (see section 3.1). The general procedure is to consider several different models, simulate the resulting NMR spectrum, and compare it to the experimentally observed line shape. Line-shape analysis can never prove that a model represents what is physically occurring in the system, but analysis of experimental line shapes can

dismiss certain models. It is hoped that a model can be developed that accounts for all attributes of the line shape and relaxation data as well as being compatible with studies involving labeling at different sites.

The first characteristic of the line shape considered was the variation in QCC$_{eff}$ and η_{eff} with increasing humidity. The simplest model considered consists of a rapid three-site jump about the C_3 symmetry axis of the methyl group. A motionally averaged line shape characteristic of fast methyl reorientation was observed in the dry dodecamer and monomer sample. To describe the methyl group dynamics in monomer studies of [$methyl$-^{2}H]-2'-deoxythymidine,[90] the three-site jump model was found to be superior to a model of free diffusion about the C_3 axis, and was subsequently used to describe the methyl motion within the dodecamer. Increasing the rate of the methyl motion will not alter the line shape, the observed line shape being in the rapid narrowing regime. This places a lower limit on the rate responsible for the spectral line shape observed, $\tau_c \ll \omega_Q^{-1} \approx 10^{-6}$ s. This conclusion is also supported by the observation that varying the interval τ_1 in the quadrupolar echo sequence from 40 to 200 μs produces little intensity loss and no distortion of the powder line shape. The short anisotropic T_{2e} effects expected for motions occurring in the intermediate regime were not observed in the dry sample. The reduction in QCC$_{eff}$ could occur due to variation in β_{pm}, which describes the angle between the methyl motional axis and the q_{zz} element of the EFG tensor, which is typically oriented coincident with the carbon–deuterium bond. This explanation has been used to describe the reduction in QCC$_{eff}$ in studies of polycrystalline amino acids.[95] However, to explain the large reductions in QCC$_{eff}$ that occur at high hydration levels, a distortion of the tetrahedral configuration of the methyl group to $\beta_{pm} = 43°$ would be required. Such a large variation in β_{pm} was considered physically unrealistic and was not pursued further. All subsequent analysis assumed $\beta_{pm} = 70.5°$, and any reduction in QCC$_{eff}$ was attributed to averaging of the quadrupolar tensor by additional internal or overall motions.

Incorporation of a two-site libration of the base plane in addition to the methyl group three-site jump was also considered. This model was evaluated previously in the dynamic studies of deoxythymidine monomer as well as analysis of the base-labeled dodecamer.[50,90] Since the methyl group three site jump motion produces an uniaxially averaged tensor, the direction of the two-site libration cannot be assigned; the averaged elements of the methyl EFG tensor being equivalent ($\overline{q_{xx}} = \overline{q_{yy}}$). Directional analysis has been discussed for other base studies,[67,68,71] the relative orientation of the EFG tensor in the molecular frame being obtained from analysis of oriented DNA samples. In the analysis of ^{2}H base labeled purine studies, it has been found that q_{xx} of the EFG tensor lies approximately in the base plane, but the present study involves the analysis of the methyl EFG tensor and no direct comparison is applicable.

The reduction in QCC$_{eff}$ at 75% RH ($W = 10.4$) and 80% RH ($W = 11.6$) can be accounted for by increasing the angle of libration from $\theta_0 = 9°$ for the dry sample ($W = 0$) to $\theta_0 = 12°$ at 80% RH ($W = 11.6$), both at a rate with $\tau_c < 10^{-6}$ s, where θ_0 is the half-angle between the two sites. This is in agreement with the [6H-

[²H]-2'-deoxythymidine studies in the same dodecamer.[50] It is interesting to consider correlation times $\langle \tau_c \rangle$ calculated from corresponding $\langle T_1 \rangle$ values for this model. Spin-lattice relaxation behavior for a model included a three-site jump about the C_3 symmetry axis and an uncorrelated small-amplitude two-site libration was determined from a formalism developed in section 2.2.1. For a site-site libration amplitude $\theta_0 = 12°$ and an angle between the C–D bond and the methyl C_3 symmetry axis $\beta_{pm} = 70.5°$, four solutions are obtained for the correlation time. The two-site libration has solutions for the correlation time, τ_c of $\sim 3.6 \times 10^{-8}$ or $\sim 4.6 \times 10^{-11}$ s, with the corresponding pair of methyl correlation time solutions being $\sim 1.5 \times 10^{-7}$ or $\sim 1.3 \times 10^{-11}$ s. The pair of solutions with slower methyl correlation times do not reproduce the observed experimental methyl line shapes. On the other hand both solutions for τ_c of the librational motion produce nearly identical methyl line shapes regardless of pulse spacing, τ_1. Simulations of base-labeled line shapes for the librational correlation time solutions show only minor variation in center intensity. Given the signal to noise observed for the base-labeled material at 80% RH (W = 11.6),[50] it would be difficult to distinguish between these two solutions. In contrast, analysis of the dry base labeled dodecamer $\langle T_1 \rangle$ produces librational correlation time solutions with distinguishable line shapes, supporting the assumption that the correct librational correlation time is on the fast side of the T_1 curve.

Attempts to extrapolate this two site librational model to 88% RH (W = 16.3) and beyond were unsuccessful. Increasing the angle of libration to account for reduction in QCC_eff resulted in a dramatic increase in η_{eff}. This was not observed experimentally, suggesting that a two site jump model is unrealistic in describing the internal dynamics of the base. A similar conclusion was reached in the analysis of relaxation rates in oriented fibers[69] where similar T_1 relaxation rates for $\Theta = 90°$ and $\Theta = 0°$ suggests the bases undergo a more symmetric motion.

Different models have been proposed to describe internal motions in DNA.[21] The diffusion-in-a-cone model[96-98] has found a wide range of applications including investigations of fluorescence polarization decay in membranes[99] and nuclear magnetic relaxation in lipids.[100] It has also been used in the analysis of ²H studies of purine-labeled nucleic acids as described in section 3.1. Use of this model to describe the restricted motion of the base may not be completely applicable to the present study due to observation of $\eta_{eff} > 0$. A symmetric motion like diffusion-in-a-cone, along with the methyl three site jump motion, will produce a symmetrically averaged EFG tensor (η_{eff} = 0), but use of this model, ignoring deviations from axial symmetry of the molecular motion, still allows an estimation of changes in internal motion with increasing hydration. Defining θ_0 as the half-angle of the cone in which the C_3 symmetry axis is allowed to freely diffuse, and ignoring the small asymmetry parameter, the effective quadrupolar coupling constant is given approximately by

$$\text{QCC}_{eff} \sim (e^2qQ/h)_{eff}^{Me} S_{zz} \qquad (97)$$

where $(e^2qQ/h)_{eff}^{Me}$ is the effective averaged quadrupolar coupling constant due to rapid methyl motion, and the uniaxial order parameter for diffusion-in-a-cone is given by

$$S_{zz} = (\cos \theta_0 + \cos^2 \theta_0)/2 \qquad (98)$$

Assuming that there are no significant librational motions present within the dry sample, application of this diffusion-in-a-cone model gives S_{zz} = 0.981 and θ_0 = 9° at 80% RH (W = 11.6), S_{zz} = 0.883 and θ_0 = 23° at 88% RH (W = 16.3), S_{zz} = 0.388 and θ_0 = 59° at 92% RH (W = 26.6), and S_{zz} = 0.291 and θ_0 = 65° at 95% RH (W = 39.8). The value for 80% RH (W = 11.6) is smaller than the reported θ_0 = 16° for 84% RH in Li-DNA,[68] which has a similar water content. It compares well with the θ_0 = 8.5° reported for salmon sperm DNA.[71] Analysis of purine base labeled dodecamer data with a diffusion-in-a-cone model resulted in similar values for the angle of fluctuation, with θ_0 = 17° at 80% RH (W = 11.6) and θ_0 = 57° at 92% RH (W = 26.6). These values for θ_0 assumed that librational motions were absent in the dry methyl-labeled dodecamer. Including the possibility of librational motions within the monomer and dry dodecamer will increase the angle of fluctuations. Besides the inability of this model to describe the intermediate rate line shape observed at 90% RH (W = 21.2) and the appearance of a nonzero asymmetry parameter, the large cone angle required to fit experimental spectra at elevated levels of hydration makes the applicability of this model to the dodecamer data questionable. Additional models need to be investigated. Of course, a nonzero asymmetry parameter can be obtained by other means than through a nonsymmetric motion, but in keeping with the model presented in the previous deoxythymidine monomer studies, these were not pursued. (See ref 90 for further discussion.)

Fluctuation of the C_3 symmetry axis within an one dimensional harmonic potential was examined to describe the changes in the dodecamer line shape with increasing hydration levels. Expressions for a one-dimensional harmonic potential, $U(\theta_0) = f\theta_0^2$, were presented in section 2.2.2. If the observed asymmetry parameter is entirely the result of fluctuations within the harmonic potential, solutions for the reduction factor Λ and η_{eff} are shown in Figure 25. The observed asymmetry parameter η_{eff} = 0.05 results from fluctuations in a potential defined by the force constant $f \approx 15k_BT$. The rms amplitude is found using the Boltzmann distribution

$$P(\theta_0) = Z^{-1} \exp (-f\theta_0/k_BT) \qquad (99)$$

and is given by

$$\langle \theta_0^2 \rangle^{1/2} = (k_BT/2f)^{1/2} \qquad (100)$$

To explain the observed asymmetry parameter the force constant would correspond to a rms displacement of 10.5°. This is in close agreement with the rms of 12° obtained from the two site jump model. The value of f corresponds to a single value of the reduction factor $\Lambda \approx 0.94$, and cannot explain the continuous reduction of Λ with a constant η_{eff}. As with the two site libration, fluctuations in a harmonic potential are unable to explain all the observed changes in line shape as a function of hydration.

An alternative model is one-dimensional harmonic diffusion on a cone, $U(\theta,\phi_0) = f'\phi_0^2 \sin^2 \theta = f\phi_0^2$, described
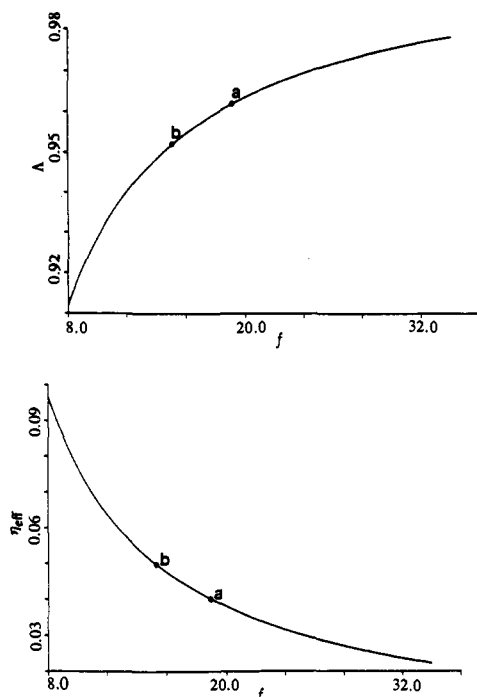
Figure 26. Observed η_{eff} and Λ for diffusion in a cone ($U = f'\phi_0^2 \sin^2 \theta$) as a function of the force constant f and the cone angle θ. Contours for specific values of η_{eff}, 0.05 (—), and Λ, 0.97 ($\cdot\cdot$), 0.96 (- -), 0.95 (—), 0.86 (- $\cdot$ -). Solution for 80% RH ($\bullet_a$) and 88% RH ($\bullet_b$) and the corresponding one-dimensional libration ($\bullet_c$).

Figure 25. Observed η_{eff} and Λ for a simple one-dimensional harmonic potential ($U = f\theta_0^2$) as a function of the force constant f. Solutions for the [methyl-^{2}H]-2'-deoxythymidine monomer ($\bullet_a$) and dry dodecamer ($\bullet_b$) are shown.

in section 2.2.2. Figure 26 presents a contour surface relevant values of η_{eff} and Λ as a function of the force constant f. The distribution is a simple Gaussian, with the root mean square amplitude being given by

$$\langle \phi_0^2 \rangle^{1/2} \sin \theta = (k_B T / 2f')^{1/2} \qquad (101)$$

Descriptions of the reorientation of a CD bond on the unit sphere are only comparable when the $\sin^2 \theta$ is included in the rms determination, thus avoiding large ellipticity effects of the harmonic potential. There are no possible solutions for $\Lambda = 0.97$ and 0.96 for the entire range of the cone angle θ. The solution for $\Lambda = 0.95$ corresponds to diffusion in a cone of $\theta \sim 40°$ with $f \approx 7k_B T$, while for $\Lambda = 0.86$ the cone angle is $\theta \approx 22°$ and $f \approx 1k_B T$. These solutions correspond to rms distributions of 15° and 40.5°, respectively. While the model can explain the line shapes for two of the hydration levels, it offers no solution for the lowest hydration levels. The variation in the cone angle θ with hydration level corresponds to the motional axis moving with respect to the C_3 symmetry axis, questioning the physical relevance of this model. There are no structural characteristics that would motivate such a process with higher water content, suggesting that this model is inadequate in describing the internal dynamics. The lack of solutions for the lower hydration levels may result from using a QCC$_{static}$ that was obtained using a two site jump model. A similar treatment of η_{eff} in the monomer using the one-dimensional harmonic potential model would produce a different QCC$_{static}$. In contrast to the two site jump model, solutions for an observed asymmetry parameter η_{eff} do not have an unique solution of Λ.

A biaxial model, consisting of motions in two perpendicular directions, has been previously presented as a model of internal base motions.[67,68,71] In all cases it is assumed that one direction of libration is within the
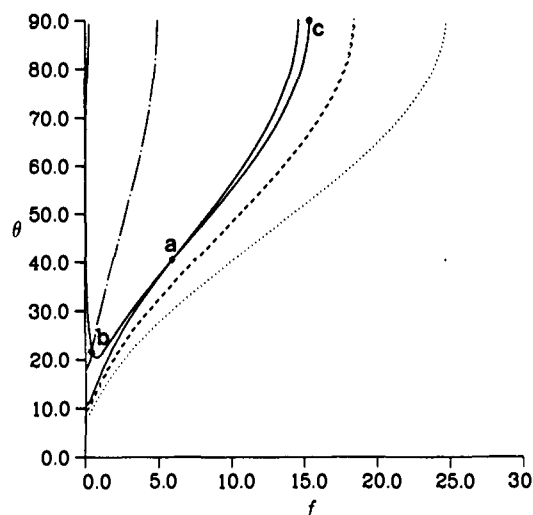
base pair plane and the second direction of libration is perpendicular to that plane. The fluctuations of the methyl C_3 symmetry axis are described by ϕ_0 for the in-plane libration, and θ_0 for the out-of-plane librations. It is not possible to determine the relationship of θ_0 and ϕ_0 to a specific direction with respect to the C_3 symmetry axis, since the methyl motion alone produces a uniaxially averaged EFG. Assignment of the directions of θ_0 and ϕ_0 is possible from an analysis of the aligned liquid crystal spectrum, which allows discrimination between twisting and tilting type motions.[101]

Changes in QCC$_{eff}$ and η_{eff} with increasing humidity can be described by increases in θ_0 and ϕ_0. Using the static value of e^2qQ/h obtained from monomer studies,[90] the line shape of the dry sample can be simulated using $\theta_0 = 9° \pm 1°$, and $\phi_0 = 7° \pm 1°$. At 75% RH ($W = 10.4$) and 80% RH ($W = 11.6$) the angles of libration increase to $\theta_0 = 12° \pm 2°$ and $\phi_0 = 10° \pm 2°$, while at 88% RH ($W = 16.3$) $\theta_0 = 19° \pm 2°$ and $\phi_0 = 17° \pm 2°$, at 92% RH ($W = 26.6$) θ_0 and $\phi_0 \approx 40° \pm 3°$, and at 95% RH ($W = 39.8$) θ_0 and $\phi_0 \approx 43° \pm 3°$. The lower hydration levels compare favorably with values reported for calf thymus Li–DNA,[68,91] while the higher hydration levels show substantially higher values of libration than those reported for salmon DNA fibers and films.[71] This increase may result from differences in the actual level of hydration, or from differences in the helix axis motion as discussed below. Analysis of the base-labeled dodecamer[50] using this four site librational model resulted in surprisingly large differences between θ_0 and ϕ_0, given the values of η_{eff} at lower hydration levels, but at 92% RH, θ_0 and ϕ_0 equaled about 38°, remarkably close to those values obtained for the methyl group. It should be noted that in the methyl line shape analysis the angles are restricted to $\theta_0 \neq \phi_0$ to fulfill the requirement $\eta_{eff} \neq 0$. These librational amplitudes are tabulated in Table IV and were obtained using a visual fit of the line shape.[101] Figure 27 shows the contour surface of a four-site libration. It immediately becomes evident that there are no solutions for $\eta_{eff} = 0.05$ and $\Lambda > 0.96$. This results in an inability to explain the observed line shape of the dodecamer at the dry or 66%

TABLE IV. RMS Deviations of Biaxial Libration with Relative Humidity for [methyl-²H]-2′-Deoxythymidine-Labeled [d(CGCGAAT*T*CGCG)]₂

% RH	W	Λ	$\theta_0,°$ deg	$\phi_0,°$ deg	$\theta_0,^b$ deg	$\phi_0,^b$ deg
dry	0.0	0.97	9 ± 1	7 ± 1	ns^c	ns^c
66	5.0	0.97	9 ± 1	7 ± 1	ns	ns
75	10.4	0.96	12 ± 2	10 ± 2	ns	ns
80	11.6	0.95	12 ± 2	10 ± 2	14.5	3.0
88	16.3	0.86	19 ± 2	17 ± 2	21.0	15.5
90	21.2					
92	26.6	0.39	40 ± 3	40 ± 3	39.5	39.5
92	29.6	0.38	40 ± 3	40 ± 3	40.0	40.0
95	39.8	0.28	43 ± 3	43 ± 3	43.5	43.5
98	69.9					

^{a} Visual fit of simulations. ^{b} Obtained using analytical expressions for a four-site libration. ^{c} ns, no solution using analytical expressions.
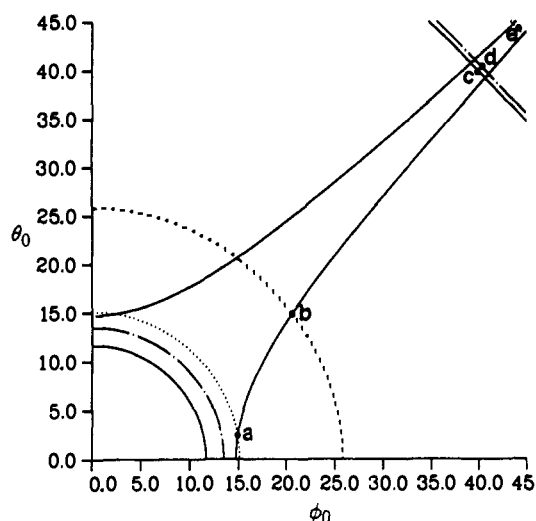

Figure 27. Contour surface for a four-site libration as a function of the displacement θ_0 and ϕ_0. Contours for specific values of Λ (concentric circles) are shown, 0.97 (—), 0.96 (— ·), 0.95 (· ·), 0.86 (– –), 0.39 (—), 0.38 (— ·), 0.28 (· ·), as is a contour for η_{eff} at 0.05 (—). Solution for different hydration levels are shown: ($\bullet_a$) 80% RH, ($\bullet_b$) 88% RH, ($\bullet_c$) 92% RH (W = 26.6), ($\bullet_d$) 92% RH (W = 29.6), and ($\bullet_e$) 95% RH.

RH humidity levels (as well as the monomer). The results for other hydration levels are shown in Table IV. There are several points that need to be addressed. The first is how a visual fit could produce solutions for the lower hydration levels, while the analytical expressions have no possible solutions. This discrepancy may lie in the smallness of the observed asymmetry parameter, and the difficulty of measuring subtle changes in the asymmetry parameter with the 1–1.5 kHz natural line broadening present. As seen in Figure 8 a variation in the observed η_{eff} of ±0.01 would produce solutions for the dry and 66% RH samples. The difficulty in measuring the small η_{eff} may also explain the discrepancy of relative differences in θ_0 and ϕ_0, when compared to the reported base values. The analytical expressions for a four-site libration produce differences in these two amplitudes that are on the same order as those reported by Huang and co-workers for the base-labeled dodecamer.[50] The lack of solutions for the lower hydration levels may also result from the method of determining QCC_{static} (see previous paragraph). Inspection of Figure 27 reveals that given an observed asymmetry parameter η_{eff}, a unique solution for QCC_{static}

is again not possible. For this reason the value of QCC_{static} obtained using the two-site libration will continue to be utilized.

If the librational motions of this four-site model are faster than the width of the rigid lattice spectrum, effective average values of QCC and η are produced. The correlation time of the libration cannot be determined from line-shape analysis, but an upper limit of $\tau_c < \omega_Q^{-1} \approx 10^{-6}$ s can be set. A thorough analysis of relaxation data is required for determination of τ_c. The two site or four site librational model adequately fits the experimental line shape for dry and 66% RH (See Figure 24A). Comparison of simulated spectra for this model to experimental spectra at 75%, 80%, and 88% RH shows only partial agreement. The line shape observed at 90% RH, however, is characteristic of motion occurring in the intermediate rate regime and cannot be reproduced by fast librations regardless of angle. The angle of libration of $\sim\pm45°$ for 92% RH and higher hydration levels is again physically debatable. It is obvious that additional motions are occurring and that other line-shape characteristics must be addressed in the analysis of spectra. One characteristic to consider is the loss in center intensity with increasing humidity. This orientationally dependent attenuation is not present in the simulations involving only methyl motions and fast librations. Also observed is a loss in signal intensity or echo attenuation with variation in pulse spacing as well as variation in relative intensity between hydration levels. The biaxial model consisting of only fast motions, shows no variation with τ_1, nor can the simple increase in the librational angle account for the loss in signal intensity. The loss in intensity and line-shape modulation with respect to pulse spacing, τ_1, may be attributed to heteronuclear dipolar dephasing.[103] Consideration of these heteronuclear dipolar interactions with surrounding protons in the DNA and water molecules is impractical, requiring knowledge of each interaction distance. Recognizing the omission of heteronuclear dipolar contributions as an approximation, these effects were not considered further. If the spectra are scaled to the apparent $\langle T_{2e} \rangle$ present from interactions at dry or 66% RH, additional changes in T_{2e} with increasing humidity can be entirely attributed to dynamic processes within the oligonucleotide.

Dodecamer Helix Motion

Changes in the observed experimental line shape can be accounted for by the appearance of a slower motion about the helix axis. Different models have been presented to describe the motion about the long axis of DNA;[46,51] the simplest is to treat the DNA molecule as a rigid cylinder undergoing free diffusion or restricted diffusion about the helix axis. Coupling of the biaxial librational model with slow motion about the helix axis adequately reproduces the observed line shapes through 90% RH (W = 21.2). The effect of helix diffusion was simulated using a jump model between nearest neighbors of equal site probability described by the equilibrium

$$S_1 \overset{k}{\rightleftharpoons} S_2 \overset{k}{\rightleftharpoons} ... \overset{k}{\rightleftharpoons} S_n \qquad (102)$$
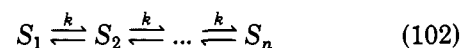
where S_i represents the ith site and k represents the rate of jumping between sites. This type of model has been used in the analysis of ^{2}H and ^{31}P line shapes in

DNA.[50,71] The relationship between k and the planar diffusion coefficient D_R can be obtained in the following manner. The number of random jumps required for an axis to reorient by an angle ξ is given by[104]

$$n_\xi = \xi^2/\theta_{ij}^2 \qquad (103)$$

where θ_{ij} is the arc angle between successive sites. The average time required to reorient the axis by one radian is

$$\tau = n_1/k = 1/k\theta_{ij}^2 \qquad (104)$$

which can be used to obtain the diffusion coefficient

$$D_R = 1/2\tau = k\theta_{ij}^2/2 \qquad (105)$$

The larger the number of sites N, or the smaller the jump size θ_{ij}, the closer to the true diffusion limit this becomes. Studies by Wittebort and co-workers[39] showed that differences in line shapes and variation in relative intensities can occur with increase of the number of sites. The six site jump model was used almost exclusively as a model of diffusion about the helix axis in the present simulations primarily to minimize computational time, but results are also presented for a larger number of sites.

The experimental line shapes of 75% and 80% RH are simulated well using the methyl rapid three-site jump, a fast four-site libration of the base plane, and a slower six-site helix motion at $k = 1$ kHz, $\theta_{ij} = 5°$ (See Figure 24), corresponding to a $D_R = 3.8$ s^{-1}. Line-shape variations are minimal in going from $N = 6$ to $N = 16$ for the 1-kHz model, corresponding to a total angular displacements of 25° and 75° or rms displacements of 8.5° and 23°, respectively. This suggests that the slow azimuthal rotation may not be truly restrictive in nature, but at a rate slow enough to appear restricted in nature on a ^{2}H NMR time scale. The observed spectrum at 88% RH is fit similarly with $k = 3$ kHz, $\theta_{ij} = 20°$, corresponding to $D_R = 1.8 \times 10^2$ s^{-1}. The observed signal to noise at 88% RH allowed only an approximate fit, but it was obvious from analysis of line-shape changes with variation in pulse spacing that the lack of anisotropic attenuation precludes models containing significantly larger angles and/or increased rates, since these produced line shapes that varied differently with inter-pulse spacing than was observed experimentally.

The experimental line shapes become difficult to interpret at higher hydrations due to local internal librations being masked by larger amplitude motions occurring at low rates. Simulation of the intermediate line shape observed at 90% RH using $\theta_{ij} = 60°$, $k = 400$ kHz, corresponding to $D_R = 2.2 \times 10^5$ s^{-1} (with the amplitude of the four-site libration unchanged from that of 88% RH), produced line shapes with the same general characteristics, but were insufficiently narrowed. Simulations where the rate or angle were varied from these values tended to produce line shapes uncharacteristic of the intermediate regime. An approximate fit can be obtained by increasing the internal fluctuations to θ_0 and $\phi_0 = 22°$ to give a librationally averaged QCC$_{eff}$ ≈ 40 kHz and $\eta_{eff} \approx 0$. One can also assume that those local motions described by the rapid four-site libration remain unchanged at hydration levels greater than 88% RH and that all subsequent variations in line shape result from motions in addition to the base libration. This is not entirely unplausible in that at $W = 16.3$ the

hydration of the oligonucleotide is complete. Between $W = 5$ and 12 the nucleotide bases are hydrated, above $W = 12$ the dodecamer is completely hydrated and additional water binds to the primary hydration level, and finally above $W = 20$ water adds to the grooves as well as between dodecamer helices.[12-14] Contributions of diffusion about an axis other than the azimuthal axis may also need to be considered. A rough estimate of contributions from diffusion about an axis perpendicular to the helix symmetry axis can be obtained from consideration of the rotational dynamics of rigid spherocylinders, and using expressions applicable to shorter DNA fragments:[105,106]

$$D_{\perp R} = \frac{3k_B T}{\pi \eta L^3}(\ln p + \delta_\perp) \qquad (106)$$

$$D_{\parallel R} = \frac{k_B T}{(3.841)\pi \eta L R^2}\left(\frac{1}{1+\delta_\parallel}\right) \qquad (107)$$

where k_B is the Boltzmann constant, L and R are the length and radius of the cylinder, T is the absolute temperature, η is the solvent viscosity, and p is the length to diameter ratio

$$p = \frac{L}{2R} \qquad (108)$$

The parameters $\delta_\perp$ and $\delta_\parallel$ are end-effect coefficients. Values of these corrections for different p ratios were presented by Tirado and Garcia de la Torre. Extensions to any arbitrary value of p are obtained using the expressions presented by Hustedt:[107]

$$\delta_\perp = -0.66181 + 0.912667\left(\frac{1}{p}\right) - 0.04242\left(\frac{1}{p}\right)^2 \qquad (109)$$

$$\delta_\parallel = 0.689236\left(\frac{1}{p}\right) - 0.20321\left(\frac{1}{p}\right)^2 \qquad (110)$$

The ratio of diffusion rate about the helix axis and the axis perpendicular to the helix is ca. 1.9 for a molecule with a length to diameter aspect ratio of ca. 1.7. A rough simulation of the contributions from motion about an axis perpendicular to the helix axis can be obtained using this ratio. Simulation using a six site jump motion about the helix axis at $k = 400$ kHz, $\theta_{ij} = 60°$, and $D_{\parallel R} = 2.2 \times 10^5$ s^{-1} and a helix "wobble" being characterized by a three-site jump at $k = 1.56$ MHz, $\theta'_{ij} = 22°$, $D_{\perp R} = 1.15 \times 10^5$ s^{-1} produced slightly improved fits of experimental spectra (see Figure 24) compared to a simple reduction of QCC$_{eff}$. This jump model for helix wobble is a crude approximation for diffusional processes about two perpendicular axis, but it does demonstrate that increases in base libration may not be required to account for the additional narrowing. The possibility of magnetic ordering was investigated for 90% RH, but an aligned phase was not observed to be a major component at this hydration level.

Parameters obtained for the six site jump model compare well to previous ^{2}H studies of DNA. Kintanar and co-workers[50] analyzed the base-labeled dodecamer and found that 80% RH, $k = 3.3$ kHz, with $\theta_{ij} = 5°$, while at 88% RH, $k = 1$ MHz, with $\theta_{ij} = 30°$. The lower humidity data correspond well with the values obtained from the methyl-labeled dodecamer while the 88% RH data differ significantly. The rate and angle values reported by Kintanar and co-workers for 88% RH were

investigated, but produced line shapes that were distinctly outside the intermediate regime. This suggests that the methyl label is a more sensitive probe of motions occurring near 50 kHz. Applying this model to longer pieces of DNA at 92% RH, Shindo and co-workers found the best fit using $k = 2$ MHz, $\theta_{ij} = 30°$, corresponding to $D_R = 2.7 \times 10^5$ s^{-1}. This value of D_R is surprisingly close to that observed at 90% RH, but simulations involving a restricted reorientation were unsuccessful, resulting in broad shoulderless methyl line shapes similar to those reported for the base. This discrepancy may be the result of the differences in DNA size, the smaller dodecamer being able to fully reorient about its helix axis at this hydration level. Above $W \approx 25$ the sample was found to align with the helix axis perpendicular to the magnetic field. Simulation of the line shapes obsereved at 92% RH ($W = 26.6$) and 95% RH ($W = 39.9$) can be obtained in a similar manner as described for lower hydration levels, except the degree of alignment must be considered.

Analysis of the echo decay time, T_{2e}, allows investigation of motional rates occurring in the dodecamer, as well as a means of discriminating between various models. There have been numerous investigations of T_{2e} relaxation in lipids and integral membrane proteins.[40,108] The T_{2e} relaxation rates are orientational dependent, and therefore would give rise to nonexponential decay recovery curves; the signal to noise ratio for the deuterated dodecamer reported in this dissertation was not sufficient to detect these deviations from exponential behavior. Powder average decay rates (denoted $\langle T_{2e} \rangle$) were therefore determined, and can be interpreted in terms of changes in the second moment of the observed line shape. The second moment, M_2, is given by

$$M_2 = \int_{-\infty}^{\infty} d\omega \; \omega^2 \, f(\omega) \Big/ \int_{-\infty}^{\infty} d\omega \, f(\omega) \qquad (111)$$

where $\omega = 0$ is the Larmor frequency ω_0, and $f(\omega)$ is the line-shape function. For symmetric powder patterns the second moment can be related to the effective quadrupolar coupling constant by

$$M_2 \approx 9\pi^2 (QCC_{eff})^2 / 20 \qquad (112)$$

A qualitative analysis of T_{2e} relaxation shows that in the slow motional limit $T_{2e} \approx \tau_c$, while in the rapid limit $T_{2e} \approx (\tau_c \Delta M_2)^{-1}$.[108] This shows that for a motion about a single axis, variation in the correlation time from the slow or rigid limit to the rapid time scale results in T_{2e} passing through a minimum. Interpretation of T_{2e} for the dodecamer would require consideration of other internal dynamics in addition to motion about the helix axis, but the appearance of a T_{2e} minimum supports the model of an increase in the rate of motion about the helix axis with higher humidity levels as proposed from line-shape analysis. As a crude approximation of the correlation time for this rotational process, changes in the second moment can be related to the loss in quadrupole echo by

$$\frac{1}{T_{2e}} = \Delta M_2 \tau_c \qquad (113)$$

For 92% RH the changes in the second moment (assuming that they result entirely from motion about the helix axis) give $\tau_c \approx 5 \times 10^{-7}$ s. This is only an ap-

proximation of the correlation time of helix motion and is complicated by the fact that changes in the second moment may result from other motions occurring within the dodecamer. Analysis of T_{2e} can still be used to discriminate between various models, by comparison to decay rates obtained from simulations. These rates were scaled to the $\langle T_{2e} \rangle$ observed in the dry sample and represent relaxation due to motional changes in comparison to the dry sample. Simulated values of $\langle T_{2e} \rangle$ are given in Table III, and compare favorably to those observed experimentally. In particular, the reversal of $\langle T_{2e} \rangle$ with increasing humidity levels is reproduced. Attempts to simulate the overall loss in echo intensity as a function of W from these models were not successful. The overall trend of signal intensity loss was observed, but the magnitude of echo attenuation was less than observed experimentally. This discrepancy may in part be due to the numerous experimental conditions that can contribute to echo intensity attenuation, or due to interactions (i.e. heteronuclear dipolar dephasing) not explicitly considered.

Spin–Lattice Relaxation in Dodecamer

As demonstrated in previous sections, measurement of spin–lattice relaxation can provide information concerning the rate and nature of motions occurring within a DNA sample. The nature of nuclear spin relaxation in hydrated nucleic acids has only recently been addressed and has the potential of providing an abundance of information on internal molecular dynamics. The models describing helix motion vary in complexity and each model invokes a number of adjustable parameters. Fitting a single $\langle T_1 \rangle$ value obtained at one magnetic field strength to a particular model of molecular dynamics cannot prove the uniqueness of the model, and in fact the solutions obtained for a single point fit are not expected to be unique within the multiple dimensional parameter space. Yet with judicious restriction of some parameters, valuable insights can be obtained. In the following sections three models of helix motion are addressed: (i) free helix diffusion, (ii) restricted helix diffusion, and (iii) collective torsional modes. Expressions for spin–lattice relaxation rates for each of these models were presented in section 2.3.

Free-Helix Diffusion

The view of motion around the helix axis as free diffusion of a rigid cylinder will now be considered. To reduce the number of parameters the following assumptions are made: (i) in the "dry" sample no azimuthal helix motions are present, and the relaxation is dominated by the methyl motion alone; (ii) The correlation time of the methyl three-site jump is fixed at $\tau_c = 3.4 \times 10^{-12}$ s based on the observed $\langle T_1 \rangle$ for the dry [methyl-^{2}H]-2'-deoxythymidine-labeled dodecamer sample; (iii) all changes in the observed spin–lattice relaxation with increasing hydration result from azimuthal motion about the helix. Using these assumptions values for $D_{\|R}$ were obtained and are shown in Table V. There are two solutions to the $\langle T_1 \rangle$ expression, but the rapid $D_{\|R}$ solution was rejected because it corresponds to a room temperature solvent viscosity that is considerably less than that of water. This model was investigated for two different orientations of the base $\beta_{mc} = 70°$ and $90°$, corresponding to the A and B

TABLE V. Parameters for Free Helix Diffusion°

% RH	W	$D_{\|R}$, s^{-1}	β_{mc}, deg	$D_{\|R}$, s^{-1}	β_{mc}, deg
66	5.0	1.22×10^7	90	1.37×10^7	70
75	10.4	1.71×10^7	90	1.95×10^7	70
80	11.6	1.70×10^7	90	1.94×10^7	70
88	16.3	1.96×10^7	90	2.24×10^7	70

° τ_c (methyl) = 3.4×10^{-12} s, β_{pm} = 70.5°, details of model presented in the text.

TABLE VI. Parameters for Restricted Helix Diffusion°

% RH	W	$D_{\|R}$, s^{-1}	β_{mc}, deg	$D_{\|R}$, s^{-1}	β_{mc}, deg	γ_0, deg
66	5.0	1.84×10^7	90	2.24×10^7	70	24
75	10.4	3.76×10^7	90	5.31×10^7	70	24
80	11.6	3.75×10^7	90	5.30×10^7	70	24
88	16.3	3.23×10^7	90	3.98×10^7	70	30

° τ_c (methyl) = 3.4×10^{-12} s, β_{pm} = 70.5°, details of model presented in the text.

forms of DNA. The diffusion coefficients obtained only increase by a factor of 1.6 with hydration to 88% RH (W = 16.3). These diffusion constants are also unrealistic, being approximately the same magnitude as the viscosity observed in 20–35% sucrose solutions (see Table D-2 in ref 107).

Restricted Helix Diffusion

Another model that has been used in the description of helix motion is diffusion within a restricted potential defined by $2\gamma_0$. Using the same assumptions presented for the free helix diffusion analysis, plus the assumption that $2\gamma_0$ = 48° (see section 2.3.2), values of $D_{\|R}$ were obtained and are shown in Table VI. Attempts to utilize the value of $2\gamma_0$ = 24°, based on the amplitude of the six-site jump used in the line-shape simulations, were unsuccessful, so the value of $2\gamma_0$ = 48° was used. The magnitude of the diffusion constant increased only slightly in comparison to the unrestricted motion. It was also found that the hydration level of 88% RH (W = 16.3) could not be explained unless the amplitude of motion was increased to γ_0 = 30°.

Collective Torsional Modes

The effects of collective helical torsional motion on the spin–lattice relaxation were also investigated. This model has been described in section 2.3.2. Employing the same assumptions that were used in the free-diffusion analysis, plus restriction of the torsional spring constant to α = 4.0 × 10^{-12} dyn cm, the changes in relaxation with hydration level were modeled by variation of the friction factor γ. Similar assumptions were made for the analysis of the base-labeled spin–lattice relaxation. Results for a base orientation angle of β_{mc} = 70° and 90° are presented in Table VII. A general comparison to the previous models can be made by determining the uniform mode diffusion coefficient, $D_{\|R}$ $\approx$ 1.2 × 10^7 s^{-1} for 66% RH, and is again unrealistically large. The near 100-fold difference in the torsional frictional constant between the methyl- and base-labeled[50] spin–lattice relaxation also reveals an inconsistency in the motional model. The removal of these inconsistencies will require further experimental investigations, including analysis of spin–lattice and quadrupolar order relaxation (and the corresponding individual spectral densities $J(m\omega_0)$) at a variety of fields.

TABLE VII. Parameters for Collective Helix Torsional Motion°

% RH	W	γ, dyn cm s	β_{mc}, deg	γ, dyn cm s	β_{mc}, deg
66	5.0	2.66×10^{-22}	90	2.37×10^{-22}	70
75	10.4	1.88×10^{-22}	90	1.68×10^{-22}	70
80	11.6	1.89×10^{-22}	90	1.69×10^{-22}	70
88	16.3	1.68×10^{-22}	90	1.49×10^{-22}	70

° α = 4.0 × 10^{-22} dyn cm, τ_c (methyl) = 3.4×10^{-12} s, β_{pm} = 70.5°, details of model in the text.

3.2.2 Backbone Dynamics in Hydrated [d(CGCGAAT*T*CGCG)]₂

Line-Shape Analysis: Fast Regime Dynamics

In section 3.1.1, ^{31}P solid state NMR studies of backbone dynamics in oriented fibers of high molecular weight DNA were reviewed. Another approach to probing the dynamics of the backbone will be described in this section, where samples of [d-(CGCGAAT*T*CGCG)]₂, selectively deuterated at the 5′-carbon, have been studied by ^{2}H NMR. As in studies of dodecamer base dynamics which were described in section 3.2, ^{2}H NMR studies will be discussed at two levels: line-shape analysis and relaxation.

The specific sample to be examined is [d-(CGCGAAT*T*CGCG)]₂, in which the 5′- and 5″-protons of dT7 and dT8 have been replaced by deuterons. The chemical synthesis and a ^{2}H NMR study of the monomeric nucleoside [5′,5″-^{2}H$_{1:1}$]-2′-deoxythymidine have been reported[90] with observed values of QCC$_{eff}$ = 164 ± 1 kHz and η_{eff} = 0.07 ± 0.01. If the observed symmetry parameter is assumed to result entirely from fast limit dynamics, a model utilizing discrete jumps between two orientations with a half-angle of θ_0 = ±12° and a QCC$_{static}$ of 175 ± 1 kHz gives the observed η_{eff}. This value of QCC$_{static}$ is consistent with the value reported by Kintaner et al.[90] for the monomer, but is high in the range for values reported for methylene deuterons.[109] The question arises: how unique are the solutions for θ_0 and QCC$_{static}$ within the framework of two site dynamics? For small values of the half-angle θ_0 it may be shown[110] that the ratio of QCC$_{eff}$ to QCC$_{static}$ and the effective asymmetry parameter are given by the following expressions:

$$QCC_{eff}/QCC_{static} = P_2(\cos \theta_0) \qquad (114)$$

$$\eta_{eff} = [1 - P_2(\cos \theta_0)]/P_2(\cos \theta_0) \qquad (115)$$

The uniqueness of QCC$_{static}$ is seen by a simple rearrangement of these two equations:

$$QCC_{static} = (1 + \eta_{eff})QCC_{eff} \qquad (116)$$

So within the framework of a two-site jump and small displacements, the solution for QCC$_{static}$ is unique for observed values of η_{eff} and QCC$_{eff}$.

Line-Shape Analysis

The ^{2}H line shape for backbone-labeled [d-(CGCGAAT*T*CGCG)]₂ is shown in Figure 28 as a function of hydration. There are several aspects of the ^{2}H line shape of the backbone-labeled [d-(CGCGAAT*T*CGCG)]₂ that need to be addressed. One of the primary changes is the reduction in QCC$_{eff}$, coupled with the observation of a nearly constant η_{eff} with increasing hydration. In modeling the local dy-
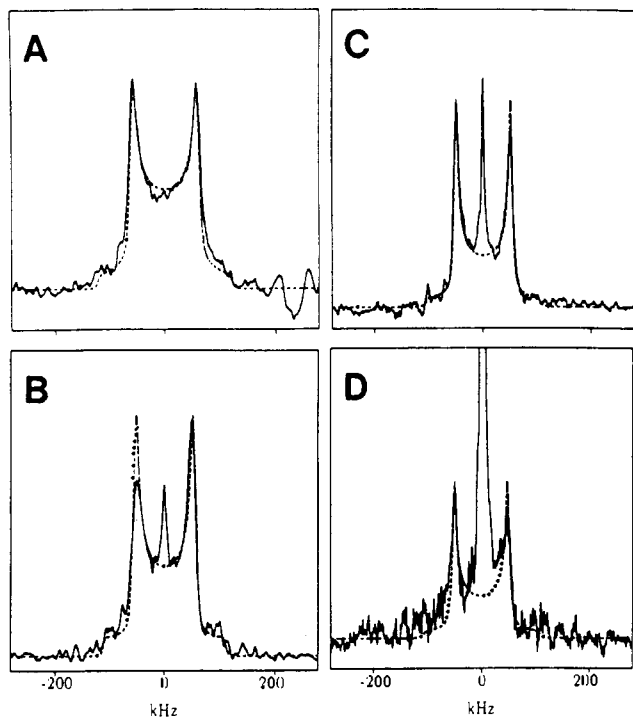
Figure 28. Experimental (—) and simulated (- -) 76.75-MHz deuterium quadrupole echo spectra of [5',5''-^{2}H$_{1,1}$]-2'-deoxy-thymidine-labeled [d(CGCGAAT*T*CGCG)]$_2$ for various levels of water content W (mol of H$_2$O/mol of water). The simulated spectra were calculated as described in the text, ignoring the central isotropic component. Using a pulse delay of 50 μs and $\pi/2$ pulse lengths varying from 2.3 to 3.0 μs, spectra were obtained for (A) 66% RH, W = 4.8, 60 000 scans; (B) 80% RH, W = 11.9, 116 750 scans; (C) 88% RH, W = 16.3, 144 000 scans; (D) 90% RH, W = 20.5, 288 000 scans.
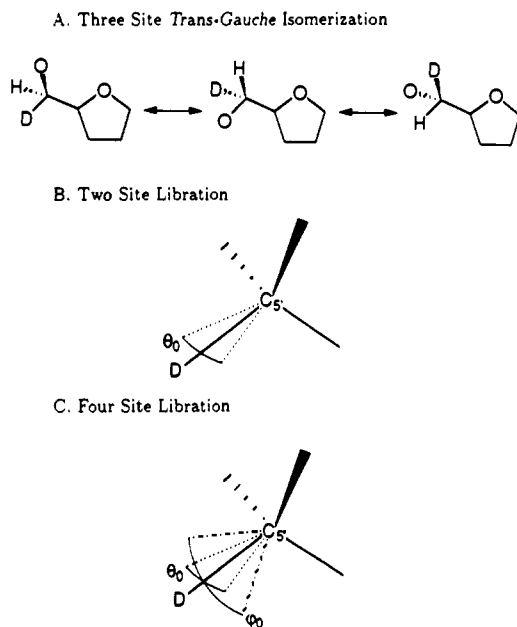

Figure 29. Representation of the different motional models considered: (A) three-site trans–gauche isomerization, (B) two-site libration of the methylene group with an amplitude θ_0, (C) four-site libration of the methylene group with amplitude θ_0 and ϕ_0.

namics of the backbone, the possibility of large conformational changes over a range of interconversion rates must be considered. In methylene chain polymers a crankshaft motion is often used to describe the molecular motions, and a similar model involving fluctu-
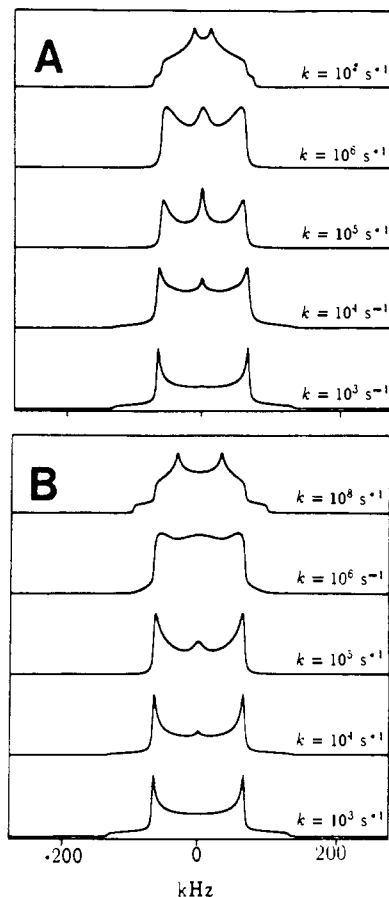

Figure 30. Simulations of backbone conformational conversions for a pulse delay of 50 μs as a function of jump rate k_{ij}. (A) Interconversion between gauche–gauche (+sc), gauche–trans (ap), and trans–gauche (–sc) with populations of 0.85 (site 1), 0.05 (site 2), and 0.10 (site 3), respectively. The site to site jump rates k_{12}, k_{13}, and $k_{2,3}$ were assumed to be equal. (B) Two-site diamond lattice jump with site population of 0.8 and 0.2 for differing jump rates k_{12}.

ations of the torsional angle ψ between the backbone conformations gauche–gauche (+sc), gauche–trans (ap) and trans–gauche (–sc),[9] with unequal site probabilities, has been applied to the dodecamer. Conformational energy surfaces for 5'-nucleotides have been computed for rotation about the exocyclic C4'–C5' bond. The +sc conformation corresponds to the global minimum, while the energy of the ap and –sc conformations were found to be only 1 kcal/mol[111] or 2 and 1.3 kcal/mol, respectively[112] above the minimum. In ref 112, Yathindra and co-workers calculated the populations for the various conformations using the expression

$$P(\chi,\phi) = 100 \times \exp\ [-V(\chi,\phi)/RT](\sum_{\chi,\phi} \exp\ [-V(\chi,\phi)/RT])^{-1}$$

(117)

where $V(\chi,\phi)$ is the potential energy. The surface was computed at 10° intervals of χ and ϕ, and values of 78% for +sc, 4% for ap, and 10% for –sc were reported. Line-shape simulations utilizing a discrete three site trans–gauche isomerization with unequal populations $p_{eq}(i)$ of 85, 5, and 10% for different jump rates k_{ij} ($i \neq j$) were initially investigated. The jump matrix $\mathbf{R}_{ij}$ used in the simulation must satisfy microreversibility, $k_{ij}p_{eq}(i) = k_{ji}p_{eq}(j)$ with k_{ii} being the negative sum of all rates depleting site i. The first model involves
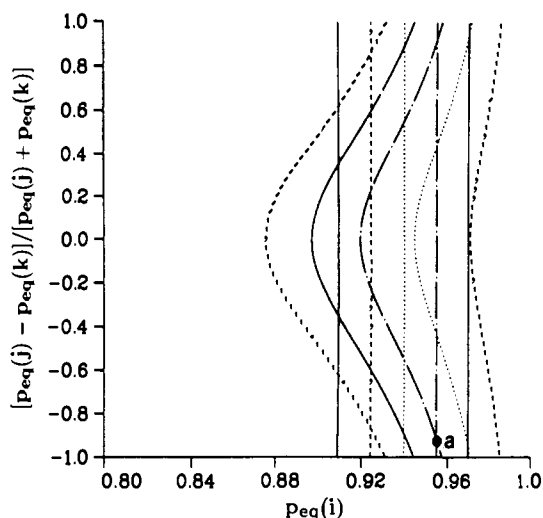
Figure 31. Variation in the reduction factor Λ and the effective asymmetry parameter η_{eff} for a discrete three-site trans–gauche isomerization as a function of the equilibrium population $p_{eq}(i)$ and the relative ratio of the remaining fractions $[(p_{eq}(j) - p_{eq}(k))/(p_{eq}(j) + p_{eq}(k))]$. Contours are for an experimentally relevant region of Λ (straight horizontal contours), 0.88 (—), 0.90 (– –), 0.92 (· ·), 0.94 (— ·), 0.96 (—), and η_{eff} (curved contours), 0.10 (– –), 0.08 (—), 0.06 (— ·), 0.04 (· ·), 0.02 (- -). The solution ($\bullet_a$) corresponds to the dry and 66% RH, W = 4.8 line shapes; the remaining hydration levels have no possible solutions.

isomerization about the C4′–C5′ bond, which is the C_3 symmetry axis for the 5′-tetrahedral carbon, as shown in Figure 29A. Variation of the line shape as a function of the jump rate k_{ij} is shown in Figure 30A. For large jump rates (fast exchange) the line shape undergoes significant averaging, leading to increased values of the effective asymmetry parameter ($\eta_{eff} > 0.2$), while exchange at intermediate rates distinct line shapes result; note particularly the disappearance of shoulders. An extension of this motional model is to restrict the motion to a two-site isomerization. Simulations using unequal site populations $p_{eq}(i)$ of 90% and 10% as a function of the jump rate k_{ij} are illustrated in Figure 30B. The differences between these simulations and experiment support the conclusion that large amplitude trans–gauche interconversion between conformations of substantial equilibrium probability do not occur in the oligonucleotide backbone at rates above $k_{ij} \approx 10^4$ s^{-1}. Figure 30A,B also reveal the insensitivity of quadrupolar echo line shapes analysis to conformational changes occurring at rates slower that $\sim 10^3$ s^{-1}.

Information for the entire range of equilibrium populations in the fast-exchange limit are easily obtained using eq 25 for a three-site isomerization, to produce surfaces of Λ and η_{eff}. Figure 31 shows a contour plot of the overlap between these two surfaces as a function of the equilibrium population $p_{eq}(i)$ and the relative distribution of the probability between the two remaining sites. The region shown is for the experimentally pertinent range (η_{eff} = 0–0.08 and Λ = 1.0–0.82).

If QCC$_{static}$ is assumed to be 175 kHz and η_{static} = 0 the line shape observed for the dry dodecamer corresponds to $\Lambda \approx 0.94$ and η_{eff} = 0.06. Inspection of Figure 31 reveals that a rapid three site trans–gauche isomerization with equilibrium population of $p_{eq}(1)$ = 0.94, $p_{eq}(2)$ = 0.05 and $p_{eq}(3)$ = 0.01 (or equivalently $p_{eq}(2)$ = 0.01 and $p_{eq}(3)$ = 0.05) will produce these fast-exchange line-shape parameters. The contour surface in

Figure 31 also reveals the lack of possible solutions that would produce averaged line shapes with η_{eff} = 0.06 and $\Lambda < 0.89$. Since the line shape observed at 75% RH (W = 10.5) corresponds to Λ = 0.87, a rapid isomerization is unable to simulate this or higher hydration levels. The lack of rapid trans–gauche isomerization of the backbone was not unexpected based on previous molecular mechanics studies[113] and molecular dynamics simulations,[114,115] in which the torsional angle ψ was the least flexible. In the molecular dynamics simulations of [d(CGCGAATTCGCG)]$_2$ and other oligonucleotides, trans–gauche isomerizations were not observed except in terminal nucleotides. Small variations in the torsional angle were observed during the 80–90 ps simulations with rms fluctuations of 7°[114] and 9°–10°.[115] Due to the inability of this three-site isomerization model to explain the observed variation of the line shape with increasing hydration, except for the limiting case of the dry dodecamer, this motional model was not pursued further.

The variation in QCC$_{eff}$ and η_{eff} has been simulated by various librational models in previous sugar and base investigations of the dodecamer. Since the static asymmetry parameter is assumed to be zero, the orientation of a librational plane with respect to a molecular or crystal frame is only possible from measurements on oriented samples. If the rate of internal libration is rapid, anisotropic librations can produce a nonzero effective asymmetry parameter η_{eff}. If additional motions occur within the sample (see later discussion) the orientation of these secondary motions can be described relative to the librationally averaged EFG tensor, but absolute orientation in a molecular or crystal frame will still require investigation of an oriented sample. While use of these models involves arbitrary orientations, consideration of the molecular or crystal environment may suggest preferred librational directions.

The simplest model considered is a two-site libration of the individual C–D bond (see Figure 29B). This model has been used to describe the base and methylene dynamics in the 2′-deoxythymidine monomer[90] and the sugar dynamics in 2′-deoxyadenosine,[118] along with the base dynamics in the labeled dodecamer.[50] Assuming QCC$_{static}$ = 175 kHz, η_{static} = 0.0, the reduction in QCC$_{eff}$ for dry (W = 0.0) and 66% RH (W = 4.8) can be accounted for by including a libration of θ_0 = 11.5° ± 1° using eqs 114 and 115. Using the relaxation expressions for a two-site libration, the $\langle T_1 \rangle$ of 505 ms for the dry (W = 0.0) dodecamer corresponds to a correlation time of 32 ps or 0.05 μs, while at 66% RH (W = 4.8) the $\langle T_1 \rangle$ of 206 ms corresponds to a two site correlation time of 85 ps or 0.02 μs. As observed in the monomer, the line shape is inconsistent with the larger correlation times. Attempts to extend this librational model to account for the 12 kHz reduction in QCC$_{eff}$ upon hydration to 75% RH (W = 10.5) were unsuccessful. The large librational angle required to produce the motional averaging results in an increased effective asymmetry parameter η_{eff} (easily seen from inspection of eq 115), a trend not observed experimentally.

Another possible model to describe the internal dynamics in the DNA backbone is a biaxial four-site jump (see Figure 29C), consisting of librations in two perpendicular planes.[50,67,71,116] The biaxial model was de-
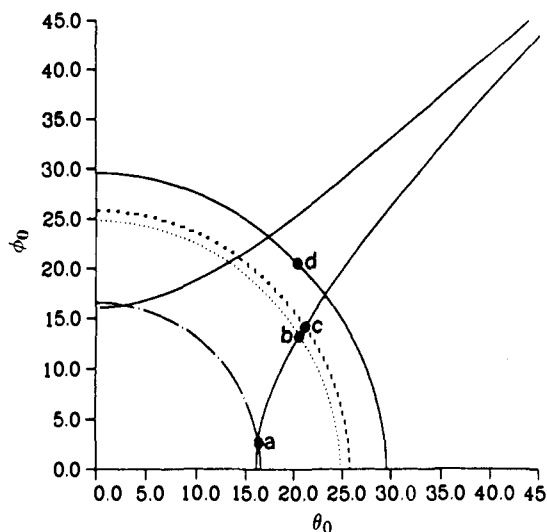
Figure 32. Variation in the reduction factor Λ and the effective asymmetry parameter η_{eff} for a discrete four-site libration as a function of the two half-angles of displacement θ_0 and ϕ_0 with equal site populations $p_{eq}(i) = 0.25$. Contours are for specific values of Λ (lower left concentric circles); 0.94 (— ·), 0.87 (· ·), 0.86 (- -), and 0.82 (—), and η_{eff} at 0.06 (—). Solutions for different hydration levels are shown: dry and 66% RH, $W = 4.8$ ($\bullet_a$); 75% RH, $W = 10.5$ ($\bullet_b$); 80% RH, $W = 11.9$ ($\bullet_c$); 88% RH, $W = 16.3$; and 90% RH, $W = 20.5$ ($\bullet_d$).

fined using θ_0 to describe librations parallel to the long helix axis of the dodecamer, and ϕ_0 to describe librations in the plane perpendicular to the helix axis. The variation in QCC_{eff} and η_{eff} with increasing relative humidity can be explained by changes in θ_0 and is presented as a contour overlay in Figure 32. Using the value $QCC_{static} = 175$ kHz and $\eta_{static} = 0.0$ the line shape of the dry ($W = 0.0$) and 66% RH ($W = 4.8$) sample were simulated with $\theta_0 = 16° \pm 2°$ and $\phi_0 = 4° \pm 2°$. At 75% RH ($W = 10.5$) the librational angles increased to $\theta_0 = 20.5° \pm 4°$ and $\phi_0 = 13.5° \pm 4°$, while at 80% RH ($W = 11.9$) the angles were $\theta_0 = 22° \pm 4°$ and $\phi_0 = 15° \pm 4°$. At 88% RH ($W = 16.3$) $\theta_0 = 20.5° \pm 3°$ and $\phi_0 = 20.5° \pm 3°$ which remained unchanged for 90% RH ($W = 20.5$). It should be noted that in the line-shape analysis the angles were restricted to $\theta_0 \neq \phi_0$ to fulfill the requirement $\eta_{eff} \neq 0$. Inspection of Figure 32 reveals that for a given Λ and η_{eff} only symmetry related solutions are possible within the range investigated.

Using the $\langle T_1 \rangle$ relaxation expressions for a four-site libration presented in section 2.3.1, the $\langle T_1 \rangle$ of 505 ms for the dry ($W = 0.0$) dodecamer corresponds to a rate of 6.5×10^9 or 5.4×10^6 Hz. Jump rates (k) are reported here, instead of the common correlation time τ_c, because the relaxation may involve a sum of exponentials relaxing at different multiples of the jump rate. This is easily evident from inspection of eq 57 for an N site jump process when $N > 3$. At 66% RH ($W = 4.8$) the $\langle T_1 \rangle$ of 206 ms corresponds to a jump rate of 2.7×10^9 or 1.3×10^7 Hz, while at 75% RH ($W = 10.5$) the $\langle T_1 \rangle$ is 59 ms with a jump rate of 1.6×10^9 or 2.2×10^7 Hz. With increase of the hydration level to 80% RH ($W = 11.9$) the $\langle T_1 \rangle$ of 41 ms corresponds to 1.3×10^9 or 2.8×10^7 Hz, while at 88% RH ($W = 16.3$) the $\langle T_1 \rangle$ of 40 ms corresponds to 1.5×10^9 or 2.4×10^7 Hz. Through the entire hydration range investigated there is only a factor of 4 variation in the rate of motion, and a factor of 2 variation in the root mean square amplitude of the

TABLE VIII. RMS Deviation of Biaxial Libration with Relative Humidity

% RH	Libration Angle, deg, of sample[a]				
	A	B[b]	C[b]	D[b]	E
dry	8 ± 1	5[b]	b	9[b]	12 ± 2
66	8 ± 1	7	10	10	12 ± 2
75	11 ± 2				17 ± 4
80	11 ± 2	9	12	14	19 ± 4
88	18 ± 2	5		16	21 ± 3

[a] A = [methyl-²H]-2'-deoxythymidine-labeled [d-(CGCGAAT*T*CGCG)]₂; B = [8-²H]-2'-purine-labeled [d-(CG*CG*A*A*TTCG*CG*)]₂; C = [6-²H]-2'-deoxythymidine-labeled [d(CGCGAAT*TCGCG)]₂; D = [2''-²H]-2'-deoxyadenosine-labeled [d(CGCGA*A*TTCGCG)]₂; E = [5',5''-²H₁:₁]-2'-deoxy-thymidine-labeled [d(CGCGAAT*T*CGCG)]₂. [b] Relative errors for libration angles were not reported for these samples, but are assumed to be similar to the errors for the methyl and 5',5''-labeled dodecamer.

four-site libration. The faster rates produced simulated line shapes that were consistent with the observed line shape in the dry and 66% RH dodecamer and were used for the remaining hydration level simulations.

It is interesting to compare the root mean square amplitude of the backbone deuterons obtained from this four-site libration model to the rms amplitude observed in previous ²H NMR investigations of the dodecamer, where the rms is defined as

$$\text{rms}(\theta_0,\phi_0) = \sqrt{\frac{\theta_0^2 + \phi_0^2}{2}} \qquad (118)$$

The results through 88% RH ($W \approx 15$) are shown in Table VIII. While the dynamic amplitude of the backbone deuterons is always greater than that observed for the base or sugar positions by 2°–6°, it never greatly exceeds the amplitude of base and sugar libration at any hydration level. The rms amplitude of 21° at 88% RH ($W = 16.3$) is smaller than the 27° fluctuations reported for the PH vector from solution NMR investigations of Hogan and Jardetzky.[15] This comparison may not be directly applicable since the dipolar relaxation involves dynamics over three bonds while the quadrupolar interaction simply involves reorientation of the EFG tensor. Rill and co-workers[117] observed the effects of intermolecular interactions on internal dynamics in the ¹³C NMR investigation of spontaneous ordering of DNA (147, 234, and 437 base pairs). At concentrations as low as 6.5 mg/mL motions of the C5' were slowed, while the dynamics of the C2' remained rapid even in the oriented phase. The concentration of the [5',5''-²H₁:₁]-2'-deoxythymidine-labeled dodecamer sample hydrated at 90% RH ($W = 25.5$) was 940 mg/mL. Due to the high concentration levels present, intermolecular interactions may account for the similarity between the observed rms amplitude of the backbone dynamics and the rms amplitude of the base or sugar 2''.

Characterization of the local mobility in nucleic acids from crystallographic data using a segmented rigid body model revealed that the phosphate backbone has the largest rms amplitude in comparison to other groups of the nucleotide.[79] The eigenvector clusters for the librational matrix were determined for the dodecamer. The rms amplitudes of the phosphate librations were found to be ca. 29° and 20°, while the librations of the
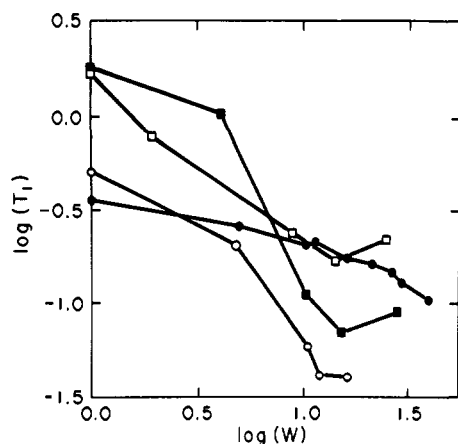
Figure 33. ^2H spin–lattice relaxation $\langle T_1 \rangle$ as a function of hydration level W for various labeled positions in the dodecamer: (O) [5',5''-$^2H_{1,1}$]-2'-deoxythymidine-labeled [d-(CGCGAAT*T*CGCG)]$_2$; (□) [8-^2H]-purine-labeled [d-(CG*CG*A*A*TTCG*CG*)$_2$]; (●) [methyl-^2H]-2'-deoxy-thymidine-labeled [d(CGCGAAT*T*CGCG)$_2$]; and (■) [2''-^2H]-2'-deoxyadenosine-labeled [d(CGCGA*A*TTCGCG)]$_2$.

ribose were 32° and 22° and the base librations were 14°, 17°, and 18°. The magnitude of these librations is significantly larger than those obtained from ^2H line-shape analysis using a four site librational model. These differences may be model dependent or reflect conformational disorder and rigid body librational disorder within the crystal.

Spin–Lattice Relaxation

The rate of these fast internal librations cannot be determined from analysis of quadrupolar echo line shapes alone except for a lower limit on the rate. While the fast librations have been modeled as a four-site jump, the exact nature of the motion, including the possibility of contributions from collective motions, cannot be determined from analysis of line shapes. A detailed investigation of spin–lattice relaxation at various magnetic field strengths, along with separation of the various spectral densities, would allow this problem to be addressed (see section 3.1.3). While such detailed analysis is not possible with the present [5',5''-$^2H_{1,1}$]-2'-deoxythymidine-labeled dodecamer, comparison of trends in the spin–lattice relaxation for various positions of the nucleotide is possible. Brandes and co-workers noted that the ratio between the ^{31}P relaxation obtained by Mai and co-workers[62] for the backbone and the ^2H relaxation of the purine bases in calf thymus DNA was approximately constant through hydration levels of $W = 20$. Similar trends were noted by Huang and co-workers[118] (see section 3.2.3) between the ^2H relaxation of the sugar 2'' and the purine base[50] within the dodecamer [d(CGCGAATTCGCG)]$_2$. These trends suggest that the backbone, sugar, and base motions are coupled. Similar comparisons can be made between all the ^2H-labeled sites of the dodecamer. Spin–lattice relaxation time as a function of hydration is shown in Figure 33. The variation in relaxation for the various positions is similar from 66% RH ($W = 4.8$) through 88% RH ($W = 16.3$), with the notable exception of the methyl-labeled position. This last observation is not surprising in that the relaxation of the methyl group is strongly influenced by the rapid (10–50 ps) motion about the C_3 symmetry axis. The trend in

the relaxation of the remaining labeled positions suggests that within the 12 base pair oligonucleotide, the motions of the backbone, the sugar 2'', and the purine bases are similarly coupled. Analysis of ^{31}P relaxation within the dodecamer is presently being pursued in our laboratory.

Slow Helix Motion

While the fast biaxial libration model describes the reduction in QCC_{eff} and η_{eff}, it does not explain all the observed variations in the line shape. Only the dry ($W = 0.0$) experimental line shape was adequately simulated using a fast librational model alone. The invariance of fast-exchange line shapes to pulse spacing is inconsistent with the observed spectra of the dodecamer sample at hydration levels above 66% RH ($W = 4.8$), which reveal a loss of center intensity with pulse spacing. Similar changes have been noted in previous investigations of ^2H base-labeled dodecamers, as described in section 3.2.1, and are characteristic of anisotropic motions in the slow and intermediate exchange regime.

The possibility of slow motion about the long helix axis in addition to fast four-site internal librations was the next model investigated. As described previously in eqs 96–99, a model of N-site nearest-neighbor jumps may be used to portray restricted diffusion about the helix axis. To model the effects of helix rotation on the line shape of the [5',5''-$^2H_{1,1}$]-2'-deoxythymidine-labeled dodecamer, the orientation of the EFG tensor with respect to the helix axis needs to be considered. Assuming model B-form DNA, the 5'- and 5''-C–D bond form angles of ca. 38° and 71° to the helix axis. The orientation of the biaxial libration was defined with displacements parallel to the helix rotation axis being defined as θ_0. It should be noted that different orientations of the biaxial librations produced effects on the simulated line shape that were small compared to the detail obtainable from the low signal to noise samples. The line shape at 66% RH ($W = 4.8$) was simulated by including a slow helix axis motion at $k = 1$ kHz, $\theta_{ij} = 5°$, corresponding to $D_R = 3.8$ s^{-1} (Figure 28A). At 75% RH ($W = 10.4$) and 80% RH ($W = 11.9$) this helix motion increased to $k = 6$ kHz, $\theta_{ij} = 5°$, $D_R = 22.8$ s^{-1} (Figure 28B). At 88% RH ($W = 16.3$) the simulation yields $k = 10$ kHz, $\theta_{ij} = 20°$, and $D_R = 609$ s^{-1} (Figure 28C). Even though the signal to noise is highly reduced, the line shape at 90% RH ($W = 20.5$) is consistent with $k = 100$ kHz, $\theta_{ij} = 20°$, and $D_R = 6092$ s^{-1} (Figure 28D).

The values for the rate and amplitude of helix motion were quite similar to those observed in previous sugar and base investigations of the dodecamer through 88% RH ($W = 16.3$). The fact that for hydration levels through $W \approx 20$ the model of fast librations combined with a slow helix motion can explain the observed line shapes for all ^2H-labeled dodecamers examined to date suggest that it is indeed a reasonable, while perhaps not unique model of dynamics in hydrated oligonucleotides.

The high hydration level of 90% RH ($W = 20.5$) could not be simulated with the values ($k = 400$ kHz, $\theta_{ij} = 60°$) obtained for the methyl-labeled dodecamer at 90% RH ($W = 21.2$), since these values produced a line shape with greater motional averaging than observed experimentally. This hydration level was not investigated for either the sugar-labeled dodecamer (see

discussion in the next section) or the base-labeled dodecamer.[50] In the investigation of the methyl and 2''-labeled dodecamer at hydration levels of $W > 20$, contributions from diffusion about an axis perpendicular to the long helix axis were also employed to explain finer aspects of the experimental data. The poor signal-to-noise observed for the [5',5''-^{2}H$_{1,1}$]-2'-deoxythymidine-labeled dodecamer does not warrant such a detailed analysis and will not be considered further. This inability to obtain rates that are consistent for the methyl- and backbone-labeled dodecamer at 90% RH may reflect subtle differences between the samples (i.e. hydration levels), or a weakness of the simplistic six-site jump to describe helix diffusion at higher hydrations.

In the analysis of the methyl-labeled dodecamer, echo decay times $\langle T_{2e} \rangle$ were used to discriminate between models of helix motion both as a function of hydration and temperature. This analysis consisted of comparing the echo decay rate from simulations to the decay rate observed experimentally. This comparison was performed for the [5',5''-^{2}H$_{1,1}$]-2'-deoxythymidine-labeled dodecamer. The rates were scaled to the $\langle T_{2e} \rangle$ observed in the dry sample and represent relaxation due to motional changes in comparison to the dry sample. These results do not compare favorably for any hydration level, with the simulated $\langle T_{2e} \rangle$ values being considerably smaller (a factor of 1.5–2.0). Variation in the rate and amplitude of helix motion required to produce similar $\langle T_{2e} \rangle$ values resulted in line-shape simulations that disagreed with experimental data. This may reflect a differential motion between the backbone and the methyl labels, but if there was additional intermediate helix motion at the 5',5''-positions, the experimental $\langle T_{2e} \rangle$ would be reduced from the observed value. It is also possible that there was backbone motion within the dry sample that was not observed in the methyl-labeled dodecamer, affecting the scaling of $\langle T_{2e} \rangle$. An alternative explanation is that the rapid 3-fold jump motion of the methyl grup reduces the effects of dipolar interactions which have been shown to modulate the echo decay,[119,120] while for the backbone-labeled sample these dipolar effects were not eliminated. Attempts to simulate the overall loss of signal intensity with variation in hydration were also unsuccessful. This discrepancy has been noted before and is most likely the result of instrumental variation during the 3–5 weeks of sample hydration.

In summary, the variation of the ^{2}H NMR spectra for the [5',5''-^{2}H$_{1,1}$]-2'-deoxythymidine-labeled dodecamer [d(CGCGAATTCGCG)]$_2$ was studied as a function of hydration level. With higher hydration levels there is a steady increase in the librational amplitude modeled using a four site jump model. The rms amplitude of this libration was only slightly larger than the motional amplitude observed in the sugar 2'' or base-labeled investigations. At higher hydration levels, slow motion about the helix axis must be included to account for the observed experimental line shapes, and is consistent with previous ^{2}H NMR studies involving the internal dynamics in synthetic oligonucleotides.

3.2.3 Furanose Ring Dynamics In [d(CGCGAATTCGCG)]$_2$

In this section we will discuss a ^{2}H NMR study of furanose ring dynamics in [d(CGCGAATTCGCG)]$_2$,

selectively deuterated at the H2''-position on the furanose rings of A5 and A6. Before proceeding, however, a brief discussion of prior knowledge on the conformation and dynamics of sugar rings in DNA will be presented. Primary sources of experimental information on localized motions of the furanose rings in polynucleotides include high-resolution NMR relaxation parameters, averaged scalar coupling constants, and X-ray diffraction data. Furanose rings in nucleosides are asymmetrically substituted and therefore the conformations assumed by the ring are not evenly weighted on the pseudorotation cycle. In fact, X-ray crystallographic studies of polynucleotides indicate that the conformations assumed by the sugar ring tend to cluster at two distinct and relatively narrow puckering conformations, namely C2'-endo and C3'-endo.[121-123]

The relative conformational energies of the C2'-endo and C3'-endo puckering modes have been the subject of several theoretical studies. For example, Levitt and Warshel[124] utilized a potential energy analysis, where the energy parameter was obtained through analysis of a large body of X-ray crystallographic, calorimetric, and spectroscopic data, and concluded that the energy barrier for the sugar conformation interconverting between C2'-endo and C3'-endo was only 1.4 kcal/mol. Olson and co-workers carried out a series of statistical computations to test various theoretical potential energy estimates of furanose pseudorotation[125,126] and suggested that the presence of endocyclic and exocyclic substituents in the sugar moiety introduces a potential barrier that opposes free pseudorotation.

NMR relaxation studies of internal dynamics in high molecular weight DNA have largely supported the occurrence of substantial and localized motions of the furanose rings on the time scale of nanoseconds. For example, on the basis of high-resolution ^{31}P and ^{13}C relaxation measurements, Jardetzky and co-workers[15] reported ^{31}P–^{1}H vector fluctuations of ±27° with a time constant of 2.2×10^{-9} s, base-plane fluctuations of ±20° with a time constant of 10^{-9} s, and fluctuations of the deoxyribose ring of ±20° to ±33° with a similar time constant. A similar view of the internal dynamics of very long DNA fragments has been reported in a series of papers by James and co-workers.[8,17]

Clore and Gronenborn[127] have reported a study of furanose ring dynamics in synthetic oligonucleotides. In that work, cross-relaxation rates between proton pairs were determined from the initial slope of the NOE build-up curves, from which the apparent correlation times were calculated using a model of internal motion which included a two-site jump and restricted diffusion or wobble within a cone, with the whole molecule assumed to undergo an isotropic tumbling motion. The results were claimed to indicate that the correlation time of the H2'–H2'' vector fluctuation to be 3-fold shorter than that of the H5–H6 vector and of the order of 10^{-9} s.

By far the most exhaustive study of sugar ring conformation dynamics has been performed by Altona and co-workers who, drawing from a large body of X-ray crystallographic data and ^{1}H NMR coupling constants, constructed a set of formulae which relate the magnitude of the scalar coupling constant between a given proton pair to the relevant bond torsional angles.[128-132] In this empirical approach, endocyclic torsional angles

TABLE IX°

5'-CGCGA*A*TTCGCG-3'[b] 3'-GCGCTTA*A*GCGC-5'

% relative humidity W (H_2O/nucleotide)	dry 0.0	66 4.1	80 10.4	88 15.3	92 28.3
T_1, s	1.80	1.04	0.110	0.070	0.089
T_{2e}, μs	330	330	190	150	112
QCC_{eff}, kHz/η	172/0.04	170/0.05	161/0.06	155/0.05	146/0.04
two-site libration	±9°	±10°	±13°	±14°	±16°
liaxial libration (±θ, ±ϕ)	±12°, ±4°	±13°, ±4°	±18°, ±8°	±18°, ±14°	±22°, ±18°
(rms)	8.9°	9.6°	13.9°	16.1°	20.1°
cone diffusion (S_{zz}, θ_0)	0.93, 17.7°	0.907, 20.5°	0.85, 26.5°	0.82, 29.0°	0.79, 31.7°

°Motional amplitudes in Table IX were calculated from a fit to QCC_{eff}. See the text for details. [b]A* refers to [2″-²H]-2'-deoxyadenosine. °Static quadrupole coupling constant (QCC) = 178 kHz, static asymmetry parameter (η) = 0.00.

in five-membered rings were described by a pseudorotation phase angle and an amplitude of puckering, and the authors suggested that conformational interconversion is a process of hindered pseudorotation with a correlation time on the nanosecond time scale, proceeding through the O4'-endo conformation and maintaining a constant puckering amplitude of ~38°.

Bax and Lerner[84] have analyzed the H2'-H2″ and H3'-H4' coupling constants of the sequence [d-(CGCGAATTCGCG)]₂ utilizing a program developed by Altona and co-workers. By confining the minor conformer to the 3'-endo conformation with a 36° amplitude of pucker, the analysis indicated that the population of the major conformer ranges from 74% to 99% with a puckering amplitude of ca. 33°-38° for the individual deoxyribose sugar moieties in the sequence.

A somewhat different view of the structure of the DNA dodecamer [d(CGCGAATTCGCG)]₂ has been reported by Reid and co-workers.[82,83] That structure, derived using distance geometry techniques, displays kinks in the C3-G4 base step and at the A6-T7 base step, which appear similar to those reported for the EcoRI restriction site DNA bound to its endonuclease.[133] Although this solution structure differs in several respects from the crystal structure as reported by Dickerson and Drew,[73] the conformations reported by both studies for the sugar rings of A5 and A6 are quite similar, the NMR study reporting ^0_1T conformations for both sugars and the X-ray study reporting $_1E$ (C1'-exo) conformations for both sugars.

Torchia and co-workers[134,135] have reported a solid-state ²H NMR investigation of sugar ring flexibility in single nucleosides where an enzymatic synthesis was used to produce 2'-deoxyguanosine-2'-d_2 and 2'-deoxythymidine-2'-d_2 (both protons at the C2' ring position were deuterated). This investigation showed significantly shorter T_1 values than expected for a rigid system: <1 s for deoxyguanosine and ~0.15 s for deoxythymidine. The authors suggested the presence of small amplitude motion of the furanose ring on a time scale of <10^{-6} s which may be independent of the nature of the base. The authors also observed only about one-half of the expected ²H signal intensity of deoxyguanosine when compared with a known weight of methylene-deuterated polyethylene and interpreted this fact as indicating that a significant fraction of the sample undergoes motion of the furanose ring on a time scale within the intermediate rate regime. The authors suggested that this may be due to interconversion between different sugar ring conformations.

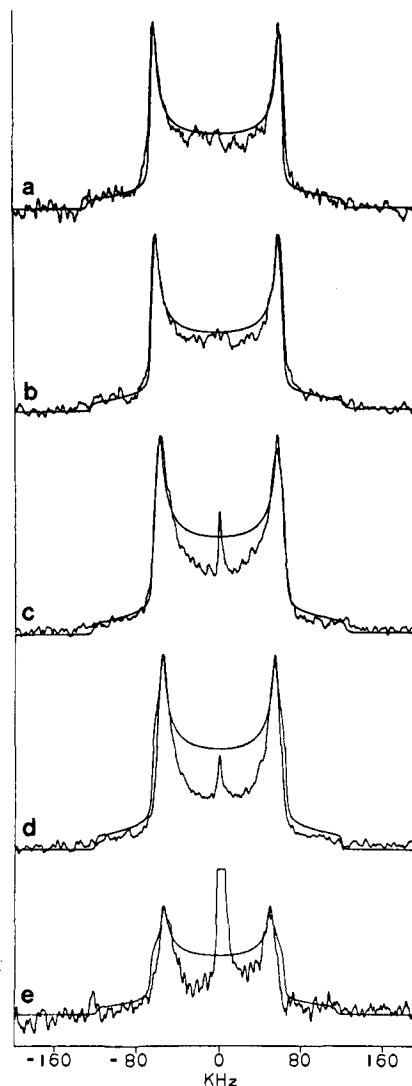The ²H NMR spectrum of the DNA dodecamer [d-(CGCGA*A*TTCGCG)]₂ deuterated at the 2″-position

Figure 34. Solid-state ²H NMR line shape of [2″-²H]·2'-deoxyadenosine labeled [d(CGCGA*A*TCGCG)]₂ as a function of hydration level for (A) dry DNA, (B) DNA equilibrated at 66% RH, (C) 80% RH, (D) 88% RH, and (E) 92% RH. Solid lines are theoretical spectra calculated assuming a two site jump model with jump amplitude ranging from ±9° for dry DNA to ±16° for DNA equilibrated at 92% RH and static parameters QCC_{static} = 178 KHz and η_{static} = 0.0.

on A5 and A6 is shown in Figure 34 as a function of hydration level. The corresponding ²H NMR spectral and relaxation parameters are given in Table IX. The water content profile (the number of moles of water per mole of nucleotide, W, versus relative humidity, RH) of this sugar-deuterated dodecamer is essentially the same as previously discussed for base- and backbone-

deuterated $[d(CGCGAATTCGCG)]_2$. Spectral data in Table IX indicate a decrease in QCC_{eff} from 172 kHz in dry samples to 146 kHz in samples equilibrated at 92% RH. The effective asymmetry parameter η_{eff} remains about constant at 0.04–0.06. As will be discussed below, the modest decrease in QCC_{eff} over the observed range of hydration suggests that any fast regime motions at the 2″-sites on A5 and A6 must be low in amplitude. Large amplitude motions ($\gg 20°$) in the fast rate regime would tend to produce far more drastic averaging of the EFG tensor, and consequently of the ^2H line shape, than would be suggested by the experimental data. However, the 30-fold decrease in $\langle T_1 \rangle$, the 3-fold decrease in $\langle T_{2e} \rangle$, the decrease in QCC_{eff} over the observed hydration range, and the distortion of the quadrupolar echo spectral line shape as a function of pulse spacing at high levels of hydration suggest the occurrence of nonnegligible dynamics at the 2″-sites of A5 and A6.

Line-shape trends shown in Figure 34 generally support the existence of significant motions of the 2″-sites of A5 and A6 in the slow and/or intermediate rate regimes at high levels of hydration. As indicated in Table IX, QCC_{eff} decreases from 172 to 146 kHz as W increases from 0 to 28.3 (92% RH), a trend that may be reproduced by a number of N-site jump or diffusive models occurring at rates in the fast regime. However, ^2H line shapes obtained from samples equilibrated at $\geq 80\%$ RH consistently show less intensity in the center of the powder pattern than would be predicted assuming that the internal dynamics can be described by small amplitude, fast motions (Figure 34C–E), a trend also observed in base-deuterated dodecamers. Such distortions of quadrupolar echo spectra are known to be produced by anisotropic motions in the slow/intermediate rate regimes.[36,136]

Although changes in the ^2H powder pattern shape as a function of hydration level for 2″-deuterated and base-deuterated DNAs are similar in a number of respects, there are also a number of differences. In base-deuterated DNA dodecamers QCC_{eff} decreases precipitously from 170 kHz at 88% RH to 71 kHz at 92% RH, whereas the QCC_{eff} of 2″-deuterated DNA dodecamers shows much less averaging over the same hydration range (Figure 34 and Table IX). Even more interesting is the comparative loss in spectral intensity as a function of hydration for base-deuterated and 2″-deuterated DNA dodecamers. In base-deuterated DNA the relative spectral intensities for the hydration series (RH) 66%:80%:88% was 1.0:~0.7:~0.2,[50] a 5-fold loss, whereas over the same hydration range, the relative spectral intensities obtained from 2″-deuterated samples were 1.0:~0.77:~0.74, indicating a reduction in relative spectral intensity of only 25%. In the following section, these observations will be evaluated with the goal of developing a motional model that describes the local dynamics of the sugar ring as well as the whole-molecule dynamics in a way consistent with studies of base and methyl-deuterated DNA dodecamers.

Line-Shape Analysis

Information on static QCC and asymmetry parameter values have been derived from ^2H NMR studies of 2′-deoxyadenosine-2″-d_1.[118] From the simulation of the

^2H line shape of the monomeric nucleoside an effective asymmetry parameter η_{eff} of 0.02 and an effective deuteron quadrupole coupling constant QCC_{eff} of 172 kHz are derived.

At low hydration levels (W), the dynamics of the 2″-deuterons on A5 and A6 may be described by simple jump or diffusive models with rates in the fast regime. Simulation of the ^2H powder pattern of the lyophilized 2″-deuterated DNA dodecamer yields a QCC_{eff} of 172 kHz with an η_{eff} of 0.04. Similarly, simulation of the ^2H powder pattern of the same sample equilibrated at 66% RH ($W = 4.1$) results in a QCC_{eff} of 170 kHz and an η_{eff} of 0.05. Assuming a QCC_{static} of 178 kHz and a η_{static} of zero, as determined from studies of 2′-deoxyadenosine-2″-d_1, described above, and assuming the dynamics of 2″-sites at A5 and A6 can be described as a 2-fold jump, the ^2H powder line shapes (Figure 34A,B) may be reproduced by a librational amplitude of $\pm 9°$ in dry DNA, increasing slightly to $\pm 10°$ at 66% RH. QCC_{eff} decreases from 161 kHz at 80% RH to 155 and 146 kHz at 88% and 92% RH, respectively, a trend that can be reproduced by assuming an increase in the librational amplitude from $\pm 13°$ at 80% RH to $\pm 14°$ at 88% RH and $\pm 16°$ at 92% RH, but the line shapes obtained at these hydration levels are not reproduced (Figure 34C–E).

Other models may be considered to describe internal motions in DNA. The biaxial jump model described above can also reproduce the QCC_{eff} trend observed in Figure 34 and Table IX. Biaxial jump amplitudes θ and ϕ are found to be $\pm 12°$ and $\pm 4°$ in dry DNA (rms = 8.9°), $\pm 13°$ and $\pm 4°$ at 66% RH (rms = 9.6°), $\pm 18°$ and $\pm 8°$ at 80% RH (rms = 13.9°), $\pm 18°$ and $\pm 14°$ at 88% RH (rms = 16.1°), and $\pm 22°$ and $\pm 18°$ at 92% RH (rms = 20°). Like the two-site jump model, however, the biaxial jump model does not reproduce the line shapes shown in Figure 34C–E.

Brandes et al.[66] have proposed the use of a diffusion-in-a-cone model to describe the restricted motion of purine-labeled polynucleotides. This model produces symmetrically averaged EFG tensors ($\eta_{eff} = 0$), if the motion occurs in the fast rate regime and if the static asymmetry parameter is zero. In the current study, as in the study of base- and methyl-deuterated DNA dodecamers,[110] deviations of observed ^2H line shapes from axial symmetry imply that cone diffusion cannot account for all the fast internal dynamics in oligonucleotides. However, ignoring deviations from axial symmetry, and defining θ_0 as the half-angle of the cone in which the C–D bond axis is allowed to freely diffuse, the amplitude of local motions may be estimated for this model, assuming the effective quadrupolar coupling constant QCC_{eff} is given by eqs 97 and 98. Assuming that cone diffusion describes the sugar ring dynamics, the model yields $S_{zz} = 0.97$ and $\theta_0 = 11.5°$ in the dry dodecamer, $S_{zz} = 0.96$ and $\theta_0 = 14.1°$ at 66% RH, $S_{zz} = 0.90$ and $\theta_0 = 21.5°$ at 80% RH, $S_{zz} = 0.87$ and $\theta_0 = 24.5°$ at 88% RH, and $S_{zz} = 0.82$ and $\theta_0 = 28.9°$ at 92% RH.

Dynamical models based on small amplitude motions in the fast state regime cannot account for ^2H line shapes observed at higher hydration levels. In particular, the central part of the experimental powder patterns are consistently too low in intensity, but this feature can be simulated by assuming the presence of

internal motions occurring at rates on the order of 10^4–10^5 Hz. To develop a model of this intermediate regime motion, we first recall the observation stated above that the quadrupolar echo intensity of the sugar-deuterated sample diminishes by only 25% in going from W = 4.1 (66% RH) to W = 10.4 (88% RH), an observation that is in contrast to studies of base-deuterated DNAs where much greater attenuations of echo intensity have been observed.[50,90] We may resolve these seemingly disparate data with the following model. Assuming that the principal axis of the EFG tensor of the D6 aromatic deuteron is approximately perpendicular to the helix axis and the principal axis of EFG tensor of the 2″-deuteron makes a small ($\leq 30°$) angle with the helix axis, the difference in echo intensity as a function of hydration for 2″-deuterated DNAs and base-deuterated DNAs may be explained if the intermediate regime motion is assumed to be a restricted reorientation about the helix axis. Fiber-diffraction studies[47-49] indicate that as DNA is progressively hydrated from W = 4.1 to W = 10, the transition from A to B form occurs, and we assume that at W = 10 the DNA is sufficiently hydrated to allow the onset of helix twisting motions at rates on the order of 10^4 Hz. This motion in turn produces an attenuation of the quadrupolar echo amplitude which is maximal for base deuterons, and less extreme for 2″-deuterons if the sugar rings exist in conformations in which the C–D vector makes a moderate angle ($< 30°$) with the helix axis. In fact, the angle between the C2′–D2″ bond axis and the helix axis is sensitive to the conformation of the sugar ring. As shown in Figure 3 (see small arrow) for the dodecamer [d(CGCGAATTCGCG)]$_2$ in the ideal B form, where the sugar rings are in the C2′-endo conformation, the C2′-D2″ bond axis of A5 makes an angle of about 20° with the helix axis. In A-form DNA, on the other hand, where the sugar rings are in the C3′-endo conformation, the same bond axis makes an angle of about 90° with the helix axis.

Restricted diffusion about the helix axis may be approximated as described in section 3.2.1 using eqs 104 and 105 to calculate the diffusion coefficient. As in our studies of base-labeled and backbone-labeled DNA dodecamers (see sections 3.2.1 and 3.2.2), the number of sites, N, was typically limited to 6 in order to minimize computational time. Increasing N beyond 6 produced subtle line-shape changes, but these changes were not considered significant given the limited signal-to-noise of our spectral data.

At low hydration levels, where torsional motions about the helix axis are negligible, the orientation of the librational axis of the sugar ring cannot be determined in a polycrystalline sample because the EFG tensor is uniaxial (η_{static} = 0). At higher levels of hydration however, the mutual orientation of the helix axis and the axis of libration of the C2′–D2″ bond becomes important. To proceed further we assume that the axis of local libration of the C2′–D2″ bond is perpendicular to the helix axis. The reduction of QCC$_{eff}$ to 161 kHz at 80% RH can then be simulated assuming a two-site libration about this perpendicular axis with an amplitude of ±13°. To invoke a slow rotation of the helix axis we assume the sugar ring exists in a conformation such as C2′-endo, where the C2′–D2″ bond makes an angle of about 20° with the helix axis. NMR studies of
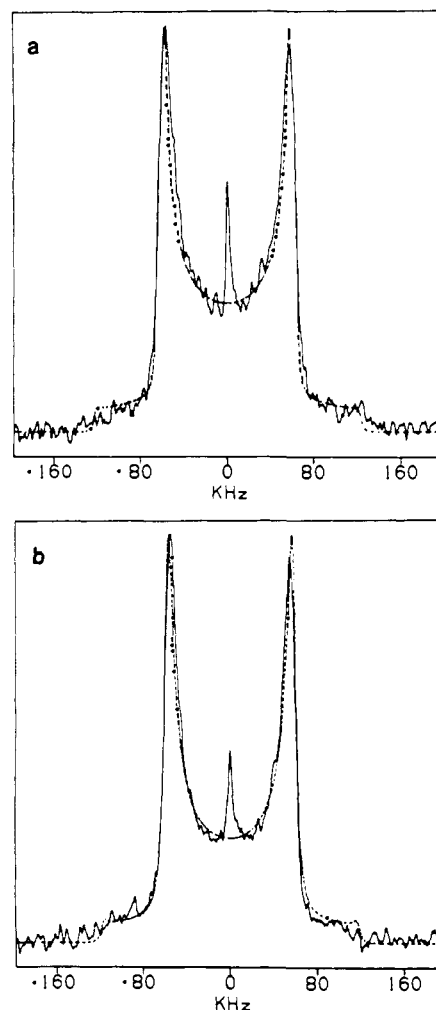

Figure 35. (A) ^{2}H NMR line shape for DNA dodecamer, deuterated at the 2″ position of A5 and A6, equilibrated at 80% RH. The broken line corresponds to a dynamical model of restricted reorientation about the helix axis, N = 6, θ_{ij} = 5°, k = 6.9 kHz. (B) ^{2}H NMR line shape for DNA equilibrated at 88% RH. The broken line corresponds to a model of restricted reorientation about the helix axis, N = 6, θ_{ij} = 20°, k = 13 kHz.

methyl-deuterated dodecameric DNA[110] indicate that at 80% RH torsional motions about the helix axis may be modeled as a six-site jump (N = 6) with a θ_{ij} of about 5° at a rate of 1 kHz. Studies of that same dodecamer deuterated at the H6 site on T7 similarly obtain a θ_{ij} of 5° at a slightly higher rate of 3.3 kHz. As shown in Figure 35A, essentially the same model of torsional motions applies to 2″-deuterated DNA dodecamers with the line shape of the 80% RH data being successfully reproduced, assuming θ_{ij} = 5° at a rate of 6.9–9.8 kHz. Assuming a slightly larger value of jump angle θ_{ij} = 10° results in a best fit for rates 4.9–6.9 kHz.

Samples hydrated at 88% RH absorbed ∼15 molecules of water per nucleotide and the DNA assumed a gel-like consistency. As indicated in Table IX, QCC$_{eff}$ decreases to 155 kHz at 88% RH from 161 kHz at 80% RH, a trend that can be reproduced by increasing the amplitude of fast libration to 14°. ^{2}H NMR studies of methyl-deuterated DNA dodecamers equilibrated at 88% RH indicate that torsional dynamics about the helix axis can be simulated using the same N site jump models as in the 80% RH case, only using somewhat larger values of θ_{ij} and slightly higher jump rates. This is a physically reasonable approach in view of the fact
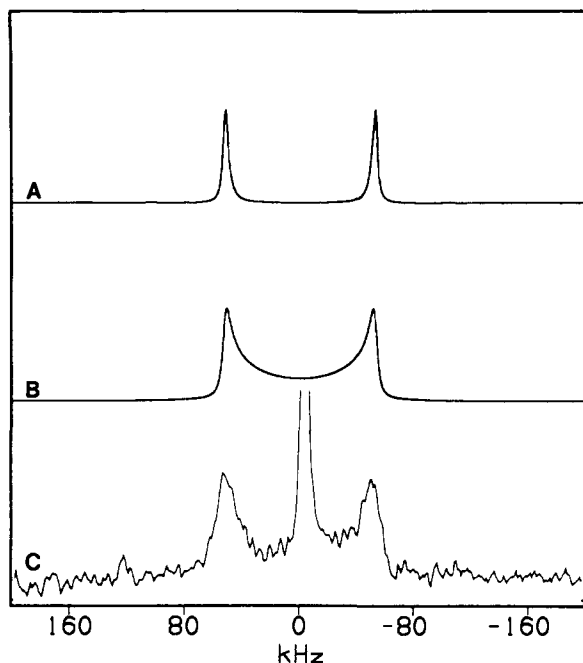
Figure 36. (A) Theoretical spectrum assuming formation of a liquid–crystalline phase with 70% of the sample existing in ordered domains with the helix axes perpendicular to the magnetic field and a Gaussian ordering profile of $\sigma = 25°$. A dynamical model of free diffusion about the helix axis at 100 kHz is assumed with a fast libration of the furanose ring about an axis perpendicular to the helix axis with an amplitude of 16°. (B) Similar model to A but adding a helix wobble of 11° at a rate of 1.5 MHz and a somewhat reduced sugar ring libration of 14°. (C) Experimental spectrum.

that further hydration of DNA above 80% RH simply adds water to spaces between DNA molecules, allowing less restricted reorientation about the helix axis. As shown in Figure 35B, the line shape of DNA equilibrated at 88% RH can be simulated, assuming $\theta_{ij} = 20°$ and a rate of about 9.8–13 kHz.

Simulation of the experimental ^2H NMR spectrum of 2″-deuterated DNA hydrated at 92% RH presents a considerable problem. ^2H NMR studies of methyl-deuterated [d(CGCGAATTCGCG)]$_2$ indicate that at a hydration level of $W = 26.6$, the DNA is partially ordered into liquid–crystalline domains in which the helix axis is oriented perpendicular to the magnetic field, with about 70% of the DNA in liquid–crystalline domains and the remaining 30% randomly ordered.[110,144] At a hydration level of $W = 29.6$ the fraction of randomly ordered DNA approaches zero. Internal motions in both domains were described by free diffusion about the helix axis at a rate of about 400 kHz, but the low signal-to-noise of the spectra of 2″-deuterated DNA at 92% RH precludes such detailed modeling of the degree of ordering and the internal dynamics. As shown in Figure 36A, however, assuming approximately the same degree of long range ordering as in the methyl-deuterated sample, together with internal motions described as a local libration of the furanose ring of ±16° and diffusion around the helix axis at a rate on the order of 100 kHz results in a rather poor fit to the experimental spectrum shown in Figure 36C.

It is not unreasonable, however, to assume that a DNA dodecamer may be undergoing restricted reorientations about axes other than the helix axis. In studies of methyl-deuterated DNA dodecamers, a rough

estimate of contributions from diffusion about an axis perpendicular to the helix axis was obtained from consideration of the dynamics of spherocylinders.[105,106] Assuming the diameter of an oligonucleotide is about 24 Å and the length is given by $N \times 3.4$ Å, where N is the number of base pairs ($N = 12$ for a dodecamer), the length-to-diameter ratio of the DNA dodecamer is about 1.7. The theory of Tirado et al.[105,106] indicates that the ratio of the diffusion coefficient for reorientation about an axis parallel to the helix axis ($D_{\parallel}$) to the diffusion coefficient for reorientation about an axis perpendicular to the helix axis ($D_{\perp}$) should equal about 1.9 for an oligonucleotide with a length-to-diameter of 1.7. Including a slow helix wobble (restricted rotation about an axis perpendicular to the helix axis) with an amplitude of 22° and a rate of 1.56 MHz in addition to unrestricted diffusion about the helix axis at a rate of 400 kHz produces slightly improved fits of experimental spectra of methyl-deuterated DNA dodecamers at hydration levels above 90% RH. Including essentially the same wobbling motion in a fit of 2″-deuterated DNA results in substantially improved fits to experimental data, except that QCC_{eff} becomes too small (<146 kHz) if the amplitude of local libration is assumed to be 16°. Reducing the libration amplitude to the value at 88% RH (±14°) resulted in the spectrum shown in Figure 36B.

Spin–Lattice Relaxation Data

Brandes et al.[69] have measured both the Zeeman relaxation time T_1 and the quadrupolar relaxation time T_{1Q} at two different values of magnetic field strength, which enables a study of the individual spectral densities $J_1(\omega_0)$ and $J_2(2\omega_0)$ as a function of frequency. In this study, T_1 at a single field strength has been measured, and although we cannot present as complete an analysis of the dynamics of the 2″-deuterated DNA dodecamer as has been applied to purine base motion in high molecular weight DNA, a comparison of trends in Zeeman relaxation as a function of hydration level with earlier studies of base-deuterated DNAs as possible.

Zeeman spin–lattice relaxation times $\langle T_1 \rangle$ for the 2″-deuterated DNA dodecamer as well as base and backbone deuterated dodecamers are plotted as a function of hydration level in Figure 33. $\langle T_1 \rangle$ for the 2″-deuterons of A5 and A6 is 1.8 s in the dry, lyophilized dodecamer, which is about equal to the value of 1.66 s reported by Kintanar et al.[50] for the H8-deuterated dodecamer, and somewhat shorter than the 7 s reported by Brandes et al. for H8-deuterated high molecular weight Li–DNA.[69] Hydration at 66% RH resulted in a moderate decrease in the $\langle T_1 \rangle$ of the 2″-deuterated dodecamer to 1.04 s in comparison to the hydrated H8-deuterated dodecamer, which decreased to 0.78 s, and the H8-deuterated high molecular weight Li–DNA, which decreased to 0.30 s. In going from 66% to 80% RH, $\langle T_1 \rangle$ of both the H8-deuterated and the 2″-deuterated DNA dodecamers decreased markedly to values of 0.11 and 0.24 s, respectively. Mai et al.,[62] in a ^{31}P NMR study of the backbone dynamics of the Na salt of calf thymus DNA, observed a similar decrease in the ^{31}P spin–lattice relaxation time and suggested that the transition from A- to B-form DNA occurs with an increase in internal motion, thus accounting for the re-

duction of T_1. Brandes et al.[45] in a ^{2}H NMR study of both the Na and the Li salts of high molecular weight DNA also observed a similar decrease in T_1, but disagreed with the attribution of this T_1 decrease to the onset of the new motional regime caused by conversion to B-form DNA produced this T_1 decrease since their Li–DNA remained in the B form throughout the hydration range covered by their study.

Brandes et al. also noted that up to a hydration level of $W = 20$, the ratio of the ^{31}P and ^{2}H spin–lattice relaxation times is approximately constant, implying that base and backbone motions are coupled. In fact, inspection of Figure 33 shows that the $\langle T_1 \rangle$ values for H8-deuterated and 2″-deuterated DNA dodecamers also vary in constant proportion as a function of hydration level between 80% and 92% RH, implying a similar coupling between base and furanose ring motions in DNA dodecamers. Models incorporating collective torsional modes into the internal dynamics of DNA have long been used to explain FPA and EPR data of DNA solutions[23–26] and may be invoked to explain the apparent coupling of the base and furanose ring motions in DNA dodecamers as well. In this picture, the increased amplitudes of the fast regime motions of the C–D bond vectors on the base and furanose rings at high levels of hydration may be due in part (or entirely) to collective motions of the polymer. In a recent study, Brandes et al. note that the large ratio of $J_1(\omega_0)$ to $J_2(2\omega_0)$ measured for H8-deuterated high molecular weight DNA excludes the possibility that in-plane torsional motions is the dominant relaxation mechanism in DNA for hydration levels up to 84% RH ($W = 13$), but note that the ratio decreases at higher hydration levels. The possibility that coupled torsions are responsible for the $\langle T_1 \rangle$ trend observed in Figure 36 remains. We note that studies of the frequency dependence and the dependence of ^{2}H relaxation on oligonucleotide length would be helpful in elucidating the nature of internal motions in synthetic DNAs. Such studies, as well as relaxation and line-shape studies of DNA oligomers selectively deuterated on the H5′/5″[62] sites, are in progress in this laboratory.

Summarizing our ^{2}H NMR study of the furanose ring dynamics of the DNA dodecamer [d-(CGCGAATTCGCG)]$_2$:

(a) The amplitude of fast regime motions of the furanose rings of A5 and A6, as elucidated by the effective quadrupolar coupling constant QCC$_{eff}$, increases from about 9° in dry, lyophilized samples to about 16° in samples equilibrated at 92% RH ($W = 28.3$), assuming a simple two site jump model, a QCC$_{static}$ of 178 kHz, and an asymmetry parameter of zero. Other simple jump or restricted diffusion models similarly yield small motional amplitudes. Assumption of a smaller QCC$_{static}$ would moderate these amplitudes even further, as would the assumption of a static asymmetry parameter greater than zero. For example, if a QCC$_{static}$ of 173.7 kHz is assumed, the amplitude of the fast regime motion of the furanose ring (modeled as a two-site jump) is only 3–4° in the dry dodecamer, ~5° for the dodecamer at 66% RH, ~9° at 80% RH, ~11° at 88% RH, and ~13° at 92% RH.

(b) Studies of ^{2}H Zeeman relaxation as a function of hydration level indicate that above 80% RH, the motions of the bases and furanose rings appear to be coupled, implying that part, or all, of the decrease in QCC$_{eff}$ may be due to collective motions of the oligomer, as opposed to an increase in the amplitude of localized motions of the furanose rings.

(c) Over the hydration range studied, there is no ^{2}H NMR evidence to suggest the occurrence of an interconversion between the C2′-endo and C3′-endo conformations (or any other conformations where the change in amplitude is greater than 16°) of the furanose rings of A5 and A6 on the nanosecond time scale or at any rate greater than 10^4 or 10^5 Hz.

(d) Changes in the ^{2}H line shape over the hydration range 66% RH ($W = 4.1$) to 92% RH ($W = 28.1$) can be accounted for by a modest increase in the amplitude of fast regime motions of the furanose rings together with the onset of reorientations about the helix axis, which increase in amplitude and rate with hydration level. Models of restricted motion about the helix axis used to fit the line shapes of 2″-deuterated DNA oligomers at 80% and 88% RH are in excellent agreement with models used in similar studies of methyl-deuterated DNA dodecamers. Rates of restricted reorientation about the helix axis derived from line-shape studies of 2″-deuterated and methyl-deuterated DNA dodecamers are also in agreement with similar studies of H8-deuterated DNA dodecamers hydrated at 80% RH, but differ by an order of magnitude for H8-deuterated dodecamers hydrated at 88% RH. Line-shape simulations in this latter case, however, were of spectra of very low signal-to-noise, and derived rates were only approximate.

(e) Line-shape data of 2″-deuterated DNA dodecamers hydrated at 92% RH are of limited signal-to-noise and therefore preclude detailed modeling of the motion of the furanose rings. However, the large QCC$_{eff}$ eliminates the possibility of large amplitude motions on the nanosecond time scale, and the general line shape is consistent with the formation of a liquid–crystalline phase.

4.0 Properties of the Aligned Phase of Oligonucleotides

Thus far investigation of structural questions in DNA by ^{2}H NMR has been limited to characterization of purine base tilt and order in oriented DNA films and fibers.[57,65–68,71] Recalling the discussion of ^{2}H NMR studies of DNA fibers in section 3.1.3, Shindo and co-workers[71] reported a base tilt of ~20° for A-form DNA and ~0° ±10° for B-form DNA. Investigation of oriented Li–DNA by Brandes and co-workers[68] found the average base tilt $\overline{\Theta}_T \approx 0°$ with $\sigma_T = 9°$ for the B-form DNA at $W \approx 10$ (mol of H$_2$O/mol of nucleotide), while Na–DNA in the A form ($W = 8.6$) resulted in $\overline{\Theta}_T \approx 23°$ and $\sigma_T \approx 4°$. The static order was also investigated, with changes in W for oriented Li–DNA and was found to decrease from $\sigma = 17°$ at $W = 0.5$ to $\sigma = 9°$ for $W = 6$ through $W = 13.4$.

The formation of a liquid-crystal phase by high molecular weight DNA at high concentration was reported long ago in the literature,[140–143] and a preliminary ^{2}H NMR investigation of the oriented phase and dynamics using the [methyl-^{2}H]-2′-deoxythymidine-labeled dodecamer has also been reported.[144,145] In the DNA dodecamer a liquid-crystal phase was found to exist for

concentrations ranging from 490 to 722 mg/mL, with the helix axis aligning perpendicular to the magnetic field. This section presents a structural investigation of the selectively deuterated synthetic oligonucleotide [d(CGCGAATTCGCG)]$_2$ in the liquid-crystal phase. Three different samples, [methyl-^{2}H]-2'-deoxy-thymidine-labeled [d(CGCGAAT*T*CGCG)]$_2$, [8-^{2}H]-2'-deoxyadenosine, [8-^{2}H]-2'-deoxyguanosine-labeled [d(CG*CG*A*A*TTCG*CG*)]$_2$, and [2''-^{2}H]-2'-deoxyadenosine-labeled [d(CGCGA*A*TTCGCG)]$_2$, were investigated. By analysis of line shapes obtained at reduced temperatures for these highly hydrated samples, information concerning the base and sugar conformation and order were obtained.

4.0.1 Analysis of Quadrupolar Line Shapes

Recall from section 2.1 that the NMR frequency for an isolated deuteron in a solid is given by $\omega = \omega_0 \pm \omega_Q$ where

$$\omega_Q = 3\pi/4\left(\frac{e^2qQ}{h}\right)[3\cos^2\Theta - 1 + \eta\sin^2\Theta\cos 2\Phi]$$

(119)

(e^2qQ/h) is the quadrupolar coupling constant (QCC) and η is the asymmetry parameter which describes the deviation from cylindrical symmetry of the electrical field gradient (EFG) tensor about the q_{zz} axis in the principal axis system (PAS). To quantitatively describe the effects of helix alignment on the resonant frequency it is convenient to introduce an intermediate helix frame of reference. Transformation between these frames using the simplifying assumption of a symmetric EFG tensor results in

$$\omega_Q = 3\pi/2\left(\frac{e^2qQ}{h}\right)[P_2(\cos\theta)P_2(\cos\beta) - 3/4\sin 2\theta$$

$$\sin 2\beta\cos(\gamma + \phi) + 3/4\sin^2\theta\sin^2\beta\cos 2(\gamma +\phi)]$$

(120)

where $P_2(x)$ are second-order Legendre polynomials. The angles θ, ϕ define the orientation of the EFG tensor in the helix axis frame, and β, γ describe the orientation of the helix axis with respect to the lab frame. A visual representation of these frames is shown in Figure 37. In particular, β describes the angle between the helix and the magnetic field, γ describes the relative rotation about the helix axis, and θ describes the angle between the C–D bond and the helix axis (making the assumption that the q_{zz} tensor element is coincident with the C–D bond), while ϕ describes the orientation of the bond about the helix axis. Since γ and ϕ commute, ϕ can be set to zero without loss of generality. For a nonzero asymmetry parameter, an additional angle χ is required to describe the orientation of the EFG tensor in the helix axis frame; ω_Q then becomes dependent on the asymmetry parameter. Internal motions also affect the observed quadrupolar frequency: anisotropic base motion modeled as restricted diffusion in two perpendicular planes,[67,68] along with the analogous effect of a four-site libration on the methyl group frequency.[144]

If the helix axis does not align perfectly in the magnetic field, there will be a distribution of β angles. Simulations of the experimental line shapes were ob-
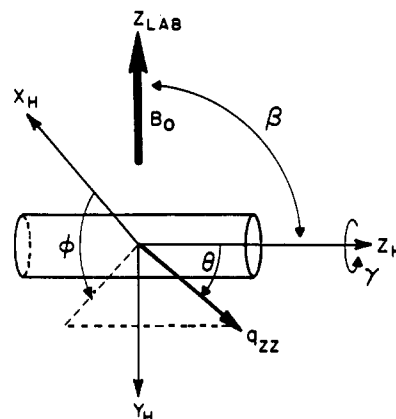

Figure 37. Illustration of coordinate system for a uniaxial EFG tensor. The orientation of the q_{zz} component of the EFG tensor with respect to the intermediate helix axis frame is described the angles θ and ϕ. The orientation of the helix frame with respect to the external magnetic field B_0 is described by β and γ.

tained with appropriate weighting of β characterized by an orientational weighting function $f(\beta)$[104,145]

$$I(\omega) = \int\int I(\omega,\beta,\gamma,\theta,\phi)f(\beta)\sin(\beta)\,d\beta d\gamma$$

(121)

Different forms of $f(\beta)$ are available, but experimental spectra were simulated by imposing domains where the helix axis is randomly oriented with domains where the helix axis is highly ordered. A Gaussian distribution was assumed for the oriented domains, the functional form of $f(\beta)$ being given by

$$f(\beta) = (P/\sigma\sqrt{2\pi})e^{-(\beta-\beta_0)^2/2\sigma^2} + (1 - P)$$

(122)

where P is the fraction of the sample in the oriented domain, β_0 is the mean angle of alignment, and σ is the standard deviation in the Gaussian distribution. Variation in the line shape with changes in these parameters has been discussed previously.[68,69,144]

4.0.2 Characteristics of the Aligned Phase

The effect of helical alignment is demonstrated by the spectra shown in Figure 38. The spectrum in Figure 38A was obtained from a sample of [methyl-^{2}H]-2'-deoxythymidine-labeled dodecamer at a reduced water content [W = 16.8 (mol of H_2O/mol of nucleotide)] which was frozen inside the magnetic field. This level of hydration was not observed to form an oriented phase during the time scale of previous investigations (24–48 h). The spectrum is characteristic of an unoriented sample and differs significantly from the experimental line shape shown in Figure 38B. Figure 38B is a spectrum of the same sample, hydrated to a level of W = 29.6 and frozen in the magnetic field. This spectrum displays the characteristic cylindrical powder pattern.[146] Further proof of alignment is given by Figure 38C, which shows the result of rotating the frozen, aligned [methyl-^{2}H]-2'-deoxythymidine-labeled sample, the initial spectrum of which is shown in Figure 38B, about the X or Y lab axis. These spectra prove that there is helix ordering with respect to the angle β, but no macroscopic order is present about α (around B_0). This is clear if one imagines that the all the dodecamer helix axes align perpendicular to the field (β = 90°), but within the plane defined by the β = 90°
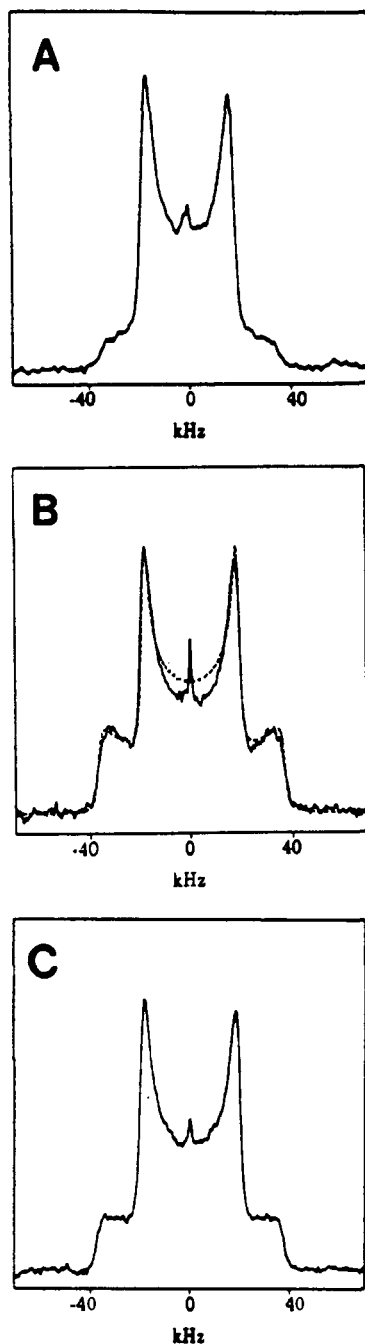
Figure 38. (A) Experimental spectrum of [methyl-^{2}H]-2'-deoxythymidine-labeled [d(CGCGAAT*T*CGCG)]$_2$ equilibrated at $W = 16.8$, representative of a line shape obtained from an unaligned sample. (B) Experimental and simulated (dotted line) spectra of the same methyl-deuterated DNA dodecamer, equilibrated at $W = 29.6$ and then frozen while in the magnetic field. (C) The same sample and preparation conditions as in B only the sample has been rotated about the X lab axis.

angle there is no macroscopic order (no order in α). When the sample is rotated about a lab X or Y axis the helix axes now have a range of β values eliminating the characteristic cylindrical line shape observed for the oriented sample. Freezing samples outside the magnetic field prevents alignment of the dodecamer when placed within the field.

4.0.3 Investigation of Conformation and Order

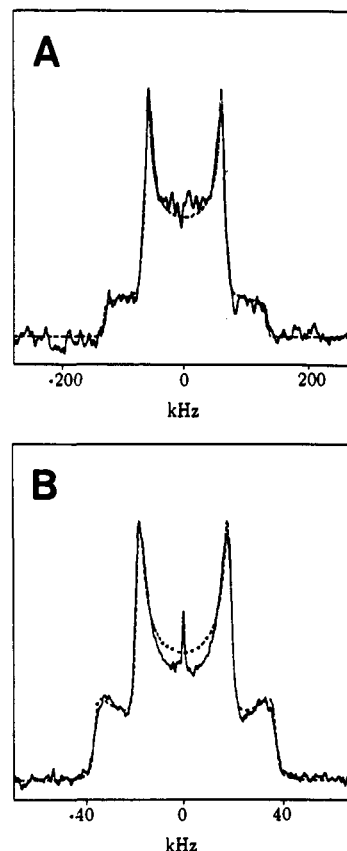From the discussion of the analysis of ^{2}H line shapes, the orientation of the C–D bond with respect to the

Figure 39. Experimental (—) and simulated (- -) 76.75-MHz deuterium quadrupole echo spectra of labeled [d(CGCGAATTCGCG)]$_2$ in the oriented liquid-crystal phase. The simulated spectra were calculated as described in the text, ignoring the central isotropic component. Using a pulse delay of 50 μs, spectra were obtained for (A) [8-^{2}H]-purine-labeled [d(CG*CG*A*A*TTCG*CG*)$_2$], 13 000 scans, $\pi/2 = 2.3$ μs, $W = 27.7$; (B) [methyl-^{2}H]-2'-deoxythymidine-labeled [d(CGCGAAT*T*CGCG)$_2$], 8000 scans, $\pi/2 = 2.5$ μs, $W = 29.6$.

TABLE X. Experimental Parameters for Magnetically Oriented [d(CGCGAATTCGCG)]$_2$[a]

	A	B	C
W (H$_2$O/nucleotide)	29.6	30.5	28.9
concn, mg/mL	654	635	685
temp, K	228 ± 3	200 ± 3	200 ± 3
$\bar{\theta}$, deg	90 ± 10	90 ± 10	22 ± 3
σ_{total}, deg	15	20	15
P	0.7	0.7	0.7

[a] A = [methyl-^{2}H]-2'-deoxythymidine-labeled [d(CGCGAAT*T*CGCG)]$_2$, B = [8-^{2}H]-purine-labeled [d(CG*CG*A*A*TTCG*CG*)]$_2$, C = [2''-^{2}H]-2'-deoxyadenosine-labeled [d(CGCGA*A*TTCGCG)]$_2$. Symbol definitions are given in Table XI.

helix axis can be determined. The oligonucleotide in the liquid-crystal phase has uniaxial order; therefore only θ, β_0, and σ can be determined. The ^{2}H NMR spectra of [methyl-^{2}H]-2'-deoxythymidine-labeled [d(CGCGAAT*T*CGCG)]$_2$, [8-^{2}H]-2'-deoxyadenosine, [8-^{2}H]-2'-deoxyguanosine-labeled [d(CG*CG*A*A*-TTCG*CG*)]$_2$, and [2''-^{2}H]-2'-deoxyadenosine-labeled [d(CGCGA*A*TTCGCG)]$_2$ are shown in Figures 39A,B and Figure 41A. The water content (W), concentration, and experimental temperatures are given in Table X. At reduced temperature the observed line shapes are characteristic of aligned samples. Use of reduced temperatures is critical to obtain line shapes that are not
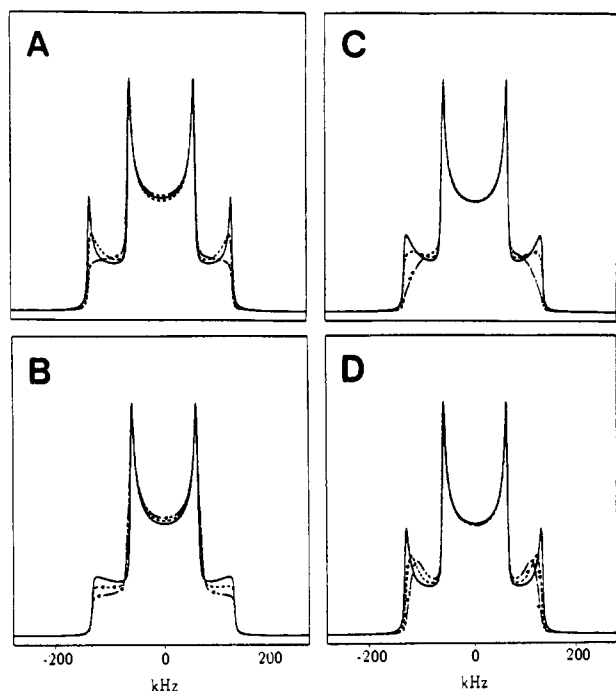
Figure 40. Simulated quadrupole echo spectra as a function of Gaussian distribution parameters. (A) Variation in σ_{total}: (—) 1°, (– –) 10°, (– - -) 20°, $\beta_0 = 90°$, $\theta = 90°$, $P = 1.0$. (B) Variation in P: (—) 1.00, (– –) 0.75, (– - -) 0.50, $\beta_0 = 90°$, $\theta = 90°$, $\sigma_{total} = 15°$. (C) Variation in θ (—) 90°, (– –) 80°, (– - -) 70°, $\beta_0 = 90°$, $\theta = 90°$, P = 1.0, $\sigma_{total} = 10°$. (D) Variation in β_0, (—) 90°, (– –) 80°, (– - -) 75°, $\theta = 90°$, $P = 1.0$, $\sigma_{total} = 5°$.

TABLE XI. Summary of Parameters Introduced in the Description and Simulation of Magnetically Oriented [d(CGCGAATTCGCG)]₂

$\bar{\theta}_R$, $\bar{\theta}_T$	average variation of roll and tilt between base pairs
Θ_R, Θ_T	average roll and tilt of base with respect to global helix axis
$\|\Theta_T\|$	average tilt magnitude with respect to global helix axis
$\sigma_{\|\Theta_T\|}$	width of distribution of tilt magnitude
$\|\Theta\|$	average orientation of base or sugar with respect to global helix axis
$\sigma_{\|\Theta\|}$	width of orientation distribution
$\bar{\theta}$	average angle between helix axis and C–D bond
$\|\theta\|$	average magnitude of C–D bond orientation
β_0	average angle between helix axis and $\mathbf{B}_0$
σ, σ_{total}	combined distribution width of helix and C–D bond orientation
σ_β	distribution width of helix axis orientation around β_0
σ_θ	distribution of C–D bond orientation about $\bar{\theta}$
P	fraction of sample oriented

highly averaged by motion about the helix axis. Examples of this motional averaging have been presented previously.[144]

Librational amplitudes were not determined in the nonselectively labeled base or sugar-labeled material due to insufficient signal to noise. Spin–lattice relaxation times $\langle T_1 \rangle$ and quadrupole echo decay times $\langle T_{2e} \rangle$ were determined only for [*methyl*-²H]-2'-deoxy-thymidine-labeled [d(CGCGAAT*T*CGCG)]₂ and have been reported in the original characterization of the liquid-crystal phase.[144]

4.0.4 Base Orientation and Order

From the spectra of the methyl- and base-labeled material information concerning the conformation and order within the base domain is obtained. The effects of the variables σ, β_0, θ, and P on the line shape of the
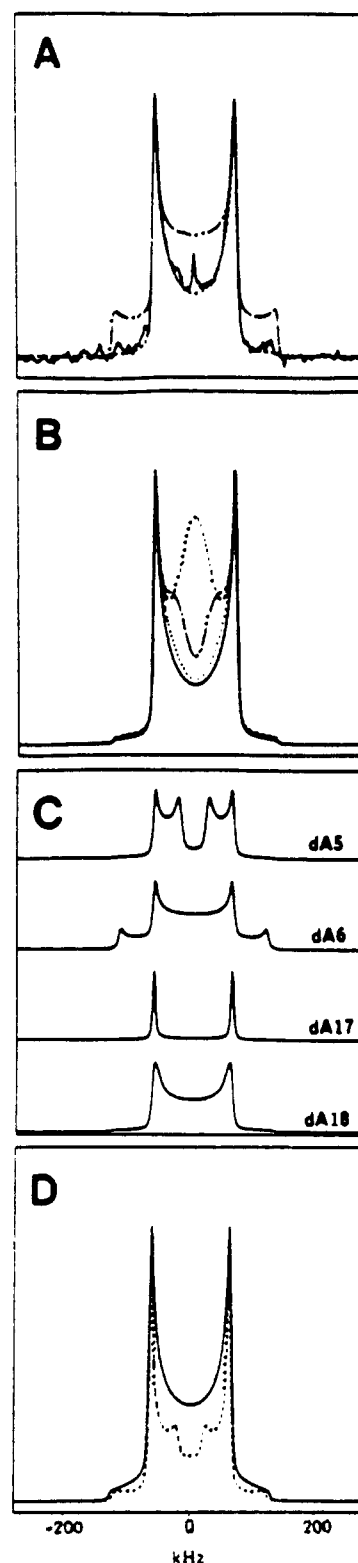
Figure 41. (A) Experimental (—) spectrum of [2''-²H]·2'-deoxyadenosine-labeled [d(CGCGA*A*TTCGCG)]₂ using 24 340 scans, $\pi/2 = 2.3\ \mu s$, $W = 28.3$; simulated (– –) spectrum for C_2-endo sugar conformation in model B-form DNA; and simulated (– - -) spectrum for C_3-endo configuration of model A-form DNA. (B) Variation in θ: (—) $\theta = 20°$, $\sigma = 15°$; (· ·) $\theta = 25°$, $\sigma = 10°$; (– - -) $\theta = 30°$, $\sigma = 5°$; (– –) $\theta = 35°$, $\sigma = 5°$. (C) Simulated spectra using solution NMR distance geometry structure for each of the 2''-labeled adenosines in the dodecamer. (D) Sum of individual simulations for (—) $\sigma = 15°$ and (– –) $\sigma = 1°$.

purine base labeled material is shown in Figure 40. Similar effects were investigated for the [*methyl*-²H]-2'-deoxythymidine-labeled dodecamer.[144] Finite

pulse effects are less pronounced in the methyl-labeled spectra due to the reduced line width resulting from the rapid 3-fold jump of the methyl group.

The spectrum of nonselectively labeled, [8-^{2}H]-2'-deoxyguanosine-[8-^{2}H]-2'-deoxyadenosine-labeled [d-(CG*CG*A*A*TTCG*CG*)]$_2$ was simulated using QCC$_{eff}$ = 178 kHz, η_{eff} = 0.08, θ = 90°, β_0 = 90°, σ = 20°, and $\bar{P}$ = 0.7 (Figure 41A). Using these effective values, the $\bar{q_{xx}}$ element of the averaged EFG tensor lies approximately within the base plane (χ = 90°), in agreement with that observed by Brandes and co-workers.[68] The random fraction value was determined from the methyl-labeled spectrum which has much higher signal to noise. The values of QCC$_{eff}$ and η_{eff} are the same as those observed in the dry dodecamer. If one uses the static values of QCC$_{static}$ = 179 kHz and η_{static} = 0.06, the observed effective values would require an additional libration in two orthogonal planes of ~±7° and ~±2°.[50] Unlike the investigation in the methyl-labeled dodecamer, the signal-to-noise of the purine-labeled material does not allow distinguishing between the effects of tilting and twisting librations on the line shape. The simulation parameters listed in Table X for the nonselectively labeled purine sample assumed that the experimental spectra can be described by a single average θ and σ_{total} (see later discussion). The experimental spectra could also be simulated using average θ values ranging from 80° to 100° with only small changes in σ. Base tilt angles exceeding this range produced simulations different from experimental data (See Figure 40C). Similarly, variation of the standard deviation σ also produced line shapes not observed experimentally (See Figure 40A). From previous investigations of the [methyl-^{2}H]-2'-deoxythymidine-labeled dodecamer, the spectrum was simulated using θ = 90°, β_0 = 90°, σ = 15°, P = 0.7, QCC$_{static}$ = 159 kHz, η_{eff} = 0.0, and a rapid three-site jump about the C_3 symmetry axis of the methyl group, along with a tilt libration θ_0 = 10° ± 3° and a twisting libration of ϕ_0 = 15° ± 3° (See Figure 41B). Since the C–D vector of the [8-^{2}H]-labeled purine is ~15° from the roll axis, to a first approximation base role and propeller twist will have a small effect on the ^{2}H NMR powder pattern. In contrast, the C_3 symmetry axis of the methyl group is ~72° from the roll axis so that the angle θ with respect to the helix axis is affected by both roll and twist. Therefore, the θ distribution found in the base- and methyl-labeled material cannot be directly compared. As pointed out by Brandes and co-workers[67] it is not possible to distinguish between a helix distribution (σ_β) or a distribution in the orientational angle θ (σ_θ). If one assumes that these distributions are independent, the standard deviation of the Gaussian distribution determined experimentally is described by σ_{total}, where

$$\sigma_{total}^2 = \sigma_\beta^2 + \sigma_\theta^2 \qquad (123)$$

If the purine- and methyl-labeled samples have the same distribution of β, the largest possible σ_β is 15° (i.e. the σ_{total} of the methyl-labeled sample, assuming σ_θ = 0°). The minimum θ distribution for the nonselectively labeled purine is therefore σ_θ ~13° using eq 123.

These values of the angle θ and the standard deviation σ_θ can be compared to those from previous structural studies, and are similar to the values obtained from X-ray investigations.[147] Since only tilt magnitude

is measured in our investigations, the average tilt magnitude $|\overline{\Theta_T}|$ and distribution $\sigma_{|\Theta_T|}$ corresponding to the crystal structure was determined. For the purine bases this is $|\overline{\Theta_T}|$ = 4.3° (i.e. θ = 85.7°) and $\sigma_{|\Theta_T|}$ = 3.1°, while the average tilt magnitude for the thymidines is $|\overline{\Theta_T}|$ = 9.3° and $\sigma_{|\Theta_T|}$ = 1.0°. Recall that there will be a small contribution from the roll to the apparent tilt values for the purine-labeled material and a larger contribution to the apparent tilt the methyl-labeled material: these contributions were not calculated. The portion of σ_{total} for the methyl-labeled sample that results from variation in base tilt cannot be determined without additional labeled samples to determine σ_β. The average tilt value determined from X-ray structural data does not conflict with what is observed experimentally, but the crystal structure shows a significantly lower distribution in $|\Theta_T|$ than the minimum θ distribution possible in the purine sample.

4.0.5 Sugar Conformation

The analysis of sugar conformation proceeds in a similar fashion. Utilizing the maximum σ_β possible (i.e. σ_β = 15°), QCC$_{eff}$ = 174 KHz, η_{eff} = 0.03, β_0 = 90°, and P = 0.7, the angle between the helix axis and the C-D bond of the C2'' position is θ = 22° (see Figure 41A). The contributions from the ca. 10% deuterium label present at the 2'-position were ignored; this omission results in a slightly increased value of θ. Using σ_β = 15° means that there is no distribution in θ. As in the previous discussion, using the value of σ_β = 13.7° and eq 111 gives σ_θ = 6.1°. Decreasing the β distribution would require an increase in the value of θ, but for values of $\theta \geq 25°$ (see Figure 41B) simulations did not reproduce the experimental line shape. These simulations were obtained using an average θ value to describe the sugar conformation, an assumption that may not be realistic considering the average involves only four 2'-deoxyadenosines (see discussion below). This range of θ values (20°–25°) corresponds well to the value of θ = 22.5° expected for the C$_{2'}$-endo configuration in model B-form DNA. As a comparison the C$_{3'}$-endo sugar conformation of A-form DNA results in the 2'' C–D bond having a θ angle of ca. 90°. Simulations for this large θ do not reproduce the experimental spectra (See Figure 41A).

These results can also be compared to the sugar conformation observed in previous structural investigations. Considering only the 2'-deoxyadenosine sugar conformations in the crystal structure of the dodecamer, one obtains $|\bar{\theta}|$ = 42.7° with $\sigma_{|\theta|}$ = 14°. Both of these values differ significantly from the θ observed experimentally. Comparison to the distance geometry solution structure (using the same assumptions about local helix axis as the base investigation) results in $|\bar{\theta}|$ = 42° with $\sigma_{|\theta|}$ = 29°. Again the average θ value and deviation are significantly larger than the value observed experimentally and are similar in magnitude to that observed in the crystal structure. Simulations for each C2'' of the 2'-deoxyadenosines and associated θ values are shown in Figure 41C, while the sum for σ_{total} = 15° and σ_{total} = 1° are shown in Figure 41D. The sum of these simulations for σ = 15° has additional center intensity in comparison to experimental spectra, while the simulations using σ_{total} = 1° has fine structure that is not

observed experimentally. Obviously an average θ value does not converge to the sum of spectra for low numbers of sites, in contrast to the case observed in the purine-labeled sample.

The possibility of sugar conformer mixtures was also investigated. Recent ^{2}H solid state NMR studies of internal dynamics in the furanose ring of [d-(CGCGAATTCGCG)]$_2$ suggest that fast, large amplitude motions such as interconversion between the $C_{2'}$-endo and $C_{3'}$-endo do not occur on the nanosecond time scale.[118] Unfortunately the analysis of ^{2}H NMR quadrupolar echo line shapes is insensitive to motions occurring at rates slower than 10^4 Hz, and in any caes may not be able to detect small populations of $C_{3'}$-endo. In contrast investigation of sugar conformations within the dodecamer by analysis of coupling constants suggests that there is rapid interconversion between two conformers,[84] with the $C_{3'}$-endo population of the 2'-deoxyadenosines calculated to be 6–7%. Simulations of mixtures between θ = 22° ($C_{2'}$-endo) and θ = 90° ($C_{3'}$-endo, A form) suggest the maximum mixture that would fit the experimental data was ~20% for the θ = 90° conformer. This value must be approached with caution since the θ value used for the $C_{3'}$-endo configuration was obtained from model A-form DNA. The complete conformation of the sugar cannot be obtained using only the 2''-labeled material. It will become necessary to utilize labels at additional positions to determine the complete sugar conformation.

4.0.6 Aligned Phase: Conclusions

We have shown that the oriented liquid-crystal phase formed by oligonucleotides at high hydration levels can be utilized to investigate molecular structure and order by solid-state ^{2}H NMR. The base orientation and sugar conformation have been investigated using the deuterated dodecamer [d(CGCGAATTCGCG)]$_2$. The loss of structural information accompanying the use of nonselectively labeled samples necessitates that selectively deuterated oligonucleotides be produced. Although selective deuteration is laborious, ^{2}H provides a complementary technique to probe the local structure of oligonucleotides currently under study by X-ray and high-resolution NMR methods. One advantage of solid-state NMR is that the growth of a diffractable crystal is not required. If selectively deuterated samples are prepared, solid-state NMR methods are free of the necessity of performing assignments of nuclear resonances, as is required by 2D NMR methods, so virtually any oligonucleotide sequence that produces a phase with an identifiable ordering axis can be investigated. In addition, the size of oligonucleotides that can be studied is limited only by the practical yield in the DNA synthetic protocols, and we anticipate the ability to study sequences up to 40–50 base pairs in the near future. The liquid–crystalline phase of oligonucleotides is lyotropic, and only exists at relatively high levels of hydration. However, phase ordering is preserved at reduced temperatures, where large amplitude microsecond time scale motions about the helix axis are effectively quenched. Ordering also occurs at easily available field strengths, for instance the methyl-labeled dodecamer was aligned at only 4.5 T. In summary solid-state NMR methods are capable of yielding structural information in addition to the internal dy-

namics of oligonucleotides. The conformation and structure of the base domains in [d-(CGCGAATTCGCG)]$_2$ agree well with the distance geometry solution structure. In contrast, the agreement between $|\bar{\theta}|$ of the 2''-orientation and either the X-ray or distance geometry solution structure is poor. The conformation of furanose rings cannot be exactly defined with only a single deuterium label; however, synthetic labeling of other ring positions are being pursued.

In addition to angular information obtained from the study of EFG and CSA tensors in aligned phases, the selective labeling of DNA oligomers with spin $1/2$ nuclei such as nitrogen-15 and carbon-13 enables the extraction of distance information from aligned and unaligned samples through the measurement of direct dipolar couplings. Griffin and co-workers[148] and Schaeffer and co-workers[149] have recently described MAS experiments which enable the measurement of distances in excess of 6 Å in biopolymers. The selective labeling of DNA and RNA oligomers with spin $1/2$ nuclei is underway in our lab with the objective of using high-resolution solid-state NMR techniques to measure distances between nonadjacent bases and distances between the ^{31}P nuclei of the backbone and various points on the bases and furanose rings.

5.0 Conclusions

To what degree has solid-state NMR advanced our knowledge of the structure internal dynamics of nucleic acids, and what are the biological implications of this information? DNA, as the repository of genetic information, interacts with various types of RNA, which in turn translate the DNA sequence into amino acid sequences. The control of genetic expression involves further interactions between nucleic acids and various regulatory proteins. High-resolution NMR and X-ray crystallographic studies of nuclear acid oligomers are motivated by a desire to understand the structural basis of these interactions. The following question arises: to what extent are the structures of DNA oligomers representative of high molecular weight DNA?

If DNA oligomers are perfectly representative of high molecular weight DNA, then structural information derived from these systems yields direct insight into biological function. However, high molecular weight DNA is known to be internally dynamic, and this review has sought to point out that the nature of the internal dynamics of nucleic acids is a question with vast implications for structural studies.

If the internal dynamics of DNA are strictly localized and thus adequately described by the methods reviewed in section 2.3.1, information derived from oligomerase systems is directly insightful. If internal motions are largely collective (see section 2.3.2), the structure of high molecular weight DNA may significantly deviate from the structures reported for DNA oligomers in crystal lattices in solution. As explained in section 1.2, collective models of DNA dynamics adequately simulate high-resolution NMR relaxation data, but the degree to which Zeeman relaxation in solution is dominated by collective versus localized motion remain in question.

Solid-state deuterium NMR studies of high molecular weight DNA have not settled the question entirely because no simple dynamical model has yet been found

which perfectly simulates $J_1(\omega_0)$ and $J_2(2\omega_0)$ for deuterated, high molecular weight DNA. If in-plane torsional motions dominate the internal dynamics of DNA, this should be reflected in simulations of experimental spectral densities. In-plane torsional models fail to simulate the J_1/J_2 ratio at low hydration levels but approach the theoretical ratio as the hydration level is increased.

Theoretical and experimental NMR studies of the dynamics of high molecular weight DNA should be continued. Theoretical models can be improved, perhaps by incorporation of additional motions such as bending of the helix axis.

What insights have solid-state NMR studies of DNA oligomers provided? First, the separation of local and overall molecular dynamics is more readily achieved because DNA oligomers to a very good approximation behave dynamically as rigid rods. Studies of selectively deuterated oligonucleotides have yielded results only partly in agreement with the view of internal DNA dynamics provided by high-resolution NMR and molecular dynamics (MD) calculations. In particular, dynamic equilibrium between conformations of the sugar rings has not been observed in solid-state NMR studies of DNA dodecamers and the experimentally observed amplitude of a backbone motions is also at variance with the predictions of some MD studies.

Solid-state NMR has great potential for studying DNA structure and DNA–drug interactions.[150] In contrast to high-resolution NMR where NOE-derived distances generally do not exceed 3–4 Å, solid-state NMR methods such as rotational resonance and rotational echo double resonance can yield internuclear distances of over 8 Å. If appropriately labeled oligonucleotides can be prepared, problems such as the nature of static bending in certain DNA sequences could be efficiently addressed.

6.0 References

(1) Watson, J. D.; Crick, F. H. *Nature* **1953**, *171*, 737.
(2) Wing, R. M.; Drew, H. R.; Takano, T.; Broka, C.; Tanaka, S.; Itakura, K.; Dickerson, R. E. *Nature (London)* **1980**, *287*, 755.
(3) Wang, A. H.-J.; Fujii, S.; van Boom, J. H.; Rich, A. *Proc. Natl. Acad. Sci. U.S.A.* **1982**, *79*, 3968.
(4) Drew, H. R.; Wing, R. M.; Tokano, T.; Broka, C.; Tanaka, S.; Itakura, K.; Dickerson, R. E. *Proc. Natl. Acad. Sci. U.S.A.* **1981**, *78*, 2179.
(5) Arnott, S.; Hukins, D. W. L. *Biochem. Biophys. Res. Commun.* **1972**, *47*, 1504.
(6) Dickerson, R. E.; Drew, H. R. *J. Mol. Biol.* **1981**, *149*, 761.
(7) Drew, H. R.; Samson, S.; Dickerson, R. E. *Proc. Natl. Acad. Sci. U.S.A.* **1982**, *79*, 4040.
(8) Nerdal, W.; Hare, D. R.; Reid, B. R. *J. Mol. Biol.* **1988**, *201*, 717.
(9) Saenger, W. *Principles of Nucleic Acid Structure*; Springer-Verlag: New York, 1984; Chapter 9.
(10) Drew, H. R.; Dickerson, R. E. *J. Mol. Biol.* **1981**, *151*, 535.
(11) Kopka, M. L.; Frantini, A. V.; Drew, H. R.; Dickerson, R. E. *J. Mol. Biol.* **1983**, *163*, 129.
(12) Falk, M.; Hartman, K. A.; Lord, R. C. *J. Am. Chem. Soc.* **1962**, *84*, 3843.
(13) Falk, M.; Hartman, K. A.; Lord, R. C. *J. Am. Chem. Soc.* **1963**, *85*, 387.
(14) Falk, M.; Hartman, K. A.; Lord, R. C. *J. Am. Chem. Soc.* **1963**, *85*, 391.
(15) Hogan, M. E.; Jardetzky, O. *J. Am. Chem. Soc.* **1980**, *19*, 3460.
(16) Bolton, P. H.; James, T. L. *J. Phys. Chem.* **1979**, *83*, 3359.
(17) Bendall, P.; James, T. L. *Proc. Natl. Acad. Sci. U.S.A.* **1983**, *80*, 3284.
(18) Bendall, P.; Laub, O.; James, T. L. *J. Am. Chem. Soc.* **1982**, *104*, 6748.
(19) King, R.; Jardetzky, O. *Chem. Phys. Lett.* **1978**, *55*, 15.
(20) Woessner, D. E. *J. Chem. Phys.* **1962**, *36*, 1.
(21) Lipari, G.; Szabo, A. *Biochemistry* **1981**, *20*, 6250.
(22) Barkley, M. D.; Zimm, B. H. *J. Chem. Phys.* **1979**, *70*, 2991.
(23) Robinson, B. H.; Forgacs, G.; Dalton, L. R.; Frisch, H. L. *J. Chem. Phys.* **1980**, *73*, 688.
(24) Robinson, B. H.; Lerham, L. S.; Beth, A. H.; Frisch, H. L.; Dalton, L. R.; Auer, C. *J. Mol. Biol.* **1980**, *139*, 19.
(25) (a) Allison, S. A.; Schurr, J. M. *Chem. Phys.* **1979**, *41*, 35. (b) Allison, S. A.; Shibata, J. H.; Wilcoxon, J.; Schurr, J. M. *Biopolymers* **1982**, *21*, 729.
(26) Langowski, J. et al. *Biopolymers* **1985**, *24*, 1023.
(27) Hard, T.; Kearns, D. R. *J. Phys. Chem.* **1986**, *90*, 3437.
(28) Schurr, J. M.; Fujimoto, B. S. *Biopolymers* **1988**, *27*, 1543.
(29) Abragam, A. *Principles of Nuclear Magnetism*; Oxford University Press: New York, 1961; p 216.
(30) Mehring, M. *Principles of High Resolution NMR in Solids*; Springer Verlag: New York, 1983.
(31) Slichter, C. P. *Principles of Magnetic Resonance*, 3rd ed.; Springer Verlag: New York, 1990.
(32) Davis, J. H. *Biochim. Biophys. Acta* **1983**, *737*, 117.
(33) Spiess, H. W. *Dynamic NMR Spectroscopy*; Springer-Verlag: New York, 1978.
(34) Haeberlen, U. *High Resolution NMR in Solids Selective Averaging*; Academic Press: New York, 1976.
(35) Brink, D. M.; Satchler, G. R. *Angular Momentum*; Oxford University Press (Clarendon): London, 1968.
(36) Spiess, H. W.; Sillescu, H. *J. Magn. Reson.* **1981**, *42*, 381.
(37) Barbara, T. M.; Greenfield, M. S.; Vold, R. L.; Vold, R. R. *J. Magn. Reson.* **1986**, *69*, 311.
(38) Torchia, D. A.; Szabo, A. *J. Magn. Reson.* **1982**, *49*, 107.
(39) Wittebort, R. J.; Olejniczak, E. T.; Griffin, R. G. *J. Chem. Phys.* **1987**, *86*, 5411.
(40) Davis, J. H. *Biochim. Biophys. Acta* **1983**, *737*, 117.
(41) Szabo, A. *J. Chem. Phys.* **1984**, *81*, 150.
(42) Wittebort, R. J.; Szabo, A. *J. Chem. Phys.* **1978**, *69*, 1722.
(43) Wallach, D. *J. Chem. Phys.* **1967**, *47*, 5258.
(44) Woessner, D. E. *J. Chem. Phys.* **1962**, *36*, 1.
(45) London, R. E. *J. Am. Chem. Soc.* **1978**, *100*, 2678.
(46) Allison, S. A.; Shurr, J. M. *Chem. Phys.* **1979**, *41*, 35.
(47) Allison, S. A.; Shibata, J. H.; Wilcoxon, J.; Schurr, J. M. *Biopolymers* **1982**, *21*, 729.
(48) Langowski, J.; Fujimoto, B. S.; Wemmer, D. E.; Benight, A. S.; Drobny, G.; Shibata, J. H.; Schurr, J. M. *Biopolymers* **1985**, *24*, 1023.
(49) Wu, P.; Fujimoto, B. S.; Schurr, J. M. *Biopolymers* **1987**, *26*, 1463.
(50) Kintanar, A.; Huang, W.-C.; Schindele, D. C.; Wemmer, D. E.; Drobny, G. *Biochemistry* **1989**, *28*, 282.
(51) Brainard, J. R.; Szabo, A. *Biochemistry* **1981**, *20*, 4618.
(52) Lipari, G.; Szabo, A. *Biophys. J.* **1980**, *30*, 489.
(53) Shindo, H.; Wooten, J. B.; Pheiffer, B. H.; Zimmerman, S. B. *Biochemistry* **1980**, *19*, 518.
(54) Landridge, R.; Wilson, H. R.; Hooper, C. W.; Wilkins, M. H. F.; Hamilton, L. D. *J. Mol. Biol.* **1960**, *3*, 19.
(55) Arnott, S.; Hukins, D. W. L. *Biochem. Biophys. Res. Commun.* **1972**, *47*, 1504.
(56) Nall, B. T.; Rothwell, W. P.; Waugh, J. S.; Rupprecht, A. *Biochemistry* **1981**, *20*, 1881.
(57) Tang, P.; Santos, R. A.; Harbison, G. S. *Adv. Magn. Reson.* **1990**, *13*, 225. Also, consult references cited in the bibliography.
(58) Strzellecka, T. E.; Rill, R. L. *J. Am. Chem. Soc.* **1987**, *109*, 4513.
(59) Flory, P. J. *Proc. R. Soc. London, Ser. A* **1956**, *234*. 60, 73.
(60) Warner, M.; Flory, P. J. *J. Chem. Phys.* **1980**, *73*, 6327.
(61) DiVerdi, J. A.; Opella, S. J. *J. Mol. Biol.* **1981**, *149*, 307.
(62) Mai, M.; Wemmer, D. E.; Jardetzky, O. *J. Am. Chem. Soc.* **1983**, *105*, 7149.
(63) Opella, S. J.; Morden, K. M. In *Dynamic Properties of Biomolecular Assemblies*; Harding, S. E., Rowe, A. J., Eds.; The Royal Society of Chemistry: Cambridge, 1989; p 196.
(64) Bendel, P.; Murphy-Boesch, J.; James, T. L. *Biochim. Biophys. Acta* **1983**, *759*, 205.
(65) Vold, R. R.; Brandes, R.; Tsang, P.; Kearns, D. R.; Vold, R. L.; Rupprecht, A. *J. Am. Chem. Soc.* **1986**, *108*, 302.
(66) Brandes, R.; Vold, R. R.; Vold, R. L.; Kearns, D. R. *Biochemistry* **1986**, *25*, 7744.
(67) Brandes, R.; Vold, R. R.; Kearns, D. R.; Rupprecht, A. *J. Mol. Biol.* **1988**, *202*, 321.
(68) Brandes, R.; Vold, R. R.; Kearns, D. R. *Biopolymers* **1988**, *27*, 1159.
(69) Brandes, R.; Vold, R. R.; Kearns, D. R.; Rupprecht, A. *Biochemistry* **1990**, *29*, 1717.
(70) Freed, J. H. *J. Chem. Phys.* **1977**, *66*, 4183.
(71) Shindo, H.; Hiyama, Y.; Roy, S.; Cohen, J. S.; Torchia, D. A. *Bull. Chem. Soc. Jpn.* **1987**, *60*, 1631.

(72) Eimer, W.; Williamson, J. R.; Boxer, S. G.; Pecora, R. *Biochemistry* **1990**, *29*, 799.
(73) Dickerson, R. E.; Drew, H. R. *J. Mol. Biol.* **1981**, *149*, 761.
(74) Dickerson, R. E.; Drew, H. R. *Proc. Natl. Acad. Sci. U.S.A.* **1981**, *78*, 7318.
(75) Kopka, M. L.; Yoon, C.; Goodsell, D.; Pjura, P.; Dickerson, R. E. *J. Mol. Biol.* **1985**, *183*, 553.
(76) Pjura, P. E.; Grzeskowiak, K.; Dickerson, R. E. *J. Mol. Biol.* **1987**, *197*, 257.
(77) Wing, R.; Drew, H.; Takano, T.; Broka, C.; Tanaka, S.; Itakura, K.; Dickerson, R. E. *Nature* **1980**, *287*, 755–758.
(78) Drew, H. R.; Wing, R. M.; Takano, T.; Broka, C.; Tanaka, S.; Itakura, K.; Dickerson, R. E. *Proc. Natl. Acad. Sci. U.S.A.* **1981**, *78*, 2179–2183.
(79) Holbrook, S. R.; Kim, S.-H. *J. Mol. Biol.* **1984**, *173*, 361.
(80) Drew, H. R.; Dickerson, R. E. *J. Mol. Biol.* **1981**, *151*, 535–556.
(81) Kopka, M. L.; Frantini, A. V.; Drew, H. R.; Dickerson, R. E. *J. Mol. Biol.* **1983**, *163*, 129–146.
(82) Hare, D. R.; Wemmer, D. E.; Chou, S.-H.; Drobny, G.; Reid, B. R. *J. Mol. Biol.* **1983**, *171*, 319.
(83) Nerdal, W.; Hare, D. R.; Reid, B. R. *Biochemistry* **1989**, *28*, 10008.
(84) Bax, A.; Lerner, L. *J. Magn. Reson.* **1988**, *79*, 429.
(85) Modrich, P. In *CRC Critical Review in Biochemistry*; Fasman, G. D., Ed.; CRC Press, Inc.: Boca Raton, FL, 1982; Vol. 13, pp 287.
(86) Langowski, J.; Alves, J.; Pingoud, A.; Maass, G. *Nucleic Acids Res.* **1985**, *11*, 501.
(87) Ehbrecht, H.-J.; Pingoud, A.; Urbanke, C.; Maass, G.; Gualerzi, C. *J. Biol. Chem.* **1985**, *260*, 6160.
(88) Lesser, D. R.; Kurpiewski, M. R.; Jen-Jacobson, L. *Science* **1990**, *250*, 776.
(89) McClarin, J. A.; Frederick, C. A.; Wang, B.-C.; Greene, P.; Boyer, H. W.; Grable, J.; Rosenberg, J. M. *Science* **1986**, *234*, 1526.
(90) Kintanar, A.; Alam, T. M.; Huang, W.-C.; Schindele, D. C.; Wemmer, D. E.; Drobny, G. P. *J. Am. Chem. Soc.* **1988**, *110*, 6367.
(91) Brandes, R.; Kearns, D. R. *Biochemistry* **1986**, *25*, 5890.
(92) Rupprecht, A.; Forslind, B. *Biochim. Biophys. Acta* **1970**, *204*, 304.
(93) Alam, T. M.; Drobny, G. P. *Biochemistry* **1990**, *29*, 3421.
(94) Huang, W.-C. Ph.D. Dissertation, University of Washington, 1989.
(95) Batchelder, L. S.; Niu, C. H.; Torchia, D. A. *J. Am. Chem. Soc.* **1983**, *105*, 2228.
(96) Warchol, M. P.; Vaughn, W. E. *Adv. Mol. Relax. Interact. Processes* **1978**, *13*, 317.
(97) Wang, C. C.; Pecora, R. *J. Chem. Phys.* **1980**, *72*, 5333.
(98) Lipari, G.; Szabo, A. *J. Chem. Phys.* **1981**, *75*, 2971.
(99) Kinoshita, K.; Kawato, S.; Ikegami, A. *Biophys. J.* **1977**, *20*, 289.
(100) Brainard, J. R.; Szabo, A. *Biochemistry* **1981**, *20*, 4618.
(101) Alam, T. M.; Orban, J.; Drobny, G. P. *Biochemistry* **1990**, *29*, 9610.
(102) Brandes, R.; Vold, R. R.; Vold, R. L.; Kearns, D. R. *Struct. Dyn. Funct. Biomol.* **1987**, 242.
(103) Heaton, N. J.; Vold, R. R.; Vold, R. L. *J. Chem. Phys.* **1989**, *91*, 56.
(104) Luz, Z.; Poupko, R.; Samulski, E. T. *J. Chem. Phys.* **1981**, *74*, 5825.
(105) Tirado, M. M.; Garcia de la Torre, J. *J. Chem. Phys.* **1980**, *73*, 1986.
(106) Tirado, M. M.; Martinez, C.; Garcia de la Torre, J. *J. Chem. Phys.* **1984**, *81*, 2047.
(107) Hustedt, E. J. Ph.D. Dissertation, University of Washington, 1989.
(108) Pauls, K. P.; MacKay, A. L.; Soderman, O.; Bloom, M.; Tanjea, A. K.; Hodges, R. S. *Eur. Biophys. J.* **1985**, *12*, 1.
(109) Rinne, M.; Depireaux, J. In *Advances in Nuclear Quadrupole Resonance*; Smith, J. A. S., Ed.; Pergamon: New York, 1974; Vol. 1, p 357.
(110) Alam, T. M. Ph.D. Dissertation, University of Washington, 1990.
(111) Saran, A.; Pullman, B.; Perahia, D. *Biochem. Biophys. Acta* **1972**, *287*, 211.
(112) Yathindra, N.; Sundaralingam, M. *Biopolymers* **1973**, *12*, 297.
(113) Kollman, P.; Keepers, J. W.; Weiner, P. *Biopolymers* **1982**, *21*, 2345.
(114) Levitt, M. *Cold Spring Harbor Symp. Quant. Biol.* **1983**, *47*, 251.
(115) Singh, U. C.; Weiner, S. J.; Kollman, P. *Proc. Natl. Acad. Sci. U.S.A.* **1985**, *82*, 755.
(116) Alam, T. M.; Drobny, G. P. *Biochemistry* **1990**, *29*, 3421.
(117) Rill, R. L.; Hilliard, P. R.; Levy, G. C. *J. Biol. Chem.* **1983**, *258*, 250.
(118) Huang, W.-C.; Orban, J.; Kintanar, A.; Reid, B. R.; Drobny, G. P. *J. Am. Chem. Soc.* **1990**, *112*, 9059.
(119) Heaton, N. J.; Vold, R. L.; Vold, R. R. *J. Am. Chem. Soc.* **1989**, *111*, 3211.
(120) Heaton, N. J.; Vold, R. R.; Vold, R. L. *J. Chem. Phys.* **1989**, *91*, 56.
(121) Saenger, W.; Hunter, W. N.; Kennard, O. *Nature* **1986**, *324*, 385.
(122) Dickerson, R. E. *J. Mol. Biol.* **1983**, *166*, 419.
(123) Arnott, S.; Hukins, D. W. L. *Biochem. Biophys. Res. Commun.* **1972**, *47*, 1504.
(124) Levitt, M.; Warshel, A. J. *J. Am. Chem. Soc.* **1978**, *100*, 2607.
(125) Olson, W. K.; Sussman, J. L. *J. Am. Chem. Soc.* **1983**, *104*, 270.
(126) Olson, W. K. *J. Am. Chem. Soc.* **1983**, *104*, 278.
(127) Clore, G. M.; Gronenborn, A. M. *FEBS Lett.* **1984**, *172*, 219.
(128) Altona, C. *Recl. Trav. Chim. Pays.-Bas.* **1982**, *101*, 413.
(129) (a) Altona, C.; Sundaralingam, M. *J. Am. Chem. Soc.* **1972**, *94*, 8205. (b) Altona, C.; Sundaralingam, M. *J. Am. Chem. Soc.* **1973**, *95*, 2333.
(130) Haasnoot, C. A. G.; de Leeuw, F. A. A.; Altona, C. *Tetrahedron* **1980**, *36*, 2783.
(131) Westhof, E.; Sundaralingam, M. *J. Am. Chem. Soc.* **1980**, *102*, 1493.
(132) de Leeuw, H. P. M.; Haasnoot, C. A. G.; Altona, C. *Isr. J. Chem.* **1980**, *20*, 108.
(133) McLarin, J. A.; Frederick, C. A.; Wang, B.-C.; Greene, P.; Boyer, H. W.; Grable, J.; Rosenberg, J. M. *Science* **1986**, *234*, 1526.
(134) Roy, S.; Hiyama, Y.; Torchia, D. A.; Cohen, J. S. *J. Am. Chem. Soc.* **1986**, *108*, 1675.
(135) Hiyama, Y.; Roy, S.; Cohen, J. S.; Torchia, D. A. *J. Am. Chem. Soc.* **1989**, *111*, 8609.
(136) Vega, A. J.; Luz, E. *J. Chem. Phys.* **1987**, *86*, 1803.
(137) Cooper, P. J.; Hamilton, L. D. *J. Mol. Biol.* **1966**, *16*, 562.
(138) Kohler, S. J.; Klein, M. P. *Biochemistry* **1976**, *15*, 967.
(139) Spiess, H. W. *J. Chem. Phys.* **1980**, *72*, 6755.
(140) Robinson, C. *Tetrahedron* **1961**, *13*, 219.
(141) Luzzati, V.; Nicolaieff, A.; Masson, F. *J. Mol. Biol.* **1961**, *3*, 185.
(142) Iizuka, E. *Polym. J.* **1983**, *15*, 525.
(143) Rill, R. L. *Proc. Natl. Acad. Sci. U.S.A.* **1986**, *83*, 342.
(144) Alam, T. M.; Drobny, G. P. *J. Chem. Phys.* **1990**, *92*, 6840.
(145) Alam, T. M.; Orban, J.; Drobny, G. *Biochemistry* **1990**, *29*, 9610.
(146) Hentschel, R.; Sillescu, H.; Spiess, H. W. *Polymer* **1981**, *22*, 1516.
(147) Fratini, A. V.; Kopka, M. L.; Drew, H. R.; Dickerson, R. E. *J. Biol. Chem.* **1982**, *257*, 14686.
(148) Levit, M. H.; Raleigh, D. P.; Creuzet, F.; Griffin, R. G. *J. Chem. Phys.* **1990**, *92*, 6347.
(149) Guillion, T.; Schaeffer, J. *J. Magn. Reson.* **1989**, *81*, 196.
(150) Tang, P.; Juang, C.-I.; Harbison, G. R. *Science* **1990**, *249*, 70.